Dissertations   Theses and Dissertations

2016

The Amino Terminal Region of Cardiac Myosin Binding Protein-C Is Necessary for Cardiac Function

Thomas Lawrence Lynch
Loyola University Chicago

Follow this and additional works at: https://ecommons.luc.edu/luc_diss

Part of the Physiology Commons

Recommended Citation

LOYOLA UNIVERSITY CHICAGO

THE AMINO TERMINAL REGION OF

CARDIAC MYOSIN BINDING PROTEIN-C IS NECESSARY

FOR CARDIAC FUNCTION

A DISSERTATION SUBMITTED TO

THE FACULTY OF THE GRADUATE SCHOOL

IN CANDIDACY FOR THE DEGREE OF

DOCTOR OF PHILOSOPHY

PROGRAM IN MOLECULAR PHARMACOLOGY AND THERAPEUTICS

BY

THOMAS L. LYNCH IV

CHICAGO, IL

DECEMBER 2016

ACKNOWLEDGEMENTS

I would like to thank all of the people who made this dissertation possible, starting with my wonderful professors in the Departments of Molecular Pharmacology and Therapeutics and Cell and Molecular Physiology at Loyola University Chicago. In particular, I would like to thank my mentor Dr. Sakthivel Sadayappan for providing me the opportunity and resources to conduct my dissertation project in pursuit of the degree of Doctor of Philosophy. His training and mentorship have been invaluable to me and I will be forever grateful to him. I would also like to thank my committee chair, Dr. Pieter de Tombe. As an expert in cardiac muscle physiology, Dr. de Tombe has been an excellent resource and source of inspiration for me. His teaching and training has allowed me to understand the intricacies of cardiac muscle contraction. I am grateful to my other committee members Drs. R. John Solaro, Adriano Marchese, and Xun Ai for their suggestions and critical evaluations, which challenged me to delve deeper into thought and experimentation during my studies. Finally, I would like to thank my Graduate Program Director, Dr. Kenneth Byron. Since I first began my graduate education at Loyola University Chicago, Dr. Byron has provided me with mentorship and support, especially during difficult times in my graduate career. His advice, guidance, and encouragement have provided me with a strong foundation upon which to build my career goals.

and support that she has provided me throughout my life and during my time at Loyola. I would also like to thank my sisters, Patricia Domico and Diana Stephenson, my grandmother, Rose, and my fiancé, Audrey Dorenbos, for all of their love and support. Thank you all.

For My Mother, Sisters, Grandmothers, and Fiancé

TABLE OF CONTENTS

LIST OF TABLES

LIST OF FIGURES

LIST OF ABBREVIATIONS

α   alpha

ADP   Adenosine diphosphate

AF   Autofluorescence

α-TM   α-tropomyosin

AV   Atrioventricular

ATPase   Adenosinetriphosphatase

β   beta

BABB   Benzyl alcohol:benzyl benzoate

BSHG   Backward second harmonic generation

C'   C-terminal

Ca^{2+} Calcium

CAD   Coronary artery disease

CICR Ca^{2+}-induced Ca^{2+} release

Cl^- Chloride

cMyBP-C   Cardiac myosin binding protein-C

CO   Cardiac output

ECG   Electrocardiogram

EDP   End-diastolic pressure

EDPVR   End-diastolic pressure-volume relationship

EDV	End-diastolic volume
EF	Ejection fraction
ELC	Essential light chain
ESPVR	End-systolic pressure-volume relationship
ESV	End-systolic volume
FL	Full-length
FS	Fractional shortening
FSHG	Forward second harmonic generation
g	Gram
GLS	Global longitudinal strain
H&E	Hematoxylin and eosin
HCM	Hypertrophic cardiomyopathy
HF	Heart failure
HFpEF	Heart failure with preserved ejection fraction
HFrEF	Heart failure with reduced ejection fraction
hGH	Human growth hormone
HR	Heart rate
HW	Heart weight
IVS	Interventricular septum
IVSd	Interventricular septum at end diastole
IVSs	Interventricular septum at end systole
K^+	Potassium
kDa	Kilodalton

k_{tr}	Rate of tension redevelopment
L	Liter
LA	Left atria
LMM	Light meromyosin
LV	Left ventricle
LVID	Left ventricular internal diameter
LVIDd	Left ventricular internal diameter at end diastole
LVIDs	Left ventricular internal diameter at end systole
LVP	Left ventricular pressure
LVPW	Left ventricular posterior wall
LVPWd	Left ventricular posterior wall thickness at end diastole
LVPWs	Left ventricular posterior wall thickness at end systole
M	Molar
mg	Milligram
MHC	Myosin heavy chain
MI	Myocardial infarction
ml	Milliliter
mM	Millimolar
mm	Millimeter
MT	Masson's Trichrome
N'	N-terminal
Na^+	Sodium
NHANES	National Health and Nutrition Examination Survey

nl	Nanoliter
nM	Nanomolar
nm	Nanometer
NSTEMI	Non-ST segment elevation myocardial infarction
NTG	Non-transgenic
PAGE	Polyacrylamide gel electrophoresis
PAS	Periodic Acid Schiff
PBS	Phosphate buffered saline
PCR	Polymerase chain reaction
PKA	Protein kinase A
PLN	Phospholamban
PV	Pressure-volume
qPCR	Quantitative real-time PCR
RA	Right atria
RLC	Regulatory light chain
RV	Right ventricle
S1	Subfragment 1
S2	Subfragment 2
SA	Sinoatrial
SDS	Sodium dodecyl sulfate
SEM	Standard error of the mean
SERCA-2	Sarco/endoplasmic reticulum Ca^{2+} transport ATPase
SHG	Second harmonic generation

SR	Sarcoplasmic reticulum
STEMI	ST-segment elevation myocardial infarction
SV	Stroke volume
TBS-T	Tris-buffered saline containing 1% Tween-20
TG	Transgenic
TL	Tibia length
TnC	Troponin C
TnI	Troponin I
TnT	Troponin T
μl	Microliter
μm	Micrometer
μM	Micromolar

ABSTRACT

Cardiac myosin binding protein-C (cMyBP-C) is a thick filament-associated protein that has been suggested to regulate cardiac contraction via its amino terminal (N') region. Following ischemic injury to the heart, cMyBP-C is cleaved into a predominant N' fragment consisting of the first 271 N' residues of cMyBP-C (domains C0 through C1 and the first 17 residues of the M-domain) that is referred to as C0-C1f. *In vitro* studies have suggested the importance of the C0-C1f region of cMyBP-C in regulating actin filament sliding over the thick filament to control cross-bridge cycling kinetics within the cardiac sarcomere. However, the necessity of the N'-C0-C1f region of cMyBP-C in regulating cardiac function *in vivo* has not been elucidated. I hypothesized that the N'-C0-C1f region of cMyBP-C is critical for normal cardiac function *in vivo*. To test this hypothesis, transgenic (TG) mice with 81 ± 2.2% expression of a truncated cMyBP-C missing the N'-C0-C1f region and 19 ± 2.2% expression of endogenous full-length (FL) cMyBP-C (cMyBP-C^{110kDa} TG mouse line) were generated and characterized in comparison to their non-transgenic (NTG) littermates between 3- and 8-months of age. Short-axis M-mode echocardiography at 3- and 6-months of age showed a significant elevation ($p < 0.05$) in left ventricular (LV) internal diameter (LVID) and LV systolic volume at end systole in cMyBP-C^{110kDa} hearts compared to NTG hearts at 6-months of age. Importantly, percent ejection fraction (EF) and fractional shortening (FS) were significantly reduced in cMyBP-C^{110kDa} hearts

compared to NTG hearts at 3-months of age ($p < 0.05$), which were even further reduced in the hearts from 6-month old cMyBP-C^{110kDa} mice compared to hearts from both 6-month old NTG mice ($p < 0.0001$) and 3-month old cMyBP-C^{110kDa} mice ($p < 0.05$), indicating progressive cardiac dysfunction in cMyBP-C^{110kDa} animals. Accordingly, global longitudinal strain (GLS) analysis revealed abnormal wall motion in cMyBP-C^{110kDa} hearts compared to NTG hearts. I further observed cardiac enlargement, determined by whole-heart confocal imaging, and an elevation in cardiac pathological hypertrophy markers, determined by quantitative real-time PCR (qPCR) and RNA-Seq, in cMyBP-C^{110kDa} compared to NTG animals. Histopathological and second harmonic generation (SHG) analyses on myocardial sections indicated increased cardiac fibrosis ($p < 0.0001$) and increased sarcomere area ($p < 0.01$) in cMyBP-C^{110kDa} hearts compared to NTG hearts. Crucially, using immunofluorescence analysis coupled with SHG imaging of isolated cardiac myocytes from cMyBP-C^{110kDa} and NTG hearts, I determined that the cMyBP-C^{110kDa} TG protein localized properly at the C-zone within the cardiac sarcomere in the classic doublet pattern of cMyBP-C localization between α-actinin. This suggested that the contractile dysfunction observed in the hearts of cMyBP-C^{110kDa} animals was due to the absence of the N'-C0-C1f region of cMyBP-C in the cMyBP-C^{110kDa} TG protein and not aberrant mislocalization of this protein. Intriguingly, increased phosphorylation of the cMyBP-C^{110kDa} TG protein at serines 282 and 302, and endogenous FL-cMyBP-C at serines 273 and 302, sites important for cMyBP-C's regulation of actomyosin interactions, was observed in cMyBP-C^{110kDa} myofilament fractions compared to

those from NTG controls. Finally, using isolated, permeabilized papillary muscle fibers from cMyBP-C^{110kDa} and NTG hearts on a steady-state force-ATPase experiment, I determined that a significant elevation in maximum force ($p < 0.01$) and rate of tension redevelopment (k_{tr}) ($p < 0.05$) were produced from cMyBP-C^{110kDa} fibers compared NTG fibers. Based upon this data, I have determined that the N'-C0-C1f region of cMyBP-C is a critical regulator of actomyosin interactions and controls aberrant contraction kinetics within the cardiac sarcomere. I conclude that the N'-C0-C1f region of cMyBP-C regulates cardiac contractility and is necessary for maintaining normal cardiac function *in vivo*.

CHAPTER ONE

INTRODUCTION

Heart failure (HF) remains a leading cause of morbidity and mortality worldwide and affects 5.7 million people in the United States (Go et al., 2013) with a significant economic burden at a cost of approximately $32 billion annually (Heidenreich et al., 2011). HF is defined as the inability of the heart to maintain a cardiac output to distal organs that is sufficient to meet metabolic demand (Gordin & Fonarow, 2016). Left ventricular (LV) remodeling is the principal cause of many forms of HF (Cohn, Ferrari, & Sharpe, 2000). Systolic HF or HF with reduced ejection fraction (HFrEF) includes ventricular dilation and a reduction in cardiac contractility and ejection fraction (EF) (Burchfield, Xie, & Hill, 2013; Chatterjee & Rame, 2008). In contrast, diastolic HF or HF with preserved EF (HFpEF) is characterized by impaired cardiac relaxation and/or an increase in ventricular stiffness leading to abnormal ventricular filling with preservation in EF (Burchfield et al., 2013; Gutierrez & Blanchard, 2004; Zile & Brutsaert, 2002). Diastolic heart failure can occur alone or in combination with systolic heart failure (Zile & Brutsaert, 2002). LV systolic dysfunction is primarily caused by end-stage coronary artery disease (CAD), with patients having a history of myocardial infarction (MI) or reduced myocardial perfusion (Dargie, 2005). Similarly, diastolic LV dysfunction is related to ischemic heart disease as well as chronic hypertension, but may arise from restrictive, infiltrative, and hypertrophic

cardiomyopathies (Andersen et al., 2013; Moller, Pellikka, Hillis, & Oh, 2006).

Myocardial remodeling leading to ventricular hypertrophy is central to the development of HF and likely occurs to maintain cardiac pump function (de Tombe, 1998). Indeed, this pathology is observed in most cases of HF in humans and in animal models (de Tombe, 1998). Cardiac myocytes and other cardiac cells are thought to be fundamentally involved in the process of myocardial remodeling (Cohn et al., 2000). In addition to LV chamber remodeling, end-stage HF involves such processes as loss of functional myocytes, hyperplasia of the extracellular matrix, and decreased myocyte function (de Tombe, 1998). The current study focuses on the latter aspect of HF, which includes the mechanisms by which decreased myocyte contractile function leads to HF. These mechanisms include alterations in (i) calcium handling, (ii) myofilament function, and the (iii) cytoskeleton (de Tombe, 1998). In particular, the work presented here directly focuses on providing a better understanding of myofilament function in health and disease through the direct study of a critical contractile regulatory protein known as cardiac myosin binding protein-C (cMyBP-C).

Since its discovery in 1973 by Offer, Moos, and Starr (Offer, Moos, & Starr, 1973), cMyBP-C's role in modulating cardiac contraction has been the topic of fervent investigation (Barefield & Sadayappan, 2010) and controversy (Pfuhl & Gautel, 2012). It has been well established that the C' region of cMyBP-C interacts with light meromyosin (LMM) and titin to position and intricately incorporate cMyBP-C into the thick filament and to anchor the thick filament

(Freiburg & Gautel, 1996; Gilbert, Cohen, Pardo, Basu, & Fischman, 1999; Miyamoto, Fischman, & Reinach, 1999; Okagaki et al., 1993; Pfuhl & Gautel, 2012). This interaction may stabilize and organize the thick filament, however, this has yet to be confirmed (Nyland et al., 2009). In stark contrast to cMyBP-C's C' region, the interactions, role, and necessity of the N-terminal (N') region of cMyBP-C remain incompletely understood (Pfuhl & Gautel, 2012). While the N' region of cMyBP-C has been shown to interact with the subfragment 2 (S2) region of myosin heavy chain (MHC) (Gruen & Gautel, 1999), the same interacting region of cMyBP-C was suggested to bind to F-actin (Razumova et al., 2006; Squire, Luther, & Knupp, 2003).

cMyBP-C is thought to be a critical contractile regulatory protein that, through its binding to actin, myosin, or both, regulates the probability of cross-bridge interaction with actin and rates of force development and relaxation (Moss, Fitzsimons, & Ralphe, 2015). Furthermore, phosphorylation of cMyBP-C within its N' region is considered to be the predominant mechanism controlling cMyBP-C's interactions and its ability to regulate contraction at the level of the sarcomere (Barefield & Sadayappan, 2010). Animal models of total cMyBP-C ablation develop hypertrophic cardiomyopathy (HCM) demonstrating the necessity of cMyBP-C in maintaining normal cardiac function (Harris et al., 2002). Intriguingly, *MYBPC3*, the gene encoding cMyBP-C, is the most highly mutated gene in human HCM accounting for approximately 40% of the identified mutations (Barefield et al., 2015), further suggesting the importance of cMyBP-C

in regulating cardiac function within the myofilament. Given that the N' region of cMyBP-C is the most critical region controlling actomyosin interactions and the kinetics of cross-bridge cycling, elucidating the necessity of the N' region of cMyBP-C *in vivo* is of critical importance to understanding the mechanisms by which cMyBP-C functions in both health and disease.

The focus of my dissertation work has been on determining the necessity of the N' region of cMyBP-C, particularly, a region referred to as C0-C1f, in maintaining normal cardiac contractile function *in vivo*. The N'-C0-C1f region of cMyBP-C is a 40 kilodalton (kDa) peptide consisting of the first 271 amino acid residues of cMyBP-C and incorporates domains C0 through C1 and the first 17 residues of the M-domain (Govindan, McElligott, et al., 2012; Govindan, Sarkey, et al., 2012; T. L. Lynch & Sadayappan, 2014; Previs, Beck Previs, Gulick, Robbins, & Warshaw, 2012; Razzaque et al., 2013; Witayavanitkul et al., 2014). The importance of the N'-C0-C1f region of cMyBP-C is several-fold. Initially, our group identified this region as a predominant N' cleavage fragment of cMyBP-C following cMyBP-C's dephosphorylation during conditions of hypoxia or ischemic injury (Govindan, McElligott, et al., 2012). In two subsequent reports, we discovered that C0-C1f was sufficient to cause contractile dysfunction in isolated rat ventricular myocytes (Govindan, Sarkey, et al., 2012) and could impair myofilament function in human cardiac myofilaments (Witayavanitkul et al., 2014). Intriguingly, a later study by Razzaque *et al.* demonstrated that endogenous expression of C0-C1f was sufficient to cause HCM and HF in mice

(Razzaque et al., 2013). Importantly, others have reported the ability of C0-C1f to inhibit actin filament sliding over myosin (Previs et al., 2012) and that the first 17 residues of the M-domain (the "f" region of C0-C1f) are crucial to this process (A. Weith et al., 2012). Together, these studies suggest the importance of the N'-C0-C1f region of cMyBP-C in regulating myofilament function both *in vitro* and *in vivo*. Therefore, we proposed that the N'-C0-C1f fragment may be the vital portion of cMyBP-C's N' region that allows this protein to control actomyosin interactions and cardiac contraction.

My central hypothesis stemming from these previous findings and that forms the cornerstone of my dissertation work is that the N'-C0-C1f region of cMyBP-C is necessary for maintaining normal cardiac function *in vivo*. I tested this hypothesis using a novel transgenic (TG) mouse model developed in our lab that is missing the N'-C0-C1f region but that still expresses the remaining 110 kDa more distal C' fragment of cMyBP-C (cMyBP-C^{110kDa} mouse model) within the cardiac sarcomere.

The experiments that I performed during my dissertation studies examined cardiac function at the level of the whole heart and at the level of isolated papillary muscle fibers using cMyBP-C^{110kDa} mice and their non-transgenic (NTG) littermates as controls. With this approach, I was able to determine that cMyBP-C^{110kDa} mice have significantly elevated levels of *MYBPC3* gene expression and do express the cMyBP-C^{110kDa} TG protein, which is not observed in NTG controls. Most significantly, my data revealed that between 3- and 6-months of

age, cMyBP-C^{110kDa} animals harbored cardiac contractile dysfunction both at the whole-organ level (Specific Aim 1) and in isolated cardiac papillary fibers (Specific Aim 2) and developed cardiac hypertrophy compared to NTG animals. Of critical importance, I determined that the cMyBP-C^{110kDa} TG protein localized properly within the cardiac sarcomere in the classical doublet pattern between α-actinin, which is the known localization pattern for cMyBP-C (Kuster et al., 2015). This suggests that the dysfunction seen in cMyBP-C^{110kDa} hearts is specifically instigated by the loss of the N'-C0-C1f region rather than aberrant mislocalization of the cMyBP-C^{110kDa} TG fragment acting as a poison polypeptide that has been suggested for the C0-C1f fragment (Govindan, Sarkey, et al., 2012; Razzaque et al., 2013; Witayavanitkul et al., 2014). Finally, I observed a significant elevation in cMyBP-C phosphorylation within the M-domain in myofilament fractions from cMyBP-C^{110kDa} hearts compared to NTG hearts.

Based upon these data, I propose that the N'-C0-C1f region of cMyBP-C is a critical regulator of actomyosin interactions and controls aberrant contraction kinetics within the cardiac sarcomere. From the results of the data generated during my dissertation studies, I conclude that the N'-C0-C1f region of cMyBP-C regulates cardiac contractility and is necessary for maintaining normal cardiac function *in vivo*, suggesting the importance of the N' region of cMyBP-C in both health and disease.

CHAPTER TWO

LITERATURE REVIEW

Cardiovascular Physiology in Health and Disease

The heart is an organ that is both powerful and complex and that has been a point of fascination for scholars, poets, and physicians for centuries (Young, 2010). Indeed, since the time of Ancient Greek philosophers such as Hippocrates, "the father of medicine," and later Aristotle, who described the heart as a three-chambered organ that was the center of vitality in the body, to Galen who believed the heart was the source of the body's innate heat and the organ most related to the soul, the heart has played a key role in understanding the function of the body (Aird, 2011). While to this day the heart remains a spiritual and religious component of the body to many, work by Sir William Harvey in the 17th century confirmed the physiological role of the heart is to propel blood to the extremities through the arteries (Aird, 2011; Silverman, 1985). His theories and experiments are summarized in his notion that "…the chief function of the heart is the transmission and pumping of the blood through the arteries to the extremities of the body. Thus, the pulse which we feel in the arteries is nothing else than the impact of blood from the heart" (Silverman, 1985). Harvey postulated but could not prove that blood travels through the right heart through the lungs and then to the left heart stating, "In the more perfect warm-blooded adult animals, as man,

the blood passes from the right ventricle of the heart through the pulmonary artery to the lungs, from there through the pulmonary vein into the left auricle, and then into the ventricle" (Silverman, 1985). By the end of the 17th century, the anatomical knowledge of the heart was quite accurate with many accepting Harvey's new theories that the heart was a pump (Silverman, 1985), a concept that still holds true today. Certainly, the heart has been a critical site for debate throughout the centuries, a debate that continues through many aspects of modern cardiovascular medicine and research today.

The primary objective of this chapter is to provide an overview of cardiac anatomy and physiology in both health and disease. I will provide an overview of the structure and physiological function of the heart and the electrical regulation that controls contraction within the heart. Finally, I will discuss HF, the final clinical entity of many cardiovascular diseases, and two cardiac pathologies, MI and cardiomyopathies, which are relevant to the background of my dissertation work discussed here.

Cardiac Anatomy

The human heart is a muscular organ that pumps blood throughout the body via the circulatory system, supplying oxygen and nutrients to tissues and removing carbon dioxide and other wastes. To do so, the heart functions as a unidirectional pump that pressurizes blood in order to perfuse the body. The heart muscle is quite remarkable beating at an average rate of 70 beats min^{-1} and contracting and relaxing more than 100,000 times a day (Pinnell, 2007). The

pump function of the heart can be explained by examining the anatomy of this organ.

The heart is located within the thoracic cavity between the lungs and behind the sternum. The upper portion of the heart is attached to the aorta, the main artery that carries blood away from the heart to the rest of the body, as well as to pulmonary arteries and veins, and the vena cava. The lower tip of the heart, known as the apex, sits just above the diaphragm and points to the left. As such, $2/3^{rd}$ of the heart's mass is on the left side of the body while the remaining $1/3^{rd}$ sits to the right. Within the thoracic cavity, the heart beats inside of the fluid-filled pericardial cavity that is composed of a membranous structure referred to as the pericardium. The pericardium contains a visceral layer outside of the heart as well as a parietal layer outside of the pericardial cavity. The primary functions of the pericardium are to lubricate the heart to eliminate friction between the heart and local organs and to hold the heart in place.

Structurally, the heart is composed of 3 layers. The outermost layer is the epicardium, which is synonymous with the visceral layer of the pericardium and, therefore, serves to lubricate and protect the external portion of the heart. The middle layer of the heart is the myocardium. The myocardium is the thick, muscular layer of the heart that comprises the majority of the mass of the heart and is responsible for cardiac contraction to pump blood throughout the body. Finally, the innermost layer of the heart is referred to as the endocardium, a simple squamous endothelial layer that prevents blood from sticking to the inside

of the heart and forming clots. In the healthy heart, the thickness of the walls varies such that the atria (discussed below) have a thin myocardial layer due to their requisite pumping to the nearby ventricles. In contrast, the ventricles (discussed below) have a larger myocardial layer than the atria in order to pump blood from the right heart to the lungs and the left heart to the body. Naturally, the ventricle of the left heart has the larger myocardial layer to pump blood throughout the body.

The human heart is a four-chambered structure consisting of two atria (right and left) and two ventricles (right and left). As mentioned above, the atria are the smaller chambers that serve to receive blood from the venous system of the body and lungs (**Figure 1**). The ventricles, however, are larger and contract with greater force to send blood arriving from the atria to the lungs and body away from the heart via arteries. The healthy heart is a unidirectional pump through which blood flows from the right to the left. To prevent backflow or regurgitation of blood into the heart, a series of valves known as atrioventricular (AV) and semilunar valves comprise a portion of the cardiac anatomy. The AV valves are located in the middle of the heart between the atria and ventricles and only allow blood to flow from the atria to the ventricles. On the right side of the heart, the AV valve is referred to as the tricuspid valve as it is made of three cusps that separate and connect to either allow blood to enter the right ventricle (RV) or to prevent regurgitation of blood back into the RV, respectively. On the
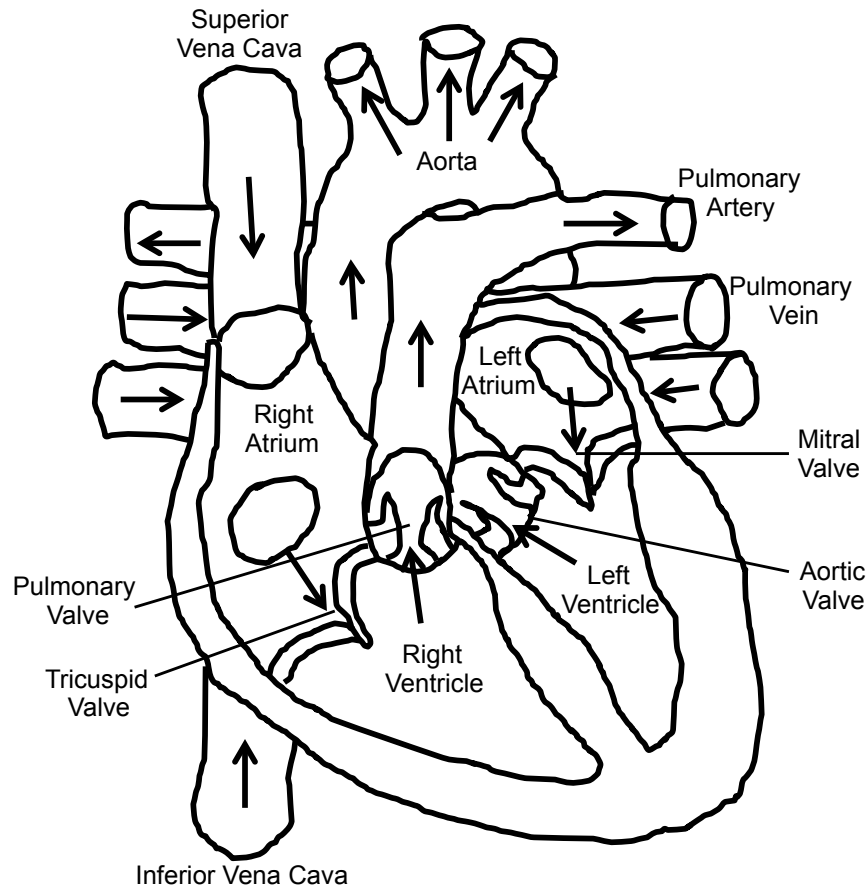
Figure 1. The Human Heart. The human heart consists of two atria (left and right) and two ventricles (left and right). Blood enters the heart from the systemic circulation through the superior and inferior vena cava and then flows unidirectionally into the RA. From the RA, blood is pumped through the tricuspid valve into the RV. From the RV, blood is pumped through the pulmonary arteries into the lungs where carbon dioxide is exchanged for oxygen. From the lungs, blood flows through the pulmonary veins into the LA where it is then pumped through the bicuspid (mitral) valve into the LV. The LV pumps blood through the aortic valve into the aorta and to the systemic circulatory system and coronary circulation. For this reason, the LV is the largest of the four heart chambers.

left side of the heart, the AV valve is referred to as the bicuspid or "mitral" valve as it has two cusps. The bicuspid valve functions similar to the tricuspid valve. The AV valves are attached to the ventricles through chordae tendineae. During contraction of the ventricles (discussed below) the chordae tendineae pull the AV valves preventing them from folding backwards into the atria and allow blood to pass through to the ventricles. The semilunar valves are situated between the ventricles and the arteries that carry blood to either the lungs or body. The semilunar valve on the right side of the heart is referred to as the pulmonary valve. The pulmonary valve prevents regurgitation of blood from the pulmonary trunk into the RV. The semilunar valve on the left side of the heart is known as the aortic valve and prevents the backflow of blood from the aorta into the LV. In contrast to the AV valves, the semilunar valves are not attached to chordae tendineae but rather, are cup shaped to catch regurgitating blood and use the pressure of the blood to close.

The propagation of electrical signals throughout the myocardium regulates contraction of the heart. In fact, the heart is capable of setting its own rhythm and conducting these electrical signals throughout the myocardium. During the cardiac contraction cycle (discussed below) the right atria (RA) and left atria (LA) contract concomitantly followed by concomitant contraction of the RV and LV. The conduction system of the heart begins with the pacemaker, a small bundle of specialized cells in the RA known as the sinoatrial (SA) node. The SA node sets heart rate by initiating depolarization, which signals the atria to contract.

Sympathetic and parasympathetic inputs to the SA node modulate heart rate (Robinson, Epstein, Beiser, & Braunwald, 1966). When the SA node fires, it initiates a wave of depolarization that spreads across the RA and LA stimulating their contraction. The signal from the SA node is picked up by another mass of conductive tissue known as the AV node, which is located in the right atrium in the lower portion of the interatrial septum. While the AV node receives its signal from the SA node and transmits this signal through the AV bundle, the AV node has its own latent pacemaker activity and can rhythmically contract at the rate of AV node firing if the SA node is injured or ablated (Olshansky & Sullivan, 2013). The AV bundle is a network of conductive tissue that travels through the interatrial septum to the interventricular septum. The AV bundle splits into left and right branches in the interventricular septum that run inferiorly to the apex and up to the free walls of the LV and RV branching into Purkinje fibers. This conduction system is known as the His-Purkinje system (Haissaguerre, Vigmond, Stuyvers, Hocini, & Bernus, 2016). From the AV node, the action potential propagates through the conduction system through Purkinje fibers allowing both ventricles to contract in concert, with the endocardium contracting slightly prior to the epicardium, and the apex contracting before the base of the ventricle. This orientation and sequence of contraction causes the ventricles to contract from the apex up, allowing efficient ejection of blood from the ventricle. Action potentials also spread from cell-to-cell due to the electrical coupling of cardiomyocytes via gap junctions (typically Connexin 43 in ventricular tissue) that

allow propagation of depolarization through cells (Kreuzberg, Willecke, & Bukauskas, 2006).

Cardiac Physiology

The primary role of the heart is to pump blood throughout the body by continuously and rhythmically relaxing to fill the heart with blood and contracting to eject blood to the lungs and body. Understanding the anatomy of the heart (discussed above) provides an understanding of its function. At any given time, the cardiac chambers are found in one of two states referred to as systole and diastole. Systole refers to the point in the cardiac cycle during which the heart muscle contracts to eject blood out of the chambers. Diastole, on the other hand, refers to the point in the cardiac cycle during which the heart and, more specifically, the heart muscle cells known as cardiomyocytes (discussed below), relax allowing the heart chambers to fill with blood. Ventricular systole is accompanied by an increase in arterial pressure that subsequently decreases during ventricular diastole. From this, we derive blood pressure. In a healthy cardiovascular system, blood pressure is typically reported as 120/80, which is systolic over diastolic pressure.

The rhythmic beating of the heart during systole and diastole is what makes the heart the engine that drives blood throughout the heart and throughout the body. Regarding blood flow throughout the heart, deoxygenated blood returning from the upper and lower portions of the body first arrives at the heart via the superior and inferior vena cava into the RA. This deoxygenated

blood is pumped through the tricuspid valve into the RV and then from the RV through the pulmonary semilunar valve into the pulmonary trunk and pulmonary arteries. Upon reaching the lungs, carbon dioxide is released and oxygen is absorbed into the blood, which then returns to the heart through the pulmonary veins into the LA. From the LA blood passes through the bicuspid valve into the LV and from the LV through the aortic semilunar valve into the aorta to the systemic circulation. Importantly, the heart, like every other organ or tissue in the body needs oxygen-rich blood to survive. As such, the heart is supplied by its own vascular system known as the coronary circulation. As oxygen-rich blood enters the aorta and travels to the systemic circulation, it also passes from the aorta into the right coronary artery and the left anterior descending coronary artery to supply the heart with blood. Blood returning from myocardial tissue does so through the coronary veins, which collect deoxygenated blood from the heart muscle and return it to the RA through the coronary sinus.

Cardiac function in terms of the contraction and relaxation of the ventricles is best described using the four phases of the pressure-volume (PV) relationship (**Figure 2**) (Kass, Yamazaki, Burkhoff, Maughan, & Sagawa, 1986; Sagawa, 1981; Suga & Sagawa, 1974). LV PV loops are derived from pressure and volume information found in the cardiac cycle diagram (**Figure 2A**). To generate a PV loop for the LV, LV pressure (LVP) is plotted against LV volume at multiple time points during a complete cardiac cycle (**Figure 2B**). The PV relationship for a single cardiac cycle is divided into 4 phases: ventricular filling (phase a;
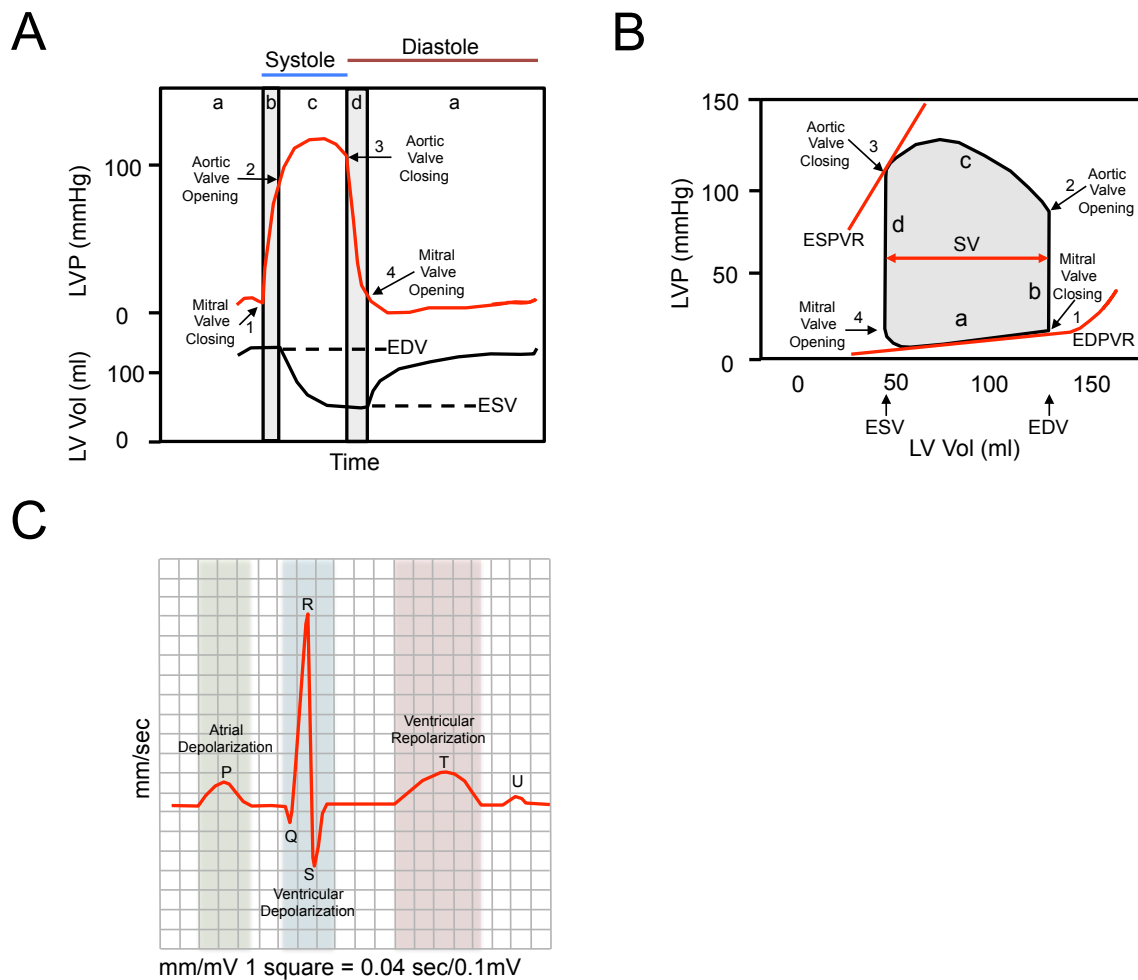
Figure 2. The Pressure-Volume Relationship. (A) The cardiac cycle as depicted by LVP and LV volume changes. (B) The PV relationship depicting LVP plotted against LV volume during the cardiac contraction cycle. (C) Depiction of an ECG recording showing points of atrial and ventricular depolarization and repolarization during the cardiac cycle.

diastole), isovolumetric contraction (phase b; systole), ejection (phase c; systole), and isovolumetric relaxation (phase d; diastole). On the PV loop, point 1 denotes the pressure and volume in the LV at the end of the ventricular filling phase (diastole) and represents the end-diastolic pressure (EDP) and end-diastolic volume (EDV) for the LV. Pressure within the LV will rise to the point where compliance declines and the elastic elements of the heart resist additional filling. At the end of diastole, the pressure exerted by the total amount of blood filling the ventricle is considered to be the preload on the heart. Next, the ventricles begin to contract isovolumetrically (phase b) leading to closure of the mitral valve and an increase in LVP with no change in LV volume as all of the valves are closed. When the LVP is greater than the aortic diastolic pressure on the distal side of the aortic valve the aortic valve opens (point 2) and ejection (phase c) begins. It is during this time that LV volume decreases as LVP increases to a peak value known as peak systolic pressure, which then decreases during LV relaxation. The level of diastolic blood pressure the heart pumps against is referred to as the afterload. When the pressure in the heart drops below the systolic blood pressure, the aortic valve closes (point 3) leading to a cessation in blood ejection, the end of systole, and the start of isovolumetric relaxation of the LV. During this time, LVP falls but LV volume remains unchanged as all valves are closed (phase d). The volume of blood in the LV at this time is known as the end-systolic (residual) volume (ESV). When the pressure in the LV is less than the pressure in the LA, the mitral valve opens (point 4) allowing the LV to fill. During this time

of ventricular filling, the LVP continues to decline as the ventricle is still relaxing. However, when the LV is fully relaxed, LVP slowly rises again as LV volume increases (phase a) and the cardiac cycle repeats. Importantly, the width of the PV loop depicts the difference between EDV and ESV, which is known as the stroke volume (SV). SV multiplied by heart rate (HR) is known as cardiac output (CO), which is the volume of blood being pumped by the heart in one minute (Vincent, 2008). Typically, at rest, the healthy heart pumps 5 to 5.5 liters of blood per minute.

In general, the filling phase of the heart follows the end-diastolic PV relationship (EDPVR), which is the passive filling curve for the LV. The slope of this curve is reciprocal of ventricular compliance. The end-systolic PV relationship (ESPVR) describes the maximal pressure that can be developed by the ventricle at any given LV volume and represents the inotropic (contractile) state of the ventricle. The PV loop cannot cross the ESPVR because this relationship describes the maximal pressure that is produced under a given inotropic state.

Electrical changes within the heart leading to atrial and ventricular depolarization and repolarization (discussed below) are the critical regulators of the rate at which the cardiac cycle occurs (HR). Such changes are measured using an electrocardiogram (ECG), which produces a waveform in response to electrical changes in the heart (**Figure 2C**). The first part of the wave is the P wave, which denotes a small increase in voltage corresponding to atrial

depolarization during atrial systole. Next, the QRS complex features a small drop in voltage (Q) a large voltage peak (R) and another small drop in voltage (S) that, together, correspond to ventricular depolarization during ventricular systole. It is also during this time that atrial repolarization occurs, which is largely undetected on the ECG. Finally, the T wave corresponds to a small peak following the QRS complex that represents ventricular repolarization during cardiac relaxation. Occasionally, a small positive U wave may also be seen following the T wave, which depicts the final stages of ventricular repolarization. Considering cardiovascular diseases, alterations in waveform and distance between the waves on an ECG are used clinically to diagnose such pathologies as heart attacks, congenital heart problems, electrolyte imbalances, etc.

Heart Failure

Abnormalities in cardiac anatomy and/or physiology are often the precursors to the development of HF. Indeed, HF is the final clinical entity of many cardiovascular diseases including CAD, diabetes, hypertension, cigarette smoking, arrhythmias, cardiomyopathies, congenital heart defects, heart valve disease, as well as alcohol and drug abuse, HIV/AIDS, thyroid disorders, excessive intake of vitamin E, radiation, and chemotherapy (Mozaffarian et al., 2016). HF describes a condition in which the heart is unable to supply sufficient blood flow to peripheral tissues and organs to meet their demand for oxygen. This often results in fatigue, shortness of breath, and decreased exercise capacity (Cowie et al., 1997). Data from the National Health and Nutrition

Examination Survey (NHANES) from 2009-2012 estimate that approximately 5.7 million Americans ≥ 20 years of age have HF (Mozaffarian et al., 2016). Projections estimate that the prevalence of HF will increase to 46% between 2012 to 2030 resulting in > 8 million people ≥ 18 years of age with HF (Mozaffarian et al., 2016). Each year, there are approximately 915,000 new cases of HF (Mozaffarian et al., 2016). While HF is a common cause of morbidity and mortality worldwide mortality declines are attributed in approaches to treat HF including the use of angiotensin converting enzyme inhibitors, β-blockers, coronary revascularization, implantable cardioverter-defibrillators, and cardiac resynchronization therapeutic strategies (Merlo et al., 2014; Mozaffarian et al., 2016). Among individuals with symptomatic HF, 55% are HFpEF. These cases are associated with a high mortality rate, comparable to that of HFrEF (Bursi et al., 2006; Mozaffarian et al., 2016). In 2012, the total cost for HF was estimated to be $30.7 billion with projections suggesting this number to rise to $69.7 billion by 2030, $244 for every US adult (Heidenreich et al., 2013; Mozaffarian et al., 2016).

Cardiac dysfunction results in changes in vascular function, blood volume, and neurohumoral status, which serve as compensatory mechanisms to maintain CO by the Frank-Starling mechanism. The Frank-Starling mechanism or Starling's Law of the heart describes the ability of the heart to change its force of contraction and stroke volume in response to changes in venous return. That is, the more the LV is stretched prior to contraction, the greater the strength of the

contraction will be. This is analogous to the notion that increasing venous return to the heart, thereby increasing LVEDP, leads to an increased stroke volume (Moss & Fitzsimons, 2002). HF typically leads to a reduction in CO due to a decline in SV resulting from systolic or diastolic dysfunction, or both. Systolic dysfunction results from a loss in either contractility (inotropy) or a loss of viable muscle as occurs following MI (discussed below). Furthermore, in chronic HF, systolic dysfunction is often the result of remodeling of the LV that leads to LV dilation (discussed below) as well as from alterations in the signaling-mechanisms regulating excitation-contraction coupling (discussed below) leading to reduced SV and a rise in preload due to incomplete emptying of the LV. This causes a rise in EDV and EDP and activates the Frank-Starling mechanism to maintain stroke volume regardless of the loss in contractility. When looking at the PV loop, the loss of inotropy accompanying systolic dysfunction decreases the slope of the ESPVR resulting in an increase in ESV, an elevation in EDV and a reduction in SV. The accompanying reduction in EF in systolic dysfunction is why this pathology is now referred to as HFrEF.

Diastolic dysfunction occurs when the LV stiffens and becomes less compliant as occurs in LV hypertrophy. This leads to impaired ventricular filling. Since ventricular filling is dependent upon venous return and the compliance of the LV during diastole, reducing ventricular compliance causes a reduction in EDV, an increase in EDP and a reduction in SV. However, depending upon how much the SV and EDV change, EF may or may not be changed. As such, HF

caused by diastolic dysfunction is referred to as HFpEF. Diastolic dysfunction may also be due to diminished ventricular relaxation resulting from impairment of calcium (Ca^{2+}) uptake into the sarcoplasmic reticulum (SR) or other mechanisms contributing to myocyte relaxation. In this case, filling of the LV is also reduced.

Myocardial Infarction

CAD is the number one cause of HF and is a pathology that reduces blood flow through the coronary arteries reducing oxygen delivery to the heart muscle (Gheorghiade et al., 2006). The result is hypoxia within the myocardium and impaired cardiac function. The final clinical entity of CAD is known as MI. MI is clinically defined by myocardial necrosis in the setting of prolonged myocardial ischemia and remains a leading cause of morbidity and mortality worldwide (Ahmad, 2012; Reichlin et al., 2009). Most MIs are caused by the occlusion of a coronary artery by thrombus formation following the rupture of an unstable atherosclerotic plaque (**Figure 3**) (Sotolongo, Smith, & Margolis, 1990). Myocardium lying distal to the occlusion will not be supplied with oxygen and nutrients and reduced perfusion will limit washout of cellular waste products. An occlusion lasting more than 20 min generates irreversible myocardial necrosis that first occurs within the endocardium and expands throughout the myocardium and epicardium (Thygesen et al., 2012). Complete necrosis of the area at risk occurs within several hours and depends upon such factors as the extent of collateral circulation and demand for oxygen and nutrients (Thygesen et al., 2012). Since the amount of tissue damage is directly related to the duration of

Aorta

Superior
vena cava

Right
coronary
artery

Myocardium

Blood clot

Atherosclerotic
plaque blocking
blood flow, oxygen
and nutrients to
distal cardiac tissue

Left anterior
descending
coronary artery

Zone of infarction
displaying myocardial
tissue death
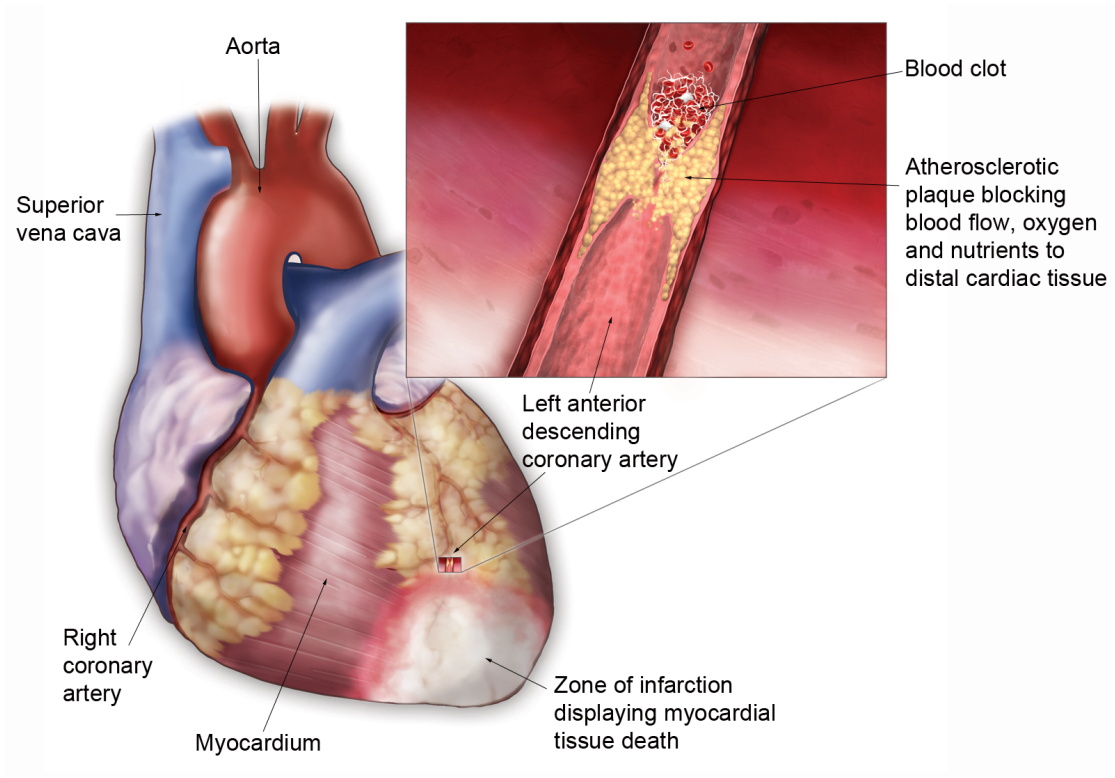
Figure 3. Myocardial Infarction. Anatomical diagram of the heart showing cardiac vasculature. Inset illustrating MI. A leading cause of MI is the rupture of an unstable cholesterol plaque promoting thrombus formation, inflammatory cell infiltration, and occlusion of a coronary artery. The loss of blood supply to distal myocardial tissue inhibits the supply of oxygen and nutrients to the infarct zone and leads to tissue necrosis following prolonged ischemia. The duration of the occlusion determines the severity of tissue damage with irreversible necrosis occurring within several hours of the infarct. Important to my dissertation work, our group recently found that cMyBP-C is degraded into an N' 40 kDa fragment (C0-C1f) following MI and that this fragment is released into the local tissue and systemic circulation. Figure from (T. L. Lynch & Sadayappan, 2014). Copyright Wiley-VCH Verlag GmbH & Co. KGaA. Reproduced with permission.

the occlusion, the therapeutic strategy is to reopen the coronary artery as quickly as possible (Sotolongo et al., 1990). Therefore, early detection of a MI is imperative for successful treatment. Large transmural infarctions can typically be detected by ECG ST-segment elevation (STEMI) (Kim, Lee, Park, Han, & Oh, 2010). However, a large proportion of infarctions do not result in clear ST-segment elevation (de Winter & Tijssen, 2012). In these non-ST segment elevation (NSTEMI) patients, diagnosis is based on the release of cardiac proteins (mostly cardiac troponins) into the circulation caused by necrotic cardiomyocytes (Hall, Hallen, Agewall, Atar, & Jensen, 2012). Unlike ECG changes in STEMI patients, an increase in serum levels of the cardiac troponins is only detectable after several hours (Ferguson, Beckett, Stoddart, Walker, & Fox, 2002; Reichlin et al., 2009).

In the healthy heart, contraction is regulated by a system that couples electrical excitation to elevated levels of intracellular Ca^{2+}, triggering an interaction between actin and myosin filaments to generate cross-bridge cycling and shortening of the sarcomere (discussed below) (Bers, 2002). However, upon ischemic injury to the heart, loss of myocardial tissue alters the contractile properties of cardiomyocytes leading to further myocyte death and exacerbating cardiac dysfunction (Zhang et al., 2010). The heart attempts to compensate for the loss of contractile activity and diminished cardiac pump function by increasing myocyte Ca^{2+} transients (Zhang et al., 2010). However, maintaining contractile function by increasing Ca^{2+} influx induces continuous pathological stress in the

post-MI heart (Zhang et al., 2010). This stress causes structural remodeling of the left ventricle (discussed below) and dysfunction leading to hypertrophy and, eventually, dilation (Dhalla, Kaura, Liu, & Beamish, 1996; Gupta, Prahash, & Anand, 2000; Zhang et al., 2010).

Important to my dissertation work, our group recently found that cMyBP-C is degraded into an N' 40 kDa fragment (C0-C1f) following MI and that this fragment is released into the local tissue and systemic circulation (Govindan, McElligott, et al., 2012; Govindan, Sarkey, et al., 2012; T. L. Lynch & Sadayappan, 2014; Razzaque et al., 2013). Notably, within cardiac tissue, C0-C1f has been demonstrated to produce significant contractile dysfunction (Govindan, Sarkey, et al., 2012; Witayavanitkul et al., 2014), and HF (Razzaque et al., 2013). The discovery and role of C0-C1f in the heart will be discussed further below.

Pathological Cardiac Remodeling

Cardiac remodeling is generally accepted as a major factor determining the clinical course of HF. Indeed, as heart disease progresses to HF, heart size is augmented, cardiac function deteriorates, and HF symptoms are manifested (Cohn et al., 2000). Cardiac remodeling is defined as genome expression resulting in molecular, cellular and interstitial changes and is manifested clinically as changes in the size, shape, and function of the heart resulting from cardiac load or injury (Cohn et al., 2000). Cardiac remodeling is influenced by several factors including hemodynamic load and neurohormonal activation among other

factors (Cohn et al., 2000). Furthermore, many changes that occur during cardiac remodeling are associated with HF progression. The cardiac myocyte is the primary cell involved in the remodeling process. However, other cardiac components including the interstitium, fibroblasts, collagen, and coronary vasculature are involved (Cohn et al., 2000). Additionally, processes relevant to cardiac remodeling include ischemic injury to the heart, cellular necrosis, apoptosis, and autophagy as well as pressure or volume overload, myocarditis, and cardiomyopathies (Cohn et al., 2000).

While the exact processes and cellular mediators of LV remodeling remain unclear, it is thought that as myocytes are stretched, norepinephrine activity and angiotensin and endothelin release are increased stimulating expression of altered proteins and myocyte hypertrophy (Cohn et al., 2000). This leads to further deterioration in cardiac function and increased neurohormonal activation. Increased aldosterone and cytokine activation may also stimulate collagen synthesis leading to fibrosis and remodeling of the extracellular matrix (Cohn et al., 2000). Although, in the series of events leading up to chronic HF, the early stages of cardiac remodeling are considered beneficial and/or compensatory as the heart attempts to maintain normal function in the face of overt stress. The cellular rearrangement of the ventricular wall associates with either maintained or improved CO as the heart hypertrophies (Cohn et al., 2000). As myocytes become elongated, the thickness of the ventricular wall increases. This stretch within myocytes may induce the expression of hypertrophy-associated genes and

the synthesis of new contractile proteins and the assembly of new sarcomeres (Cohn et al., 2000). It is thought that the pattern in which new sarcomeres are deposited determines whether cardiomyocytes increase their diameter or elongate (Francis & McDonald, 1992). Progressive dilation of the LV by cellular elongation is associated with an elevation in the volume of blood in the LV (increased preload) but a reduction in EF. Evidently, as the heart remodels, it changes its geometry and mass, which may adversely affect cardiac function leading to a maladaptive response (Cohn et al., 2000; Struijker-Boudier, Smits, & De Mey, 1995; K. T. Weber & Brilla, 1991). This plasticity of the LV is known as pathological remodeling (Burchfield et al., 2013). Surprisingly, in addition to myocyte hypertrophy, under certain conditions these cells may also atrophy leading to shrinkage of the heart and a reduction of LV mass (Ambardekar & Buttrick, 2011).

The majority of clinically used therapies targeting HF with cardiac remodeling are for patients with HFrEF. However, as indicated previously, approximately 50% of HF patients are HFpEF (Borlaug & Paulus, 2011; Burchfield et al., 2013). CAD is a leading cause of HFrEF (Dorn, 2009) and most of the knowledge regarding LV remodeling comes from patients and animal models of MI (Burchfield et al., 2013). Current clinically proven therapies used in the treatment of pathological ventricular remodeling that have been shown to reduce morbidity and mortality include angiotensin-converting enzyme inhibitors, angiotensin receptor blockers, beta (β)-blockers and mineralocorticoid receptor

antagonists that have been shown to reduce cell death, hypertrophy, and fibrosis (Xie, Burchfield, & Hill, 2013). It has been further suggested that glucagon-like peptide-1 may be effective in treating metabolic imbalances (Xie et al., 2013). Ventricular assist devices have been shown to provide mechanical support by unloading the failing myocardium and limiting ventricular dilation while implantable cardioverter-defibrillators and cardiac resynchronization therapy target electrophysiological remodeling events. Lastly, although controversial, cell replacement therapy to replace lost cardiomyocytes may prove to be a promising future therapeutic (Xie et al., 2013).

Within the categories of HFrEF and HFpEF, a wide range of etiologies dictates disease pathogenesis. HCM, a HFpEF disorder, is one such pathology use to parse out these etiologies (Burchfield et al., 2013) as it is associated with multiple distinct genetic variants that provide information regarding phenotype and disease outcome (Maron & Maron, 2013). HCM is caused by mutations in genes encoding sarcomeric proteins (Barefield, Kumar, de Tombe, & Sadayappan, 2014) that control myocyte contraction and Ca^{2+} handling. Of the identified genes, *MYBPC3* is the most highly mutated gene in human HCM accounting for approximately 40% of all known mutations (Barefield et al., 2015). As many HFpEF patients have normal extracellular matrix proteins, myocyte stiffness resulting from sarcomeric abnormalities appears to contribute to disease pathogenesis. As such, early genetic testing for HCM may assist in the accurate and early diagnosis of HFpEF (Burchfield et al., 2013). In contrast to HCM, DCM

represents a HFrEF disorder that has been shown to be linked to mutations in 50 sarcomeric genes (McNally, Golbus, & Puckelwartz, 2013). Similar to HCM, not all DCM patients display the same phenotype and often mutations within the same gene or the same genetic variant can cause HCM or DCM rendering diagnosis and risk prevention difficult (Burchfield et al., 2013). Conclusively, the cardiac myocyte appears to be at the center of cardiac remodeling and the etiology of HFpEF and HFrEF, indicating the need to better understand myocyte function in health and disease.

The Structure and Function of the Cardiac Myocyte

The myocardium is a highly organized tissue consisting of smooth muscle cells, fibroblasts, and cardiac myocytes (Walker & Spinale, 1999). The cardiac myocyte is the fundamental unit of contraction within the myocardium as well as the most physiologically energetic cell in the body, continuously contracting 3 billion times in the average human lifespan (Severs, 2000; Walker & Spinale, 1999). This leads to the pumping of 7,000 liters of blood per day along 100,000 miles of blood vessels (Severs, 2000). This next section will highlight the structural components of the cardiomyocyte and their function during cardiac contraction.

Basement Membrane

The basement membrane covers the outermost portion of the cardiac myocyte, forming a boundary between the extracellular and intracellular space. The primary constituents of the basement membrane include type IV collagen,

two glycoproteins known as laminin and fibronectin, as well as proteoglycans (Walker & Spinale, 1999). The basement membrane of the cardiomyocyte forms an interface with the extracellular space with anchoring fibers that adhere the basal lamina to collagen (Walker & Spinale, 1999). The primary function of the basement membrane is to form barrier between the extracellular space and the cardiac myocyte, influencing the exchange of macromolecules between them. The basement membrane also serves as an interface for myocyte continuity with the extracellular matrix (Walker & Spinale, 1999).

Sarcolemma

Within cardiomyocytes, the sarcolemma is formed from a melding of the plasma membrane and the basement membrane, allowing the sarcolemma to interact with both the extracellular and intracellular environment (Walker & Spinale, 1999). The sarcolemma is composed of a lipid bilayer, having a hydrophobic core. Along with receptor membrane proteins, integrins, which are attached to the intracellular side of the sarcolemma, adhere the cardiac myocyte to the extracellular matrix and basement membrane forming a collagen-integrin-cytoskeletal relation that may be essential for the transduction of cell shortening and ejection of blood from the ventricle (Hsueh, Law, & Do, 1998; Walker & Spinale, 1999).

Formed by the sarcolemma are intercalated disks and transverse tubules, or T tubules. Intercalated disks serve to conduct the action potential (discussed below) between myocytes and to provide a mechanical linkage between

myocytes (Walker & Spinale, 1999). T tubules are invaginations of the sarcolemma that contain and bring a high proportion of L-type Ca^{2+} channels in the proximity of the SR near Ca^{2+} release channels in the SR. As such, T tubules are a critical component in excitation-contraction coupling. The primary function of the sarcolemma is to provide a barrier for diffusion. Although, the sarcolemma also contains receptors, pumps, and channels that are essential to cardiomyocyte contraction (Walker & Spinale, 1999).

Sarcolemmal Pumps and Ion Channels

In accordance with the review on the structure and function of the cardiac myocyte by Walker and Spinale (Walker & Spinale, 1999), describing the pumps and channels of the cardiac myocyte sarcolemma is most understandable in the context of the phases of the action potential (**Figure 4**). Phase 4 of the action potential is referred to as the resting membrane potential, which is sustained by an inward potassium (K^+) rectifier and the sodium (Na^+)/K^+ adenosinetriphosphatase (ATPase), the Na^+/Ca^{2+} exchanger, and the sarcolemmal Ca^{2+} ATPase (**Figure 5**). As the sarcolemma is only permeable to K^+ during this time, the K^+ equilibrium potential is responsible for the resting membrane potential of the myocyte. In general, the K^+ rectifier brings K^+ into the myocyte, the Na^+/K^+ extrudes three Na^+ for two K^+ ions, and the Na^+/Ca^{2+} exchanger and sarcolemmal Ca^{2+} ATPase extrude Ca^{2+} from the myocyte (**Figure 5**) (Walker & Spinale, 1999). Although, the Na^+/Ca^{2+} exchanger is bidirectional and is the primary system leading to Ca^{2+} efflux from the myocyte.
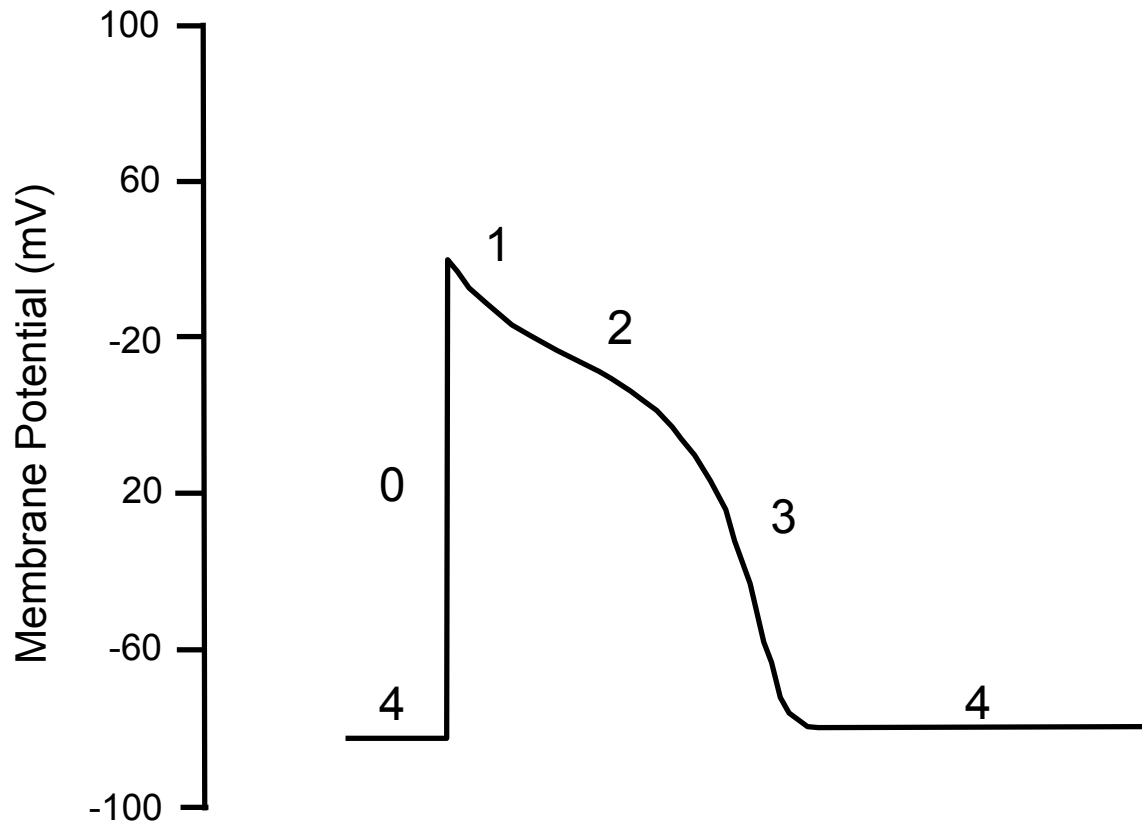
Figure 4. The Phases of the Ventricular Myocyte Action Potential. The action potential is generated from sarcolemmal protein interactions and consists of 5 phases. Phase 0 of the action potential is depicted as an upstroke to represent rapid cellular depolarization, which is followed by a brief early repolarization in Phase 1. During Phase 2, the action potential plateaus and then rapidly repolarizes in Phase 3. Phase 4 depicts the resting membrane potential.
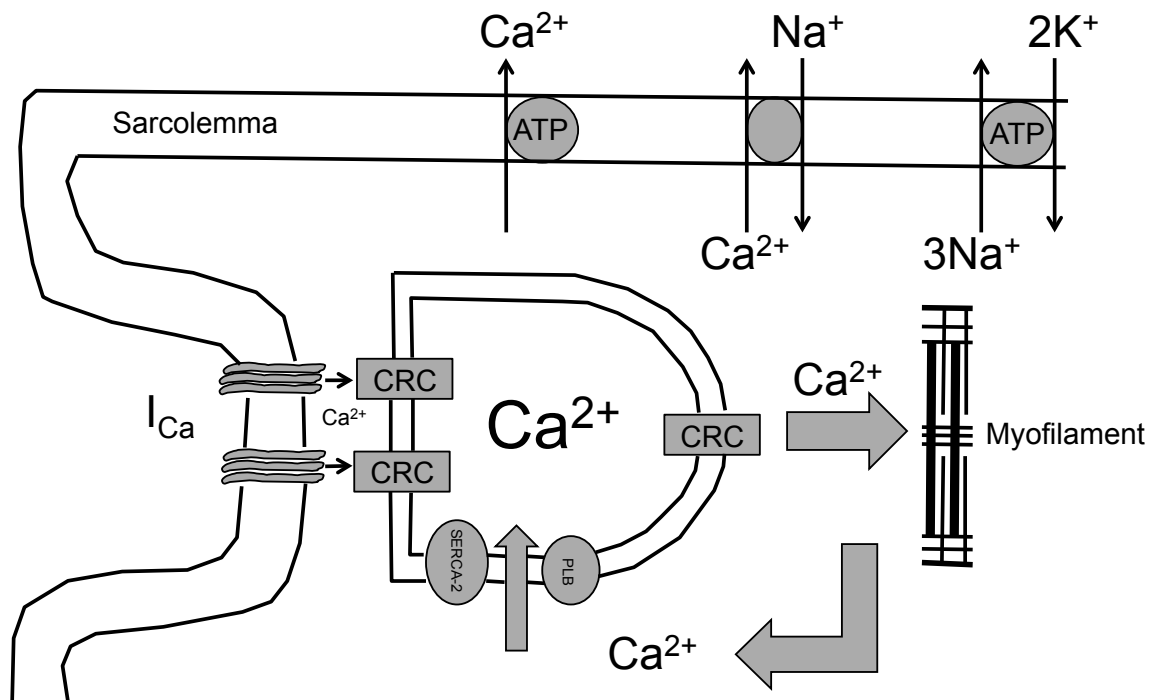
Figure 5. Excitation-Contraction Coupling in the Cardiac Myocyte. Ca^{2+} is removed from the cardiomyocyte by the Na^+/Ca^{2+} exchanger and the Ca^{2+}-ATPase located in the sarcolemma. The release of Na^+ extracellularly by the Na^+/K^+ ATPase contributes to the resting membrane potential. The Na^+/Ca^{2+} exchanger is reversible. Upon myocyte depolarization, L-type Ca^{2+} channels are activated resulting in Ca^{2+} influx into the cardiac myocyte (I_{CA}). This Ca^{2+} activates Ca^{2+} release channels on the sarcoplasmic reticulum. The subsequently released Ca^{2+} triggers myocyte contraction through actin-myosin cross-bridge formation. Cross-bridges are disengaged by the removal of Ca^{2+} from the cytosol by the actions of SERCA-2, the Na^+/Ca^{2+} exchanger, and the sarcolemmal Ca^{2+} ATPase.

Phase 0 of the action potential is due to activation of the fast Na^+ channel, which allows Na^+ to flow into the myocyte along electrical and chemical concentration gradients. Early repolarization of the myocyte is due to rapid inactivation of the Na^+ channels and activation of two outward currents. The movement of chloride (Cl^-) ions down their electrical and chemical gradient allows chloride into the cell and, also, the efflux of K^+ down its electrochemical gradient. Together, these events give rise to the brief, small repolarization of the membrane potential during phase 1 of the action potential (Walker & Spinale, 1999).

Phase 2 of the cardiac action potential represents a plateau caused by the influx of Ca^{2+} through L-type Ca^{2+} channels and an efflux of K^+ through the K^+ rectifier, a process that occurs during phase 0 and peaks during phase 2 (Balke & Shorofsky, 1998; Mukherjee & Spinale, 1998; Walker & Spinale, 1999). Phase 3 depicts myocyte repolarization due to increased K^+ conductance through the delayed rectifier K^+ channels that are activated at the end of the plateau phase. During this time, all other currents, as well as Na^+ and Ca^{2+} movement are inactivated allowing for the membrane potential to be restored to the resting state (phase 4).

Sarcolemmal Receptor Systems

Within the cardiac myocyte, muscarinic, alpha (α), endothelin, and β-adrenergic receptor systems are present (Walker & Spinale, 1999). Of particular importance, the β-adrenergic receptor system is a common clinical target. The β-

adrenergic receptor exists in either activated or inactivated states with the inactive state dominating at equilibrium (Johnson, 1998; Walker & Spinale, 1999). Both catecholamines and synthetic β-adrenergic agonists bind this receptor leading to its conformational change and activation of a guanine nucleotide-dependent coupling protein. Subsequently, adenylate cyclase is stimulated and cyclic adenine monophosphate production is elevated, which activates the catalytic subunits of protein kinase A (PKA). PKA activation leads to phosphorylation of specific targets within the myocyte, including the sarcolemmal L-type Ca^{2+} channel, phospholamban (PLN), troponin I (TnI), along with other proteins, altering their activity (Walker & Spinale, 1999).

Myocyte Cytoskeleton

The myocyte cytoskeleton is a vital interface between the contractile apparatus and the extracellular environment and may alter the form and function of the myocyte. Cytoskeletal proteins include α-actinin, talin, and desmin, which meet where integrins enter the cytosol of the myocyte. Importantly, phosphorylation of these proteins may change cellular conformation and, thereby, function. Furthermore, the giant protein titin gives the myocyte viscoelastic properties that may inhibit hyperstretching of the myocyte (Horowits, Kempner, Bisher, & Podolsky, 1986; Morano et al., 1994; Walker & Spinale, 1999). Tubulins, which include α- and β-tubulin are also important cytoskeletal proteins that are involved in assembly of the myocyte and transduction of mechanical signals to the nuclear envelope and may influence myocyte

contractility (Walker & Spinale, 1999).

Sarcoplasmic reticulum

Located within the SR membrane, the sarco/endoplasmic reticulum Ca^{2+} transport ATPase (SERCA-2) regulates Ca^{2+} accumulation within the myocyte. Along with the Na^+/Ca^{2+} exchanger and sarcolemmal Ca^{2+} ATPase, SERCA-2 plays an important role in the uptake of cytosolic Ca^{2+} in the contraction cycle allowing for cytosolic Ca^{2+} concentrations to change more than 100-fold during the excitation-contraction coupling process (discussed below) (Walker & Spinale, 1999). SERCA-2 transports 2 moles of Ca^{2+} into the SR for every 1 mole of ATP hydrolyzed (Barry & Bridge, 1993; Walker & Spinale, 1999). While SR Ca^{2+} uptake is mediated by SERCA-2, SERCA-2 activity is reversibly regulated by PLN (Kranias & Hajjar, 2012). As a generalization, in the dephosphorylated state, PLN inhibits SERCA-2 activity (Kranias & Hajjar, 2012). When phosphorylated, PLN relieves this inhibition on SERCA-2 activity (Kranias & Hajjar, 2012). As such, the phosphorylation status of PLN is crucial to the rate and extent of Ca^{2+} removal from the cytosol, thereby regulating the process of excitation-contraction coupling.

Located at the interface between the SR and the T tubules are the calcium release channels known as the ryanodine receptors (RYRs) (Lanner, Georgiou, Joshi, & Hamilton, 2010). RYRs are responsible for Ca^{2+} release from the SR store and are highly sensitive to changes in cytosolic Ca^{2+} (Lanner et al., 2010; Walker & Spinale, 1999). A small, rapid influx of Ca^{2+} through L-type Ca^{2+}

channels causes a rapid, large release of Ca^{2+} into the myocyte cytosolic space (**Figure 5**) (Walker & Spinale, 1999). This process triggers the contractile apparatus within the myocyte leading to cellular contraction (Lanner et al., 2010; Walker & Spinale, 1999).

Contractile Apparatus

The central focus of my dissertation work has been the mechanical processes underlying the function of the contractile apparatus of the cardiac myocyte. Within the cardiac myocyte, the sarcomere is the basic unit of contraction and is composed of interdigitating thick and thin filaments (**Figure 6**). The thick filament includes titin and myosin while the thin filament includes actin, the troponins, and α-tropomyosin (α-TM). The cardiac sarcomere consists of distinct regions and is defined as the segment between two neighboring Z-lines. In electron micrographs of cross-striated muscle, the Z-line appears as a series of dark lines. Surrounding the Z-line is the I-band (for isotropic), which contains only the thin filaments with no thick filament superimposition. Next is the A-band (for anisotropic), which contains the entire length of a single myosin thick filament, as well as thin filament proteins. Within the I-band is a region referred to as the H-zone, which contains the thick myosin filaments that are not superimposed by thin filaments. Finally, within the H-zone is a thin M-line, which is formed from cross-connecting constituents of the cytoskeleton.
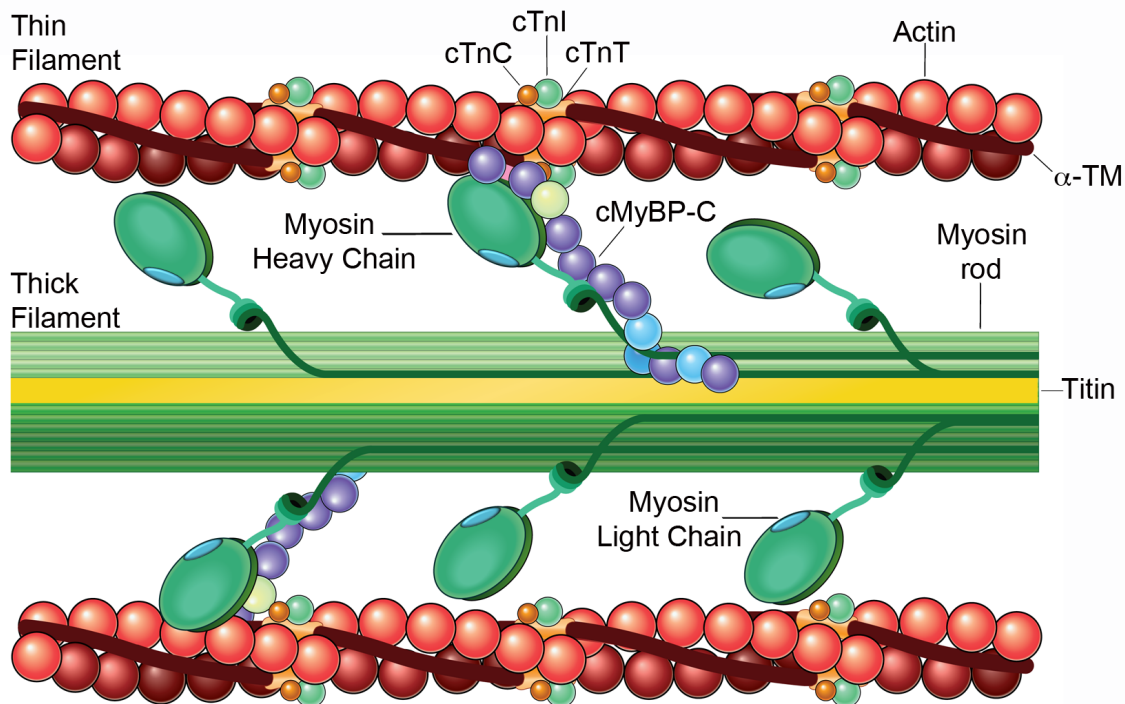
Figure 6. The Structure of the Cardiac Sarcomere. The cardiac sarcomere consists of the thick-filament proteins myosin and titin and the thin filament proteins actin, α-TM, and troponins I, C, and T. cMyBP-C is a sarcomeric protein that participates in stabilizing sarcomere structure and regulating the kinetics of cross-bridge cycling by controlling the interaction between actin and myosin filaments. Figure from (T. L. Lynch & Sadayappan, 2014). Copyright Wiley-VCH Verlag GmbH & Co. KGaA. Reproduced with permission.

Important to my dissertation work, localized within the cardiac sarcomere in a region referred to as the C-zone that is set within the A-band is the contractile regulatory protein cMyBP-C. cMyBP-C regulates actomyosin interactions and the kinetics of cross-bridge cycling in a phosphorylation dependent manner (Barefield & Sadayappan, 2010; T. L. Lynch IV et al., 2015), which will be discussed later in detail. The resting length of the cardiomyocyte has been shown to be in the range of 1.8 to 2.4 micrometers (μm). The elevation of intracellular Ca^{2+} levels within the myocyte triggers interactions between thick and thin filament proteins leading to ATP hydrolysis and the development of cellular tension (Walker & Spinale, 1999).

Myosin consists of a globular head and a filamentous tail. The globular head is the site of ATPase activity and contains the actin binding sites. Within the thin filament, actin is the primary contractile protein that comes in two forms, G- and F-actin. F-actin composes the backbone of the thin filament while G-actin provides stability (Walker & Spinale, 1999) and contains two myosin-binding sites. In the presence of ATP, myocyte contraction is orchestrated by the interaction between the globular myosin heads and the G-actin monomer in the presence of ATP. This results in cross-bridge formation and shortening of the sarcomere. α-TM, another thin filament protein, lies on either side of actin and provides rigidity to the thin filament while also blocking the myosin binding sites on actin. The troponin complex consists of cardiac troponin C (TnC), troponin T (TnT), and TnI. While also providing structural integrity to the sarcomere, the

troponins are crucial regulators of cross-bridge formation. By binding to α-TM, TnT anchors the troponin complex to the thin filament. When phosphorylated, TnI weakens the affinity of Ca^{2+} for TnC and thereby inhibits the binding of myosin to actin by preventing the shift of the troponin complex and α-TM off of the myosin binding sites on actin (Walker & Spinale, 1999). However, when Ca^{2+} binds to TnC, a conformational change occurs leading to dislocation of the troponin complex and α-TM from the myosin binding sites on actin leading to actin-myosin interactions, cross-bridge formation, and sarcomere contraction.

Mitochondria

As contraction of the myocyte is an ATP dependent process, the cardiac myocyte is rich in mitochondria to maintain high ATP stores. Within the myocyte, the mitochondria comprise approximately 40% of the cell volume (Walker & Spinale, 1999), underscoring the enormous demand for energy required by the myocyte. Within the myocyte, the high concentrations of phosphocreatine, which are higher than the levels of adenosine diphosphate (ADP), serve as the primary source of high-energy phosphate transfer between the mitochondria and cytosol (Walker & Spinale, 1999). The high-energy phosphate of ATP is transferred to phosphocreatine, which is reconverted into ATP for use in cellular processes including excitation-contraction coupling (discussed below). An additional role of mitochondria within the cardiac myocyte is to take up and buffer large quantities of cytosolic Ca^{2+}, thereby protecting the myocyte from Ca^{2+} overload (Walker & Spinale, 1999).

Excitation-Contraction Coupling

By definition, excitation-contraction coupling is the process by which action potentials generate contraction of the myocyte, thereby linking electrical excitation to contraction (**Figure 5**) (Pinnell, 2007; Walker & Spinale, 1999). Excitation-contraction coupling is produced through the fluctuation of intracellular Ca^{2+} from 100 nanomolar (nM) to 10 micromolar (μM). As described earlier, action potential propagation through the T tubule system of the myocyte activates voltage-sensitive L-type Ca^{2+} channels and triggers Ca^{2+} conductance from the extracellular space into the cytosol (Balke & Shorofsky, 1998; Mukherjee & Spinale, 1998; Walker & Spinale, 1999). However, because the quantity of Ca^{2+} entering into the cell through L-type Ca^{2+} channels is so small compared to Ca^{2+} release from the SR, this "trigger" Ca^{2+} does not contribute substantially to cross-bridge formation and contraction (Walker & Spinale, 1999). Furthermore, it is this influx of extracellular Ca^{2+} that triggers further Ca^{2+} release from the SR via RyRs in a process known as Ca^{2+}-induced Ca^{2+} release (CICR) (Pinnell, 2007).

As described earlier, Ca^{2+} release from the SR initiates a series of interactions within the sarcomere, best explained by the sliding filament theory. Under conditions of low intracellular Ca^{2+}, phosphorylated TnI decreases the affinity of cytosolic Ca^{2+} for TnC, allowing for the strong interaction between TnI and actin. Under these conditions, the troponin-tropomyosin complex blocks the myosin binding sites on actin. As intracellular Ca^{2+} is increased, Ca^{2+} binds to TnC, shifting TnI affinity from actin to TnC and promoting movement of the

troponin-tropomyosin complex off of the myosin binding sites on actin. When the myosin head is bound to ATP it forms a low energy configuration not bound to actin. When the myosin head hydrolyzes ATP to ADP and inorganic phosphate, it forms a high-energy configuration and binds to actin forming a cross-bridge. The myosin head then releases ADP and inorganic phosphate, returning to its low-energy configuration and moving the thin filament 10 nanometers (nm) relative to the thick filament (Walker & Spinale, 1999) towards the center of the sarcomere. This is known as the power-stroke. Finally, binding of a new molecule of ATP releases the cross-bridge and allows for formation of a new one, repeating the cycle. The contraction process is dynamic and depends upon the number of cross-bridges formed, the duration of the action potential, the Ca^{2+} levels in the cytosol, and ATP stores. Additionally, the strength of contraction can be altered by increasing the amount of free Ca^{2+} or by altering myofilament sensitivity to Ca^{2+} (Pinnell, 2007). The latter occurs during stretching of the myocyte and is responsible for the Frank-Starling mechanism discussed earlier. Cross-bridge cycling will occur until Ca^{2+} is removed from the cytosol by energy-dependent mechanisms or by a reduction in ATP stores.

Active relaxation of the myocyte depends upon SERCA-2, which is regulated by PLN. As discussed above, every mole of ATP that is hydrolyzed corresponds to two moles of Ca^{2+} being transported back into the SR. Other mechanisms contributing to Ca^{2+} removal include the Na^+/Ca^{2+} exchanger, the sarcolemmal Ca^{2+} ATPase, as well as Ca^{2+} binding proteins such as calmodulin

and calsequestrin (Walker & Spinale, 1999). Importantly, variations in active relaxation during the excitation-contraction process will alter diastolic performance of the myocyte.

Myocyte Contraction

Myocyte contraction is the dénouement of successful action potential transduction and Ca^{2+} release into the cytosol. In basic research, over the past two decades, technological advancements have made it possible to study cardiac contraction from the level of the whole heart using *in vivo* echocardiography imaging on live animals to *in vitro* studies at the level of the single isolated myocyte. By studying the single myocyte, one is able to examine and modulate sarcolemmal receptor systems and contractile performance in the absence of loading conditions and neurohormonal activity (Walker & Spinale, 1999). A prominent example has been the alteration of the β-adrenergic receptor system. Incredibly, we are now able to even isolate electrically responsive myocytes from myocardial biopsies and measure contractile performance. Such techniques provide basic research scientists the ability to test the mechanisms regulating excitation-contraction coupling in health and disease, leading to a better understanding of the biophysics and mechanics of muscle contraction.

In addition to studying the single isolated myocyte, the mechanics of cardiac myocyte contraction can also be studied using an isolated muscle strip. During my dissertation studies, I used isolated mouse papillary muscle fibers to determine mechanical differences between healthy and HF hearts. The papillary

muscle is convenient for such studies as the fibers within this muscle run in approximately the same direction (Pinnell, 2007). In one type of assay, the muscle is anchored at both ends and placed under an initial tension (preload). As the initial length of the fiber is increased, mimicking alterations in preload, so too is the tension generated during isometric contraction. This leads to an elevation in the force of contraction and SV, which produces the familiar Starling curve. This is explained by the notion that the overlap of actin and myosin under resting conditions is not optimal, which is improved by increasing length of the muscle (sarcomere). The result is an augmentation of actin and myosin overlap and the amount of tension that is produced. However, under physiological conditions, this mechanism has been shown to not account for the shape of the Starling curve possibly indicating other processes such as stretch-induced sensitivity increases in troponin for Ca^{2+} (length-dependent Ca^{2+} sensitivity) and the enhancement of intracellular free Ca^{2+} (Pinnell, 2007).

Isotonic contraction of a muscle refers to shortening of a muscle against a load. In this situation, the muscle maintains the same tension but shortens/changes length. Afterload is represented by the amount of weight moved by the muscle. Throughout contraction, if force is maintained constant, one can measure both the change in muscle length and force with respect to time. Increasing afterload decreases the amount and velocity of shortening, and vice versa. Importantly, if the muscle is stretched to increase preload, an increase in velocity and shortening will be observed at a particular level of

afterload. In contrast to isotonic contraction, as indicated above, isometric contraction refers to a situation in which the muscle changes or develops tension without shortening/changing length. This is the type of contraction used in my fiber studies. *In vivo*, during the cardiac contraction cycle, isometric contraction occurs when both the AV and seminlunar valves are closed. Although tension develops, blood is not ejected from the ventricle, as muscle fiber shortening is absent. Once the semilunar valves open, the contraction becomes isotonic and tension is maintained. At this point, blood is ejected and isotonic shortening occurs (Pinnell, 2007).

The Frank-Starling Relationship

As discussed earlier, the Frank-Starling relationship refers to the process by which increasing muscle length (or ventricular volume) leads to enhanced contractile performance during the subsequent contraction (Moss & Fitzsimons, 2002). Thus, increased venous return to the ventricles leads to a greater SV and increased blood volume ejection from the heart. The cellular basis of the Frank-Starling relationship is not well understood (Moss & Fitzsimons, 2002). As mentioned above, a common thought for the mechanism underlying the Frank-Starling relationship is that increasing sarcomere length reduces the lateral spacing between thick and thin filaments leading to increased cross-bridge interaction and increased contractile force. Interestingly, in permeabilized myocardium held at a constant length, osmotic compression can increase force at every Ca^{2+} concentration indicating that the same Ca^{2+} sensitivity of force

observed at long lengths can be achieved at short sarcomere lengths by reducing fiber diameter (Moss & Fitzsimons, 2002). Furthermore, osmotic compression can eliminate the length dependence of Ca^{2+} sensitivity (McDonald & Moss, 1995; Moss & Fitzsimons, 2002). Therefore, lattice filament spacing is a key contributor to the Frank-Starling relationship. This was elegantly shown by Konhilas *et al.* who used X-ray diffraction to quantify lateral spacing of thin and thick filaments in cardiac muscles while also measuring force and length (Konhilas, Irving, & de Tombe, 2002). In this study, the authors reported a decrease in filament lattice spacing upon stretching of the muscle or osmotic compression with dextran (Konhilas et al., 2002). Dextran reduced the stretch-dependent decrease in filament lattice spacing but did not alter the length dependence of Ca^{2+} sensitivity of force. Also, osmotic compression mimicking lattice spacing of longer sarcomere lengths did not alter Ca^{2+} sensitivity of force. Primarily, the authors suggested that compression of lattice spacing at short sarcomere lengths to mimic the spacing observed at long lengths does not mirror the increased Ca^{2+} sensitivity seen at longer lengths (Konhilas et al., 2002; Moss & Fitzsimons, 2002). This data contrasted to many findings that have only mimicked length-dependent changes in Ca^{2+} sensitivity by altering fiber diameter, besides altering muscle length (Fuchs & Smith, 2001; Fuchs & Wang, 1996; McDonald & Moss, 1995; Moss & Fitzsimons, 2002). As such, Konhilas *et al.* proposed that the effect of myofilament lattice spacing on myofilament Ca^{2+} sensitivity is variable and depends upon the extent of compression of the lattice

(Konhilas et al., 2002). Indeed, it has been suggested that cross-bridge formation increases the affinity of Ca^{2+} for TnC (Hofmann & Fuchs, 1988; Moss & Fitzsimons, 2002). However, this is a chicken-and-egg situation. Does, increased Ca^{2+} binding result from cross-bridge binding or does increased Ca^{2+} binding promote additional cross-bridge binding to the thin filament and increased force? Another variable may include the effect of stretch on thick filament structure or strain of the elastic protein titin such that reducing strain diminishes the length dependence of Ca^{2+} sensitivity of force in the heart (Cazorla, Vassort, Garnier, & Le Guennec, 1999; Cazorla, Wu, Irving, & Granzier, 2001; Fukuda, Sasaki, Ishiwata, & Kurihara, 2001; Moss & Fitzsimons, 2002). Furthermore, length-dependent changes in cooperative processes in the myocardium that modulates activation may contribute to the effect of myofilament lattice spacing on myofilament Ca^{2+} sensitivity (Moss & Fitzsimons, 2002).

Cooperation in cross-bridge binding is the process in which the initial recruitment of cross-bridge binding facilitates further binding, which leads to increases in force at any given Ca^{2+} concentration. Stated differently, cooperative recruitment of cross-bridges to the thin filament is triggered by binding of Ca^{2+} to TnC followed by the spread of cross-bridge binding away from the Ca^{2+} bound TnC, leading to increases in force at any given Ca^{2+} concentration. At low Ca^{2+} concentrations, this mechanism would predominate, as few TnC's would have Ca^{2+} bound leaving many extended regions of the thin filament available for cooperative activation (Moss et al., 2015). However, at saturating concentrations

of Ca^{2+}, this mechanism would not predominate, as the thin filament would be fully activated with no regions available for recruitment of cross-bridges (Moss et al., 2015). Therefore, any changes in force observed would be largely due to increases in Ca^{2+} concentration and the kinetics of force development would approach the fundamental rate of cross-bridge cycling (Moss et al., 2015). Relating back to the Frank-Starling mechanism, at long sarcomere lengths, increased cooperativity could result from increased probabilities of initial cross-bridges binding to actin due to decreased lattice spacing. Importantly, the contractile regulatory protein cMyBP-C has also been suggested to play an important role in cooperative cross-bridge recruitment to the thin filament, as discussed below.

Cardiac Myosin Binding Protein-C

Central to my dissertation has been studying the necessity of the N' region of cMyBP-C in maintaining normal cardiac function *in vivo*. Currently, studying the function of cMyBP-C in health and disease is the focus of many labs worldwide given its important role in regulating actomyosin interactions and the kinetics of cross-bridge cycling and high mutation rate in human cardiomyopathy. While this protein has been well studied since its initial discovery and while researchers are coming ever closer to definitively defining its true function and mechanism of action in the cardiac sarcomere, the exact role and mechanisms by which cMyBP-C regulates cardiac contraction remain incompletely understood. As such, the results of my dissertation work have provided direct

evidence for the importance of this protein in maintaining normal cardiac function *in vivo* and have, hopefully, provided a better understanding of the mechanistic function of cMyBP-C in both health and disease, as discussed below. In the next section, I will describe the discovery of cMyBP-C, its structure and localization within the cardiac sarcomere, the current understanding of its role in health and disease, and, finally, the discovery and importance of a specific N' region of cMyBP-C that is the focus of my dissertation work.

Discovery, Isoforms, and Localization of cMyBP-C

Between 1971 and 1973, Offer, Moos, and Starr discovered MyBP-C in mammalian skeletal muscle as an impurity of isolated myosin (Offer et al., 1973; Starr & Offer, 1971). Starr and Offer were the first to separate several unidentified myosin-associated proteins using sodium dodecyl sulfate (SDS) polyacrylamide gel electrophoresis (PAGE) (Ackermann & Kontrogianni-Konstantopoulos, 2010; Starr & Offer, 1971). MyBP-C was originally referred to as C-protein due to its localization on SDS-PAGE as band *C* and was later characterized as an approximately 1270 amino acid (mice) 140 kDa (runs at 150 kDa on SDS-PAGE) myosin binding protein using several experimental techniques including gel filtration, ammonium sulfate fractionation, and single molecule electron microscopy (Ackermann & Kontrogianni-Konstantopoulos, 2010; Hartzell & Sale, 1985; T. L. Lynch & Sadayappan, 2014; Offer et al., 1973; Starr & Offer, 1971).

The MyBP-C family consists of three isoforms including slow skeletal, fast

skeletal, and cardiac, which are encoded by the genes *MYBPC1*, *MYBPC2*, and *MYBPC3*, respectively, and which localize to chromosomes 12, 19, and 11, respectively (Ackermann & Kontrogianni-Konstantopoulos, 2010). The cloning and sequencing of these isoforms from various species including human, chicken, rabbit, and mouse indicated an approximately 65% sequence identity among the individual isoforms across species, with an approximately 50% homology shared among the human cardiac, slow, and fast forms of MyBP-C (Ackermann & Kontrogianni-Konstantopoulos, 2010; Furst, Vinkemeier, & Weber, 1992; Reinach, Masaki, & Fischman, 1983; F. E. Weber, Vaughan, Reinach, & Fischman, 1993; Yasuda, Koshida, Sato, & Obinata, 1995). In mammals, cMyBP-C is expressed early in development along with titin and myosin (Ackermann & Kontrogianni-Konstantopoulos, 2010). However, the skeletal isoforms of MyBP-C are detectable only at later stages of development following the expression of titin and myosin with the slow isoform preceding the expression of the fast isoform (Ackermann & Kontrogianni-Konstantopoulos, 2010). The slow and fast MyBP-C isoforms can coexpress in the same muscle type and coexist in the same sarcomere (Ackermann & Kontrogianni-Konstantopoulos, 2010) with slow MyBP-C having been found to express in both slow and fast-type skeletal muscles and fast MyBP-C expression having been found to be largely restricted to fast skeletal muscles (Lin et al., 2013). Intriguingly, slow and fast MyBP-C expression was shown to be upregulated in myopathic skeletal muscles from *mdx* mice (Lin et al., 2013). Also, the expression of the fast isoform was

demonstrated to be elevated in cMyBP-C null hearts undergoing dilation (Lin et al., 2013). Moreover, expression of slow MyBP-C has been detected in the RA and the interatrial septum of the heart (Dhoot & Perry, 2005). The expression of the cardiac isoform of MyBP-C is restricted to the developing and mature heart (Ackermann & Kontrogianni-Konstantopoulos, 2010). However, in avian species, cMyBP-C is expressed transiently in some skeletal muscles during embryogenesis, but was shown to be dispensable for the development of mammalian skeletal muscle with no functional or structural consequences in adult myocytes from cMyBP-C deficient animals and dystrophic mice (Lin et al., 2013).

The implementation of X-ray diffraction and immunoelectron microscopy allowed for determination of the location of MyBP-C at striped intervals within the C-zone of the A-band of rabbit skeletal muscle (Craig & Offer, 1976). This finding further confirmed MyBP-C's association with myosin thick filaments. Later studies demonstrated that MyBP-C arranges in a doublet pattern along the length of the A-band on either side of the H-zone in 7-9 transverse stripes separated at approximately 43 nm, with approximately 2-4 molecules of MyBP-C associating with each myosin cross-bridge (Ackermann & Kontrogianni-Konstantopoulos, 2010; Bennett, Craig, Starr, & Offer, 1986; Pepe, 1975; Pepe, Ashton, Street, & Weisel, 1986; Rome, Offer, & Pepe, 1973). More recently, a similar striping pattern of the cardiac isoform of MyBP-C in cardiac muscles was shown (P. Luther et al., 2008). While myosin tails comprise the backbone of the thick

filament, their heads point outwards and may extend towards actin. The heads are arranged along three-stranded helices with three pairs of heads at each 14.3 nm layer and an axial repeat of 43 nm. The defined spacing of cMyBP-C stripes indicates that only every third level of myosin heads in the C-zone are associated with a molecule of cMyBP-C (Craig & Offer, 1976). As such, cMyBP-C is likely only activated during thick-thin filament interaction in the central part of the sarcomere during the contraction cycle when the myosin-actin interaction extends into the central region of the A-band (Barefield & Sadayappan, 2010).

In total, cMyBP-C comprises 2% of the contractile proteins within the heart and has been suggested to play a role in myofibril organization and assembly during myofibrillogenesis and muscle regeneration (Ehler, Rothen, Hammerle, Komiyama, & Perriard, 1999; Schultheiss et al., 1990). Of particular interest, mouse cardiomyocytes from hearts in which cMyBP-C was either knocked-out (-/-) (Harris et al., 2002) or ablated by C-terminal truncation (t/t) (McConnell et al., 1999) developed abnormal sarcomere structures with the absence of M-lines and modifications in thick filament size (Barefield & Sadayappan, 2010). Although these animals are viable, they develop severe cardiac remodeling and contractile dysfunction by 3 months of age demonstrating that while cMyBP-C is necessary for sarcomere organization and for proper contractile dysfunction, it is dispensable for sarcomere formation during embryogenesis (Barefield & Sadayappan, 2010). Importantly, cardiomyocytes from heterozygous mice with either cMyBP-C knockout (+/-) or C-terminal truncation (+/t) develop normal

sarcomeres and have normal contractile function, indicating haploinsufficiency resulting from a null allele is not sufficient to trigger cardiac remodeling (Barefield & Sadayappan, 2010).

Molecular Structure of cMyBP-C

Structurally, cMyBP-C contains eight immunoglobulin I-like domains, three fibronectin type III domains, a proline-alanine-rich region between domains C0 and C1, and a 100 residue long phosphorylatable M domain, also referred to as the MyBP-C motif (**Figure 7**) (T. L. Lynch & Sadayappan, 2014). While all three MyBP-C isoforms share a highly homologous modular architecture, specific to the cardiac isoform is an extra immunoglobulin domain at its N' region (C0), an LAGGGRRIS insertion in the M domain, and an insertion loop of 28 residues within the C5 domain (**Figure 7**) (Barefield & Sadayappan, 2010; Flashman, Redwood, Moolman-Smook, & Watkins, 2004). The M domain has a unique structure that has been suggested to have a more N' region that is flexible and mostly disordered and a C' region containing three α-helices in a three-helix bundle (Craig, Lee, Mun, Torre, & Luther, 2014). Most notably, the mouse cardiac isoform contains four phosphorylation sites at serine residues within the M domain at positions 273, 282, 302, and 307 corresponding to human residues 275, 284, 304, and 311 (Jia, Shaffer, Harris, & Leary, 2010), which are phosphorylated by PKA (Gautel, Zuffardi, Freiburg, & Labeit, 1995). As I have used mouse models during my dissertation studies, I will focus on the mouse
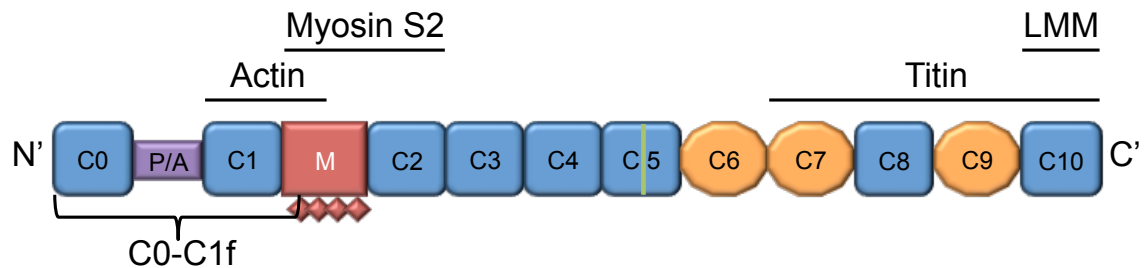
Figure 7. The Structure of Cardiac Myosin Binding Protein-C. cMyBP-C contains eight immunoglobulin I-like domains (blue), three fibronectin type III domains (orange), a proline-alanine-rich region between domains C0 and C1 (purple), and a 100 residue long phosphorylatable M domain (red), also referred to as the MyBP-C motif. Phosphorylation sites at serine residues 273, 282, 302, and 307 (mouse sequence) within the M domain are depicted as diamonds. Specific to the cardiac isoform of MyBP-C is an extra immunoglobulin domain at its N' region (C0), an LAGGGRRIS insertion in the M domain, and an insertion loop of 28 residues within the C5 domain (green line). Indicated at the N' region of cMyBP-C is the C0-C1f region (below), which contains domains C0 through C1 and the first 17 amino acid residues of the M domain. Relevant cMyBP-C protein interaction partners are indicated (above).

phosphorylation sites in the experiments presented here. In addition to PKA, additional kinases have been found to phosphorylate cMyBP-C at these and other sites within the protein. These kinases include calmodulin kinase II, protein kinase C, protein kinase D and the 90 kDa ribosomal S6 kinase (Bardswell, Cuello, Kentish, & Avkiran, 2012; Knoll, 2012; Kuster et al., 2012) (Pfuhl & Gautel, 2012). Recent evidence also established that glycogen synthase kinase 3 beta phosphorylates cMyBP-C in the proline-alanine-rich linker region on Ser-128 (Ser-133 in humans) (Kuster, Sequeira, et al., 2013). Importantly, during the development of HF, total phosphorylation of cMyBP-C has been shown to be decreased, with a major loss of tri-phosphorylated protein (Decker et al., 2005; Sadayappan et al., 2005). Furthermore, it has been shown that the reduction in cMyBP-C phosphorylation is accompanied by contractile dysfunction, reduced force generation, and increased cleavage of cMyBP-C (discussed below) (Decker et al., 2005; Sadayappan et al., 2006b). Clearly, phosphorylation of cMyBP-C is a critical regulator of its interactions and function within the cardiac sarcomere (Barefield & Sadayappan, 2010).

Physical Interactions and Function of cMyBP-C

An important feature to consider when elucidating the function of cMyBP-C is that this protein (and the skeletal isoforms) contains no enzymatic activity indicating that it must accomplish its biological function in the myocardium through its interaction with other molecules (**Figure 7**). cMyBP-C is not known to bind to Ca^{2+}, nucleic acids, or sugars (Pfuhl & Gautel, 2012). While it has been

shown to have a binding site for zinc in domain C1 (Ababou et al., 2008), this interaction is of low affinity and likely lacks physiological importance (Pfuhl & Gautel, 2012). As such, protein-protein interactions are likely the primary mechanism by which cMyBP-C functions. It is well established that the C' region of cMyBP-C interacts with the LMM region of myosin and with titin to position and intricately incorporate cMyBP-C into the thick filament and to anchor the thick filament (Freiburg & Gautel, 1996; Gilbert et al., 1999; Miyamoto et al., 1999; Okagaki et al., 1993; Pfuhl & Gautel, 2012). This interaction may stabilize and organize the thick filament, however, this has yet to be confirmed (Nyland et al., 2009). In stark contrast to cMyBP-C's C' region, the interactions, role, and necessity of the N-terminal (N') region of cMyBP-C remain incompletely understood (Pfuhl & Gautel, 2012). As such, understanding the necessity of the N' region of cMyBP-C in cardiac function has been the principal focus of my dissertation work.

Beginning with the interactions of cMyBP-C with the thick filament, following cMyBP-C's discovery, it was suggested that myosin contains at least two sites at which cMyBP-C may bind, one in the LMM region and one in the S2 region (Starr & Offer, 1978). Myosin is a hexameric protein containing two heavy chains (MHC) and two light chains (regulator and essential light chain, RLC and ELC, respectively) (Ackermann & Kontrogianni-Konstantopoulos, 2011). The rod (LMM region) of myosin is comprised of a coiled-coil helix that, towards its N' region, unwinds at each MHC producing a catalytic head, the subfragment 1 (S1) region.

The S1 region of myosin has ATPase activity and is involved in the formation of cross-bridges with actin (Ackermann & Kontrogianni-Konstantopoulos, 2011; Rayment, Rypniewski, et al., 1993; Woodhead et al., 2005). The lever arm, or S2 region of myosin divides the S1 region from the rod portion of myosin and transduces the chemical energy produced from ATP hydrolysis into mechanical movement of myosin along the thin filament (Rayment, Holden, et al., 1993). Bound to the S1 region is RLC and ELC, which regulate the speed and force of contraction (Colson et al., 2010; Morano, 1999). Intriguingly, cMyBP-C has been shown to interact at its C0 domain with RLC (Ratti, Rostkova, Gautel, & Pfuhl, 2011). More recently, the S2 binding site for cMyBP-C was mapped to the vicinity of the S1-S2 junction on myosin and to the N' cardiac C1C2 fragment (Ababou, Gautel, & Pfuhl, 2007; Ababou et al., 2008; Gruen & Gautel, 1999). Importantly, the M and C2 domains have been shown to bind directly to the first 126 residues of the S2 fragment (Ababou et al., 2007; Gruen & Gautel, 1999) while the C1 domain binds the hinge region between the S1 heads and S2 fragment (Ababou et al., 2008). Critical to cMyBP-C's regulation of actomyosin interactions, it has been extensively reported that phosphorylation of serines 273, 282, and 302 (and more recently 307) within the M domain of cMyBP-C by PKA following β-adrenergic receptor activation abolishes the interaction of the M domain with myosin's S2 region (Gruen, Prinz, & Gautel, 1999; Sadayappan et al., 2009; Sadayappan et al., 2005; Sadayappan et al., 2006a). In studies of intact myocardium in mouse models, PKA phosphorylation of cMyBP-C led to an

increase in cross-bridge turnover rate and accelerated the rise of force development under submaximal Ca^{2+} activation but had no effect on the kinetics of force development at saturating Ca^{2+} concentrations (Barefield & Sadayappan, 2010; Stelzer, Patel, Walker, & Moss, 2007). This supports the observation that cMyBP-C functionally interacts with myosin's S2 region to affect contractile function (Barefield & Sadayappan, 2010; Stelzer et al., 2007). Furthermore, phosphorylation has been proposed to cause rearrangement of the structure of the M-domain and may expose additional serine residues for phosphorylation by kinases, establishing a hierarchy of phosphorylation (Bezold, Shaffer, Khosa, Hoye, & Harris, 2013; Karsai, Kellermayer, & Harris, 2013; Previs et al., 2012; A. Weith et al., 2012). Recently, Moss *et al*. have proposed a mechanism by which cMyBP-C phosphorylation modulates the cooperative recruitment of cross-bridges (discussed above) to regulate contraction and speed the rate of force development (Moss et al., 2015). In their model, Moss *et al.* suggest that cMyBP-C is able to slow the cooperative recruitment of cross-bridges by placing a physical restraint on myosin leading to a reduction in myosin binding to actin and slowing the cooperative spread of cross-bridge binding. However, when phosphorylated, cMyBP-C relieves its constraint on myosin increasing the probability of myosin binding to actin or of its own binding to the thin filament (discussed below) (Moss et al., 2015). This would then increase the activation state of the thin filament and accelerate cross-bridge binding while augmenting the rate of force development (Moss et al., 2015). The variable phosphorylation

of cMyBP-C in mono-, di- and tri-phosphorylated forms has been shown to correlate with the rate of movement of labeled thin filaments over bound myosin in motility assays such that increased phosphorylation led to increased rate of movement (A. E. Weith et al., 2012). This implies that the actions of cMyBP-C can be modulated based upon degree of phosphorylation rather than a complete on/off mechanism (Moss et al., 2015). Remarkably, during the development of HF, total phosphorylation of cMyBP-C is decreased, with a major loss of tri-phosphorylated protein (Decker et al., 2005; Sadayappan et al., 2005). Intriguingly, reduced phosphorylation of cMyBP-C is accompanied by contractile dysfunction, reduced force generation, and increased cleavage of cMyBP-C (Decker et al., 2005; Sadayappan et al., 2006b). Therefore, in my dissertation work, I have examined the phosphorylation status of cMyBP-C in a novel mouse model that lacks the C0-C1f region of cMyBP-C in the heart and develops HF (discussed below). While it is evident that total phosphorylation of cMyBP-C by PKA alters the orientation of the thick filament (discussed below) and myosin kinetics, how the phosphorylation of cMyBP-C coordinates with phosphorylation of thin filament proteins leading to the regulation of Ca^{2+} sensitivity requires further elucidation (Barefield & Sadayappan, 2010).

As indicated previously, cMyBP-C interacts at its C10 domain with myosin's LMM region (Flashman, Watkins, & Redwood, 2007; Miyamoto et al., 1999). Furthermore, domains C8-C10 have been shown to bind with titin, which is also tightly bound to the thick myosin filament (Kontrogianni-Konstantopoulos,

Ackermann, Bowman, Yap, & Bloch, 2009). Interestingly, it was demonstrated that cMyBP-C binds to the first immunoglobulin domain of an 11-domain super-repeat in the A-band portion of titin, thereby contributing to cMyBP-C's periodicity within the C-zone (Freiburg & Gautel, 1996). While the C' region of cMyBP-C may interact with the rod domain of myosin contributing to stability of the thick filament, it is the binding of the N' region of cMyBP-C that regulates contraction (Flashman et al., 2004; Oakley, Chamoun, Brown, & Hambly, 2007). Indeed, considering both of these interactions, determining the consequences of cMyBP-C ablation in the heart is a relevant question. As such, two mouse models were developed to examine the effect of the absence of cMyBP-C on cardiac function (Harris et al., 2002; McConnell et al., 1999). While the t/t mouse model generated by McConnell *et al.* displayed a null cMyBP-C background and developed cardiac hypertrophy and contractile dysfunction while remaining viable, this model was not a genetic model of cMyBP-C ablation as it expressed detectable levels of the cMyBP-C protein (McConnell et al., 1999; Sadayappan & de Tombe, 2012). Therefore, to test the hypothesis that cMyBP-C is essential for sarcomere assembly, structure, and function, a cMyBP-C knockout mouse model was generated in which exons 3-10 of *MYBPC3* were replaced with a gene encoding *neomycin* resistance (Harris et al., 2002). Accordingly, there was no detectable cDNA and protein for cMyBP-C in these animals. cMyBP-C knockout animals developed cardiac hypertrophy and reduced diastolic and systolic function but were viable (Harris et al., 2002). These data suggest that while cMyBP-C is not

necessary for cardiac development, it is essential for normal contractile function. *In vitro* studies on myocytes and tissue from cMyBP-C knockout hearts demonstrated their reduction in myofilament Ca^{2+} sensitivity of tension (Harris et al., 2002), deficit in diastolic relaxation and increased LA myofilament Ca^{2+} sensitivity (Pohlmann et al., 2007), acceleration of stretch activation (Stelzer, Dunning, & Moss, 2006) and force development (Stelzer, Fitzsimons, & Moss, 2006), and loss of PKA mediated stretch activation (Stelzer, Patel, & Moss, 2006). Additionally, cMyBP-C knockout mice failed to compensate for increased load and demonstrated a significant reduction in systolic and diastolic function when challenged with pressure overload (Brickson et al., 2007). Finally, ablation of cMyBP-C led to radial displacement of myosin cross-bridges in cMyBP-C knockout myofibrils compared to wild-type controls (Colson, Bekyarova, Fitzsimons, Irving, & Moss, 2007). Together, these data suggest that cMyBP-C serves as a mechanical tether on myosin acting as a structural restraint on myosin heads and that phosphorylation or ablation of cMyBP-C releases this constraint resulting in the acceleration of myocardial force generation (Sadayappan & de Tombe, 2012).

From the current available data in the cMyBP-C field it is evident that through the interactions at its N' and C' regions, cMyBP-C appears to contribute to the structure of the cardiac sarcomere and the regulation of cross-bridge formation, thereby controlling the kinetics of contraction. Several models have been proposed to explain how cMyBP-C regulates the formation of actomyosin

cross-bridges. In terms of cMyBP-C's regulation of contraction, the "tether model" suggests that both of the myosin binding sites on cMyBP-C act together to limit the movement of the S1 head relative to LMM and actin, restricting the formation of actomyosin cross-bridges (Calaghan, Trinick, Knight, & White, 2000). In this model, PKA phosphorylation of serines 273, 282, and 302 within the M domain regulates the interaction between cMyBP-C and myosin (Ackermann & Kontrogianni-Konstantopoulos, 2011; Barefield & Sadayappan, 2010). The proposed mechanism is that when dephosphorylated, the N' region binds to myosin and limits its interaction with actin but when phosphorylated, this inhibition is relieved allowing myosin to interact with actin and form cross-bridges (Ackermann & Kontrogianni-Konstantopoulos, 2011). Generally, this model focuses on the dynamic and highly regulated interaction of cMyBP-C with both actin and myosin filaments. Regarding the topology of cMyBP-C within the sarcomere, two models have been proposed. The "collar model" suggests that a trimer of cMyBP-C molecules wraps around the rod domain of myosin (Ackermann & Kontrogianni-Konstantopoulos, 2011; Moolman-Smook et al., 2002) while the "axial model" proposes that the C' region of cMyBP-C runs along the length of the rod domain (Ackermann & Kontrogianni-Konstantopoulos, 2011; Squire et al., 2003). The collar model stipulates that cMyBP-C forms a dimer through C' interactions. Indeed, the interactions between domains C5 with C8 and C7 with C10 have been demonstrated (Flashman, Korkie, Watkins, Redwood, & Moolman-Smook, 2008; Moolman-Smook et al., 2002). However, X-

ray diffraction, computational modeling and electron microscopy with three-dimensional reconstructions of cardiac thick filaments supported the axial model and the notion that domains C8, C9, and C10 lay along the length of the myosin rod (Rome et al., 1973; Squire et al., 2003; Zoghbi, Woodhead, Moss, & Craig, 2008). However, the axial model does not refute the dimerization of cMyBP-C. Regardless of the model, it still stands that the N' region of cMyBP-C extends into the interfilament space where it binds the S2 portion of myosin and, possibly, actin (discussed below). As cMyBP-C is approximately 40 nm in length (Hartzell & Sale, 1985), it is capable of spanning the interfilament space where it can interact with both thick and thin filament proteins as the distance between these proteins is approximately 9-16 nm (Julian, Moss, & Waller, 1981).

While the N' region of cMyBP-C has been shown to interact with the S2 fragment of myosin (Gruen & Gautel, 1999), the same interacting region of cMyBP-C was suggested to bind to F-actin (Razumova et al., 2006; Squire et al., 2003). The ability of MyBP-C to bind to actin was suggested soon after its discovery (Moos, 1981; Yamamoto, 1986) and the interaction between actin and MyBP-C was later found to occur at the N' region (Gautel et al., 1995). This interaction was initially thought to occur between domains C0 and C1 in the proline-alanine rich region (Squire et al., 2003; Squire, Roessle, & Knupp, 2004). However, this interaction was controversial and no experimental or theoretical evidence for the proline-alanine rich sequence as an actin-binding region had surfaced (Pfuhl & Gautel, 2012). Instead, the M domain, between domains C1

and C2, was then suggested to bind to actin (Razumova, Bezold, Tu, Regnier, & Harris, 2008; Saber, Begin, Warshaw, & VanBuren, 2008; A. Weith et al., 2012; Whitten, Jeffries, Harris, & Trewhella, 2008). However, other recent work has suggested that the C0 domain is the actin-binding site (Kensler, Shaffer, & Harris, 2011; Lu, Kwan, Trewhella, & Jeffries, 2011; Mun et al., 2011; Whitten et al., 2008). Interestingly, it was also suggested that there is no specific interaction of the N' fragment of cMyBP-C with F-actin but rather it is the C' region that binds with high affinity (Rybakova, Greaser, & Moss, 2011). Yet, it is well established that this region of cMyBP-C binds unequivocally with the myosin filament backbone and titin, leaving the F-actin binding site on cMyBP-C questionable (Pfuhl & Gautel, 2012).

Further work on the interaction of cMyBP-C with actin had more convincingly revealed that domains C0C2 and C1C2 bound with high affinity to F-actin and that C0-C1 bound extremely weakly suggesting that domain C0 and the C0-C1 linker is not involved in F-actin binding (Shaffer, Kensler, & Harris, 2009). Additional work suggested that the M domain linker between domains C1 and C2 contained multiple binding sites capable of binding F-actin (Mun et al., 2011). Importantly, using *in vitro* motility assays, it has been demonstrated that actin filament sliding over myosin is slowed by N' fragments of cMyBP-C to the same extent as whole cMyBP-C (Razumova et al., 2006). These results suggested that cMyBP-C either slowed the myosin detachment rate from actin (Razumova et al., 2006) or tethered the thick filament to the thin filament (Razumova et al., 2006;

A. Weith et al., 2012). Intriguingly, using an assay that better mimicked the *in vivo* situation, the sliding of F-actin over native cardiac thick filaments was slowed specifically in the C-zone, which was ablated by the removal of C0-C1 and the first 17 residues of the M-domain (the C0-C1f region [**Figure 7**]) (Previs et al., 2012; A. Weith et al., 2012). Critically, this finding is central to the hypothesis of my dissertation work and suggests the fundamental importance of the C0-C1f region of cMyBP-C, particularly, the first 17 residues of the M domain (the "f" region of C0-C1f), in regulating cMyBP-C's interaction with actin. Additionally, this finding suggests a potential functional importance of the C0-C1f region of cMyBP-C in this protein's ability to regulate cross-bridge formation and contraction within the sarcomere, myocyte, and whole heart. Therefore, to determine the necessity of the C0-C1f region of cMyBP-C in maintaining normal cardiac function *in vivo*, our lab has developed a TG mouse model lacking the C0-C1f region of cMyBP-C, but that still expresses the remaining 110 kDa more C' region of cMyBP-C in the heart (cMyBP-C^{110kDa} mouse model). Characterization of this mouse model has been the primary focus of my dissertation work presented here. Following the reports by Previs *et al*. and Weith *et al*., additional work using yeast two-hybrid experiments led to the conclusion that the C1 and M domains were necessary for actin binding as replacement of endogenous cMyBP-C with actin binding-ablated cMyBP-C resulted in its abnormal sarcomeric distribution and altered sarcomeric structure (Bhuiyan, Gulick, Osinska, Gupta, & Robbins, 2012). Furthermore, electron tomography

observations show MyBP-C extending from thick to thin filaments in the intact sarcomere, indicating that the N' region of MyBP-C binds to the thin filament (P. K. Luther & Craig, 2011; P. K. Luther et al., 2011). Together, these results suggest that cMyBP-C binding to actin is physiologically relevant and that slowing of actin filament sliding may be one mechanism by which cMyBP-C regulates cardiac contractility (Mun et al., 2014).

Electron microscopy and neutron scattering studies of F-actin decorated with N' fragments of cMyBP-C have shed light onto the nature of the actin-cMyBP-C complex. These data suggest that the C0 and C1 domains bind near subdomain 1 and the DNase I binding loop of actin (Whitten et al., 2008) while the M domain bridges over subdomain 2 and that domains C2 and C3 extend above the filament (Mun et al., 2011). This suggests that the N' region of cMyBP-C may modulate thin filament activation by interfering with or displacing α-TM binding in its low Ca^{2+} blocked position on actin. This notion was confirmed in an important study using electron microscopy and light microscopy to demonstrate that under low Ca^{2+} conditions, the C0C2 region of cMyBP-C binds to thin filaments and displaces α-TM toward the high Ca^{2+} (closed) position in which myosin binding sites on actin are exposed (Mun et al., 2014). This suggested that cMyBP-C could activate the thin filament, which the authors further confirmed in a motility assay. They showed that C0C2 has no effect on α-TM position under high Ca^{2+} conditions but inhibits maximal sliding velocity in the motility assay (Mun et al., 2014). Of particular importance to my dissertation work, the authors

found that the C0-C1f fragment of cMyBP-C binds the thin filament under low Ca^{2+} conditions but does not displace α-TM or activate thin filament sliding. However, C0-C1f was still able to inhibit thin filament sliding at high Ca^{2+} to the same extent as the larger C0C2 N' fragment (Mun et al., 2014). These findings suggest that regions of the M-domain beyond the first 17 amino acids appear to be required for fully productive binding to thin filaments. Indeed, as mentioned earlier, yeast two-hybrid and NMR data suggest that positively charged residues of the M domain beyond the first 17 are important for actin binding (Bhuiyan et al., 2012; Howarth, Ramisetti, Nolan, Sadayappan, & Rosevear, 2012). Together, these data suggest that the N' region of cMyBP-C may play two physiological roles in intact muscle. First, at low levels of Ca^{2+}, cMyBP-C may displace α-TM from the blocked position (in which α-TM blocks the binding of myosin to actin) thereby activating the thin filament (Mun et al., 2014). Second, the N' region of cMyBP-C may govern maximal sliding velocity at high Ca^{2+} by a potentially independent molecular mechanism (Mun et al., 2014), perhaps by placing a load on the thin filament, reducing its rate of sliding. Interestingly, it has also been suggested that cMyBP-C phosphorylation within the M domain can reduce, but not abolish, cMyBP-C binding to actin and that under these conditions, α-TM is only slightly displaced (Barefield & Sadayappan, 2010; Craig et al., 2014). In the intact myocardium, this may translate to a reduction in cMyBP-C's slowing of filament sliding or a reduction in its ability to activate the thin filament (Craig et al., 2014). Given the complexity of the interactions of cMyBP-C's N' region and

the dual biphasic activation and inhibition observed in actin motility assays, Walcott *et al.* developed a novel mathematical model for the interaction of cMyBP-C with the contractile proteins actin and myosin and the regulatory protein α-TM to explain the elusive mechanism of cMyBP-C function (Walcott, Docken, & Harris, 2015). The authors referred to this as the drag-activation-competition model (Walcott et al., 2015).

The complex activating and inhibitory effects of cMyBP-C have proven challenging to explain by a single mechanism. Although activation might be explained by the ability of cMyBP-C N' domains to bind actin and shift α-TM and expose the myosin binding sites on actin, inhibition may be due to competition of cMyBP-C with myosin heads for binding to actin (Moos, Mason, Besterman, Feng, & Dubin, 1978) or by transient links formed between cMyBP-C and the flow cell surface in the motility assay creating a viscous drag that slows motility (A. Weith et al., 2012). In their model, Walcott *et al.* propose that myosin competes with cMyBP-C binding to actin. Once bound, either cMyBP-C or myosin displaces α-TM towards its open position. If nearby molecules bind, they activate intervening molecules. However, if distant molecules bind, they do so independently (Walcott et al., 2015). Further explained, the authors propose that the mechanism of drag-activation-competition for cMyBP-C is consistent with actin motility data in that cMyBP-C binding to actin is capable of displacing α-TM at low Ca^{2+}, activating the thin filament. However, increasing cMyBP-C concentration leads to competition for binding sites between myosin and cMyBP-

C as the higher cMyBP-C concentration leaves fewer sites available for myosin binding. Then, links formed by cMyBP-C binding to actin or the flow cell surface creates a viscous drag that slows actin filament sliding motility (Walcott et al., 2015).

Considering the complex functional implications for an actin-cMyBP-C interaction, a crosslink between the thick and thin filaments would likely slow down actin filament sliding but would not alter maximum force (Pfuhl & Gautel, 2012). If the interaction of cMyBP-C with the thin filament extends to the troponin-α-TM complex, this may alter contraction such that the concentration of Ca^{2+} required to reach half-maximal contraction would be modified producing a left-shift in the force/pCa (pCa = -log[Ca^{2+}]) curve (Pfuhl & Gautel, 2012). This shift has been observed in systems in which N' fragments of cMyBP-C were added (Harris, Rostkova, Gautel, & Moss, 2004; Herron et al., 2006; Kunst et al., 2000; Razumova et al., 2008; Razumova et al., 2006). Additionally, a competition of cMyBP-C with the S1 head region of myosin has been suggested to lead to a reduction in velocity and maximum force (Pfuhl & Gautel, 2012).

Recently, Kampourakis *et al*. have attempted to clarify the function of the regulatory N' C1C2 region of rat cMyBP-C by examining the effect(s) of these regions on thick and thin filament structure using intact sarcomeres from skinned rat ventricular trabeculae (Kampourakis, Yan, Gautel, Sun, & Irving, 2014). They show that the C1C2 region of cMyBP-C induced larger structural changes in thin filaments than did Ca^{2+} activation, even when active force was blocked by

blebbistatin, indicating that C1C2 directly activates the thin filament (Kampourakis et al., 2014). In contrast, they further demonstrate that structural changes in thick filaments induced by C1C2 were smaller than those associated with Ca^{2+} activation, which were abolished or reversed upon blebbistatin treatment. Furthermore, they suggest that low concentrations of C1C2 do not alter resting force but increase Ca^{2+} sensitivity and reduce cooperativity of force and structural changes in both filament types. They conclude that the N' region of cMyBP-C stabilizes the "on" state of thin filaments and the "off" state of thick filaments and that this is how cMyBP-C regulates cardiac contractility. However, given the complexity of cMyBP-C's interactions, future research is required to confirm the true mechanism of action of this protein in the cardiac muscle. This will be particularly important in understanding the role of this protein in various cardiovascular diseases and in the development of novel therapeutics to treat these pathologies.

cMyBP-C in Disease

While the project that I have undertaken for my dissertation work has been mechanistic in nature, that is, examining the function of the N' region of cMyBP-C in regulating cardiac contraction, the implication is that this work will lead to a better understanding of how cMyBP-C functions in both health and disease. Therefore, it is essential to mention relevant pathologies in which cMyBP-C has been shown to participate. Over the past decade, over 200 mutations have been identified in the *MYBPC3* gene, several of which are at the N' region of cMyBP-C

(Ackermann & Kontrogianni-Konstantopoulos, 2011). These mutations include missense, nonsense, deletion/insertion, and frame-shift mutations that are linked to the development of modest and late onset familial HCM (Ackermann & Kontrogianni-Konstantopoulos, 2011). Consequently, *MYBPC3* is the most highly mutated gene in human HCM accounting for approximately 40% of the identified mutations (Barefield et al., 2015), further suggesting the importance of cMyBP-C in regulating cardiac function within the sarcomere. Mutations within *MYBPC3* have also been identified in patients with DCM (McNally et al., 2013). Most of the mutations that occur in the *MYBPC3* gene are nonsense and frame-shift mutations leading to C' truncated forms of cMyBP-C that cannot incorporate into the sarcomere leading to a loss in the regulation of contractile function by cMyBP-C (Oakley, Hambly, Curmi, & Brown, 2004). However, missense mutations have also been identified to cause a less severe cardiomyopathic phenotype (Xu, Dewey, Nguyen, & Gomes, 2010) and do not appear to alter the structure or stability of the protein but may weaken the myosin binding capacity of cMyBP-C (Ababou et al., 2008). In addition to cardiomyopathies, cMyBP-C has been shown to play a role in the ischemic myocardium during MI.

cMyBP-C Cleavage During Ischemic Injury

Considering the involvement of cMyBP-C in cardiovascular pathologies, our lab has recently focused on the role of this protein during MI (Govindan et al., 2013; Govindan, McElligott, et al., 2012; Govindan, Sarkey, et al., 2012; Kuster, Barefield, Govindan, & Sadayappan, 2013; T. L. Lynch & Sadayappan, 2014;

Witayavanitkul et al., 2014). As mentioned earlier, the central focus of my dissertation research has been on elucidating the necessity of the N'-C0-C1f region of cMyBP-C in maintaining normal cardiac function *in vivo*. The critical importance of C0-C1f in relation to its interactions with myosin and actin was previously discussed above. To provide additional background information into the functional importance of this region, I will next describe the discovery of the C0-C1f fragment and its recently identified pathogenicity to the heart as discussed in my recently published review article on this topic (T. L. Lynch & Sadayappan, 2014).

Throughout ischemia and in early reperfusion, increased levels of Ca^{2+} activate the Ca^{2+}-dependent protease calpain, which degrades intracellular proteins, including contractile proteins, during myocardial necrosis (Kusuoka & Marban, 1992). Post-ischemic dysfunction has been associated with Ca^{2+}-dependent degradation of α-actin (Matsumura, Kusuoka, Inoue, Hori, & Kamada, 1993) and cTnI (Gao et al., 1997). Models of ischemia-reperfusion also show degradation of cTnT and myosin light chain-1. Previous work has identified cMyBP-C as a substrate for calpain proteases (Previs et al., 2012; Sadayappan, Greis, & Robbins, 2008), and that dephosphorylation makes cMyBP-C susceptible to proteolysis. Tandem mass spectrometry analyses revealed that the calpain cleavage site in cMyBP-C is set within the M-domain at 272-TSLAGAGRR-280 in mice. This finding indicated that the predominant 40 kDa cleavage fragment of cMyBP-C was the C0-C1f region. Following ischemic injury,

the 40 kDa fragments of cMyBP-C could be readily detected in cardiac tissue (Sadayappan et al., 2008). Furthermore, in an *in vivo* rat model of MI and in samples from post-MI patients, it was determined that C0-C1f is released into the systemic circulation, where it was suggested to serve as a biomarker for ischemic injury (Govindan, McElligott, et al., 2012; Kuster et al., 2014). Furthermore, cMyBP-C dephosphorylation was found to correlate with its increased degradation and release *in vitro* and in ischemic areas of the *in vivo* MI heart (Govindan, McElligott, et al., 2012). Remarkably, constitutive phosphorylation of cMyBP-C prevented its degradation and was found to be cardioprotective (Sadayappan et al., 2006a). The removal of the N' residues of cMyBP-C by a Ca^{2+} activated protease raises many interesting questions, especially when considered along with the evidence that the major regulator of actomyosin interaction is found within the M-domain, which is also the location of the cleavage site. It is possible that cleavage of cMyBP-C may provide a short-term advantage in terms of increased contractility, although the long-term effects of this modification may be deleterious, which I am to prove here. Given the role of the N' region of cMyBP-C as a regulator of actin-myosin interaction, the released C0-C1f fragment was also suggested to be involved in pathological dysfunction following ischemic injury to the heart (Sadayappan et al., 2008).

The N'-C0-C1f Cleavage Fragment of cMyBP-C is Pathogenic

Pathogenic consequences of cMyBP-C degradation in the heart post-MI could arise through disruption of normal full-length (FL) protein function, through

direct pathogenicity of C0-C1f within the sarcomere, or both. The pathogenic properties of C0-C1f were determined upon adenoviral infection of neonatal rat ventricular cardiomyocytes and adult rabbit ventricular cardiomyocytes with FL cMyBP-C, C0-C1f, or the 110 kDa C-terminal fragment of cMyBP-C that remains following the removal of C0-C1f (Govindan, Sarkey, et al., 2012). This work revealed that C0-C1f binds to the actin thin filament within the cardiac sarcomere. Using liquid chromatography-tandem mass spectrometry analysis, it was determined that the C0-C1f fragment contains several acetylation sites that may be involved in regulating the interaction between actin and myosin filaments (Govindan, Sarkey, et al., 2012). Furthermore, C0-C1f expression significantly elevated caspase-3 activity, as well as the release of lactate dehydrogenase, which is an indicator of increased cell injury, demonstrating the toxicity of this fragment to cardiomyocytes (Govindan, Sarkey, et al., 2012). C0-C1f reduced cell viability, altered Ca^{2+} handling, and significantly decreased sarcomere length shortening and the velocities of contraction and relaxation by inhibiting actomyosin function (Govindan, Sarkey, et al., 2012). It was later established *in vivo* that the TG expression of the C0-C1f fragment could cause sarcomere dysgenesis, altered cardiac geometry, and myofibrillar disarray as well as fibrosis, myocardial hypertrophy, and HF in mice between twelve and seventeen weeks of age (Razzaque et al., 2013). Most recently, Witayavanitkul *et al.* examined the association between C0-C1f and altered contractility in human cardiac myofilaments *in vitro.* They found that C0-C1f decreased myofilament

Ca^{2+} sensitivity and maximum force generation, but increased cooperative activation, the kinetics of cross-bridge cycling, and tension cost at short sarcomere lengths (Witayavanitkul et al., 2014). Furthermore, it was shown that C0-C1f interacted with actin and α-TM to exert its effects by reducing contractility, suggesting that reduced cardiac function following MI may result from C0-C1f taking on the characteristics of a poison polypeptide by interfering with the ability of native cMyBP-C to interact normally with the thin filament (Witayavanitkul et al., 2014). Overall, delineating the toxic effects of cMyBP-C degradation and the subsequent release of C0-C1f on sarcomere function has provided insight into the mechanisms underlying contractile dysfunction in MI patients. Therefore, preserving the phosphorylation status of cMyBP-C may be necessary to protect from its degradation and from the pathogenic consequences of C0-C1f in the post-MI heart.

CHAPTER THREE

HYPOTHESIS AND AIMS

Together, the data implicating the importance of the C0-C1f region in controlling cMyBP-C's N' interactions at the thick and thin filament, as well as the data supporting the pathogenicity of this fragment when expressed separate from the FL protein, suggest a critical importance of this region in regulating actomyosin interactions and the kinetics of cross-bridge cycling. However, to date, there have been no *in vivo* studies examining whether the N'-C0-C1f region of cMyBP-C is necessary for maintaining normal cardiac function. Therefore, throughout my dissertation studies, I characterized a novel mouse model developed in our lab that lacks the N'-C0-C1f region but that still expresses the remaining 110 kDa more distal C' region of cMyBP-C within the cardiac sarcomere (cMyBP-C^{110kDa} mouse model) to determine whether the C0-C1f region of cMyBP-C is necessary for regulating cardiac contractility and maintaining normal heart function *in vivo*. **My central hypothesis was that the N'-C0-C1f region of cMyBP-C is critical for normal cardiac function *in vivo*.** To test this hypothesis, I developed two Specific Aims.

In **Specific Aim 1**, I elucidated the necessity of the N'-C0-C1f region of cMyBP-C on regulating cardiac morphology and contractile function at the whole-organ level and performed studies to initially characterize the novel cMyBP-C^{110kDa} mouse model. **I hypothesized that the N'-C0-C1f region of cMyBP-C is**

necessary for maintaining physiological global cardiac function and morphology. To test this hypothesis, I performed echocardiography and histological and morphometric analyses on hearts from cMyBP-C^{110kDa} and NTG mice to assess cardiac function and morphology. mRNA levels of pathological hypertrophy markers were measured to evaluate pathological remodeling in cMyBP-C^{110kDa} versus NTG hearts. RNA-Seq was performed to assess alterations in global gene expression levels in the hearts of cMyBP-C^{110kDa} mice compared to NTG mice. Immunofluorescence analysis and coupled with second harmonic generation (SHG) imaging of isolated cardiac myocytes revealed the incorporation status of the cMyBP-C^{110kDa} TG protein into the cardiac sarcomere of cMyBP-C^{110kDa} hearts. Additionally, FL cMyBP-C and cMyBP-C^{110kDa} TG protein levels and phosphorylation status were determined by Western blot analysis in myofilament fractions from cMyBP-C^{110kDa} and NTG hearts.

In **Specific Aim 2**, I determined how the absence of the N'-C0-C1f region of cMyBP-C in cMyBP-C^{110kDa} hearts alters myofilament function to elucidate whether this region is necessary for controlling physiological contraction kinetics in the heart. **I hypothesized that the absence of the N'-C0-C1f region of cMyBP-C in cMyBP-C^{110kDa} mice disrupts steady-state myofilament function.** To test this hypothesis, I performed a steady-state fiber force-ATPase experiment using isolated cardiac LV papillary muscle fibers from cMyBP-C^{110kDa} and NTG mice at 3-months of age. The parameters measured included force

production, Ca^{2+} sensitivity of force development, tension cost, cross-bridge stiffness and rate of tension redevelopment (k_{tr}).

The results of the data I present here directly address these two Specific Aims and support the proposal that the N'-C0-C1f region of cMyBP-C is a critical regulator of actomyosin interactions that controls aberrant contraction kinetics within the cardiac sarcomere and that the N'-C0-C1f region of cMyBP-C is necessary for maintaining normal cardiac function *in vivo*.

CHAPTER FOUR

MATERIALS AND METHODS

cMyBP-C^{110kDa} Mouse Model

To determine whether the N'-C0-C1f region of cMyBP-C is necessary for cardiac function, I characterized cardiac function in a novel mouse model developed in our lab that lacks the N'-C0-C1f region of cMyBP-C but that still expresses the remaining more distal C' fragment of cMyBP-C (110 kDa region). We referred to this mouse as the cMyBP-C^{110kDa} mouse model (**Figure 8**). The data obtained from these animals was compared to age-matched NTG controls expressing only endogenous cMyBP-C in their hearts (**Figure 8**). All experiments conducted during my dissertation work were performed on animals between 3- and 8-months of age. Prior to my involvement in this project, my PhD mentor Dr. Sakthivel Sadayappan developed the cMyBP-C^{110kDa} mouse model. Briefly, the cMyBP-C wild type cDNA (~3.82 kb) was made by polymerase chain reaction (PCR) and multiple clones were completely sequenced. cMyBP-C cDNA was subjected to site direct mutagenesis in which the first 813 nucleotides were removed, resulting in loss of the C0-C1f region. The presumptive mutant PCR products were cloned into pCR-Blunt II-TOPO vector (Invitrogen) for sequence confirmation. The sequence encoding the c-Myc epitope (10 amino acids, EQKLI
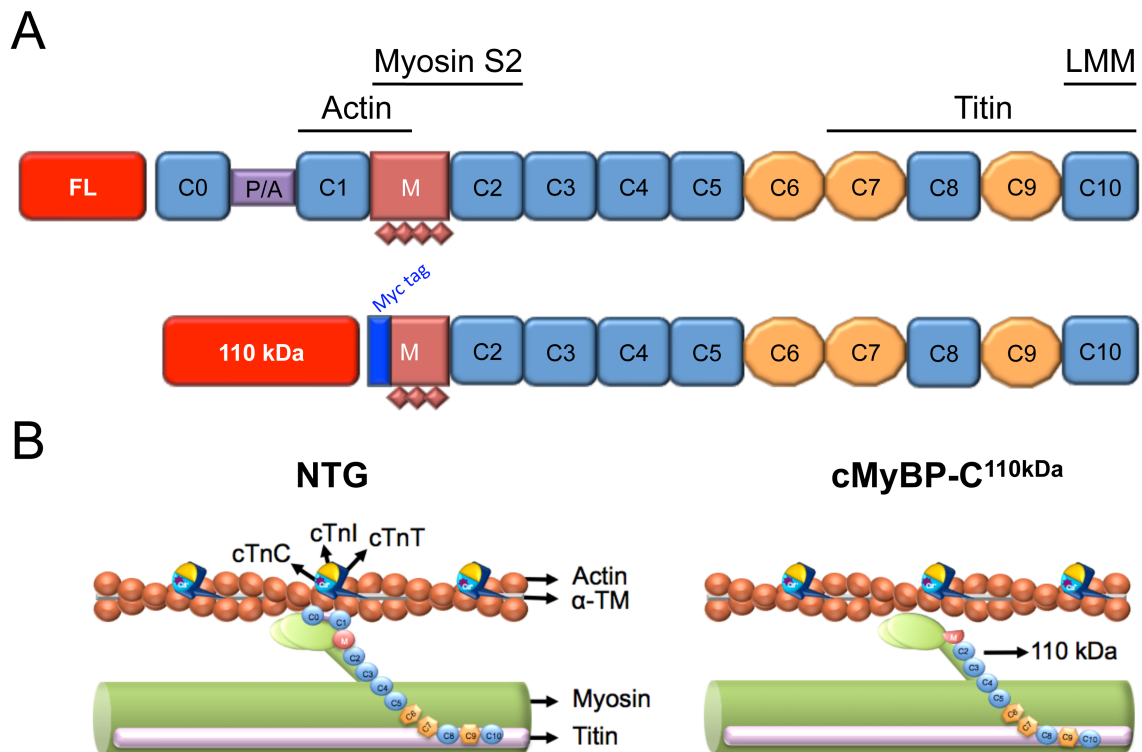
Figure 8. The cMyBP-C[110kDa] Transgenic Protein. (A) Illustration of endogenous full-length (FL) cMyBP-C and the cMyBP-C[110kDa] TG protein missing the N'-C0-C1f region (first 271 amino acid residues of FL cMyBP-C corresponding to domains C0 through C1 and the first 17 amino acid residues of the M domain) of cMyBP-C. cMyBP-C domains C0 through C10 are shown in FL cMyBP-C. The cMyBP-C[110kDa] TG protein is c-Myc-tagged at its N' region prior to the residue that would correspond to the endogenous residue at position 272 of FL cMyBP-C. Phosphorylation sites within the M domain are depicted as diamonds. Deletion of C0-C1f results in loss of the PKA recognition motif for phosphorylation at serine residue 273. Protein-protein interaction domains and binding partners are indicated. (B) Representation of the predicted myofilament protein organization within the sarcomeres of NTG and cMyBP-C[110kDa] hearts. NTG hearts are expected to express the FL endogenous cMyBP-C protein while cMyBP-C[110kDa] hearts are proposed to express the cMyBP-C[110kDa] TG protein lacking the C0-C1f region. Removal of the N'-C0-C1f region of cMyBP-C is hypothesized to be deleterious to the ability of cMyBP-C to regulate cardiac contractile function through its N' region. This is suggested to result in aberrant cardiac contractile function in cMyBP-C[110kDa] hearts leading to myocardial remodeling and HF.

SEEDL [Roche]) was incorporated into the primer such that the tag was placed after the initiator methionine residue at the N' region of the protein prior to the residue that would correspond to the endogenous residue at position 272 of FL cMyBP-C. This allowed us to distinguish and determine the localization of the cMyBP-C^{110kDa} TG protein compared to endogenous FL cMyBP-C by immunofluorescence techniques (described below). Previous *in vivo* studies showed that the c-Myc epitope tag at this location does not interfere either with normal sarcomerogenesis or the recombinant cMyBP-C's capability to incorporate into the sarcomere (Yang, Hewett, et al., 2001; Yang, Osinska, Klevitsky, & Robbins, 2001; Yang et al., 1998, 1999). After the correct sequence was confirmed, the entire cDNA fragment was ligated into a vector containing an α-MHC promoter using the unique *Sal* I site (**Figure 9**) (Gulick et al., 1997). The construct was then re-sequenced to ensure the correct orientation. The final construct was digested free of the vector with *Not* I, purified from agarose gels, and used to generate multiple TG lines on an NTG background (C57BL/6 strain) to obtain replacement of endogenous cMyBP-C in the heart with the cMyBP-C^{110kDa} TG protein. Founders were identified by PCR using primers corresponding to the 5'-UTR's with an internal control. Mouse line 62 was the line of choice for all experiments conducted during my dissertation work as it had the highest levels of replacement of endogenous cMyBP-C with the cMyBP-C^{110kDa} TG protein, based upon previous work done by our former postdoctoral researcher Dr. Diederik W.D. Kuster (**Figure 10**). Following selection of line 62, I
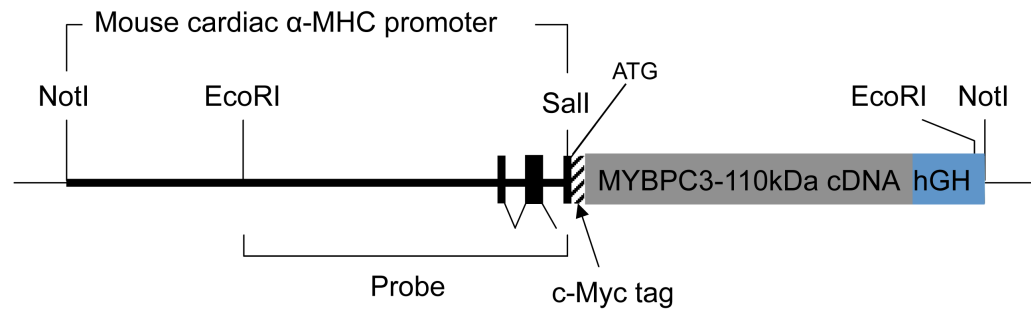
Figure 9. cMyBP-C^{110kDa} Vector Construct. DNA vector construct containing the cDNA coding region for the cMyBP-C^{110kDa} TG protein. The 5' c-Myc tag was inserted immediately after translation start codon (ATG). The entire cDNA fragment was ligated into the α-MHC promoter vector at the unique *Sal* I site. The α-MHC promoter allows for cardiac specific expression of the TG protein. The dark vertical boxes represent the three (non-coding) exons of the 5' untranslated region of α-MHC that are included in the promoter. The human growth hormone (hGH) sequence at the 3' end of the construct served as a polyadenylation sequence to maintain mRNA stability. The construct was sequenced to ensure the correct orientation and sequence. The final construct was then digested free of vector sequence with *Not* I, purified from agarose gels and used to generate multiple TG lines on an NTG background (C57BL/6 mouse strain) to obtain replacement of endogenous cMyBP-C in the heart with the cMyBP-C^{110kDa} TG protein.
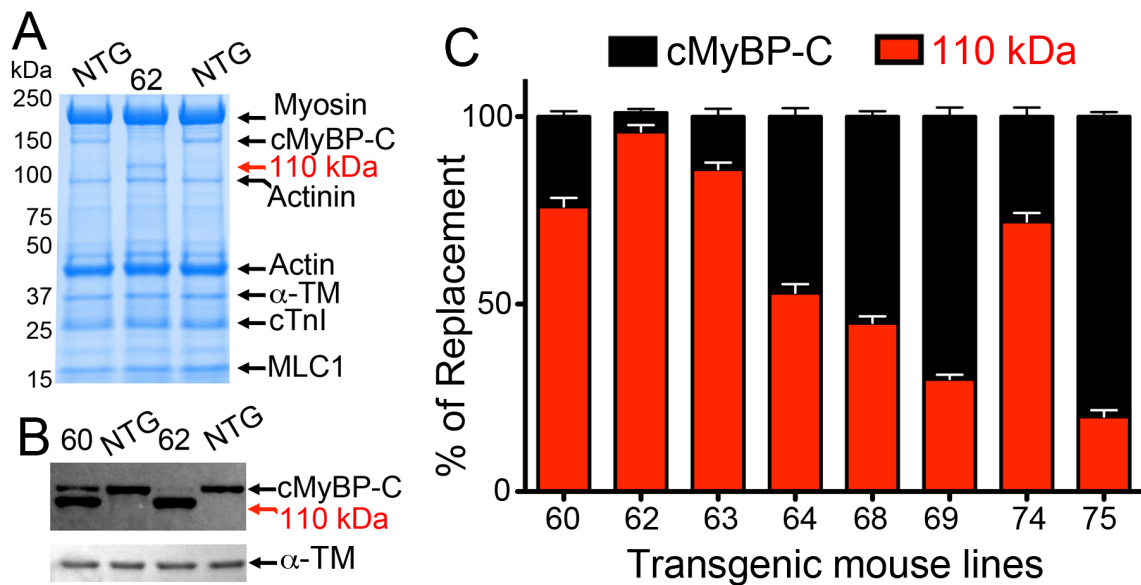
Figure 10. Initial cMyBP-C^{110kDa} Transgenic Mouse Line Characterization.
(A) SDS-PAGE gel Coomassie stained to show myofilament fractions from NTG and cMyBP-C^{110kDa} line 62 mouse hearts. Myofilament proteins are indicated, including the cMyBP-C^{110kDa} protein (red script), which is present only in the myofilament fraction from cMyBP-C^{110kDa} line 62 heart. (B) Western blot analysis using myofilament fractions from NTG and cMyBP-C^{110kDa} lines 60 and 62 mouse hearts. Relative protein abundance of endogenous FL cMyBP-C and the cMyBP-C^{110kDa} TG protein are shown. The endogenous FL cMyBP-C protein is more highly expressed in cMyBP-C^{110kDa} line 60 mouse hearts than in line 62 hearts. Endogenous FL cMyBP-C expression is highest in NTG hearts, which do not express the cMyBP-C^{110kDa} TG protein. (C) Quantification of percent replacement of endogenous FL cMyBP-C (black bars) with the cMyBP-C^{110kDa} TG protein (red bars) in several cMyBP-C^{110kDa} TG mouse lines. cMyBP-C^{110kDa} TG mouse line 62 showed the highest percent replacement of the endogenous FL cMyBP-C protein with the cMyBP-C^{110kDa} TG protein and was used for all experiments performed throughout my dissertation studies.

then joined this project and performed the experiments described below to characterize the cMyBP-C^{110kDa} mouse model (mouse line 62). All of the experiments using animals detailed in this work were approved by the Institutional Animal Care and Use Committees at Loyola University Chicago and followed the policies of the *Guide for the Use and Care of Laboratory Animals* published by the National Institutes of Health.

Echocardiography

To assess cardiac function in NTG and cMyBP-C^{110kDa} animals at 3- and 6-months of age, non-invasive M-mode echocardiography was performed using a VisualSonics Vevo 2100 imaging system (FUJIFILM VisualSonics Inc.) with an MS-550D 22-55 MHz transducer. Under isoflurane anesthesia (5% for knock-down and 1.5% for sedation), the hearts were monitored to assess function and morphology. Chamber dimensions and wall thicknesses at end diastole and systole were measured using short-axis M-mode images (**Figure 11**) and the Vevo2100 analysis package (FUJIFILM Visual Sonics Inc.), as described previously (T. L. Lynch IV et al., 2015). From these values, percent FS (measured as ((LVID;d – LVID;s) / LVID;d) x 100) and percent EF were determined. Parasternal long-axis M-mode images were used to measure percent global longitudinal strain (GLS), which was quantified using VevoStrain software in Vevo Lab (FUJIFILM VisualSonics Inc.).
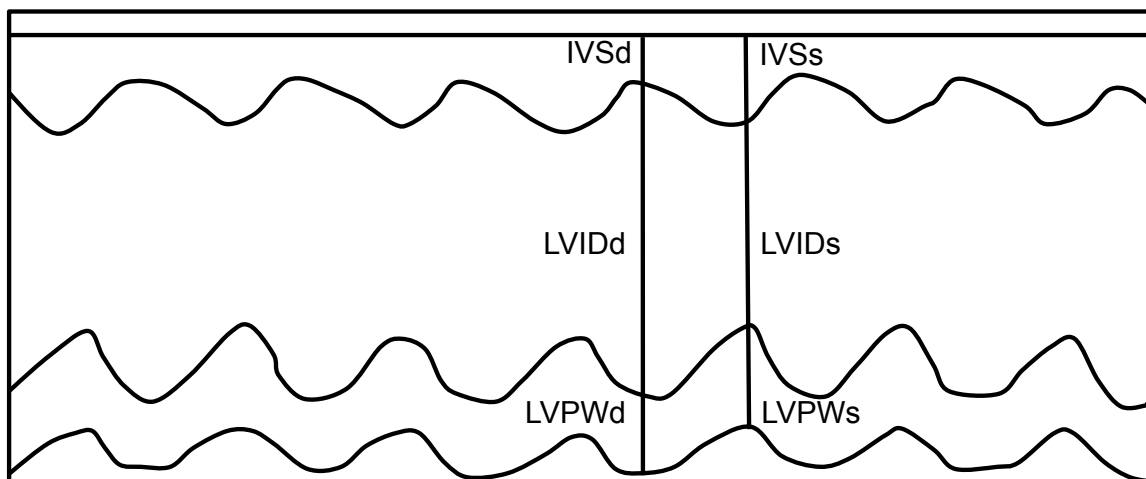
Figure 11. Echocardiography. Representative cartoon depiction of M-mode echocardiography showing the thickness of the interventricular septum (IVS) at end diastole (IVSd) and systole (IVSs) as well as LVIDd, LVIDs, and LV posterior wall thickness (LVPW) at end diastole (LVPWd) and systole (LVPWs). From these measurements, quantifications of percent EF and percent FS were calculated.

Histopathology

To assess the gross morphology of NTG and cMyBP-C^{110kDa} hearts, the

hearts were removed from anesthetized mice and were then drained of blood

and fixed in 10% formalin. Hearts were bisected longitudinally or cross-sectioned

at the base and dehydrated with a graded series of alcohols before being

embedded in paraffin. Then, 5 µm step-serial sections were taken from NTG and

cMyBP-C^{110kDa} hearts, which were stained with hematoxylin and eosin (H&E) or

Masson's trichrome (MT). The H&E and MT stained sections were imaged using

the slide scanning system (Nanozoomer RT 2.0, Hamamatsu Corporation,

Tokyo, Japan) and a 20x Uplansapo objective at a resolution of 0.23 µm under

bright field mode. To analyze the cellularity (nuclear area) and fibrosis, high-

resolution images were exported from whole heart scanned sections. Images

were thresholded based on RGB values for either nuclei (using the H&E labeled

sections) or fibrosis (using MT labeled sections) and the area of pixels occupied

by these components were quantified in the program Axiovision (version 4.9.1,

Carl Zeiss Microimaging).

Mouse Ventricular Myocyte Isolation

To determine whether cMyBP-C^{110kDa} incorporates properly within the

cardiac sarcomere of cMyBP-C^{110kDa} mice, cardiomyocytes were isolated from

cMyBP-C^{110kDa} hearts as well as NTG hearts for comparison. Prior to isolation, all

animals were placed under isoflurane anesthesia (5% for knock-down) followed

by cervical dislocation. Hearts were immediately harvested from the chest by

cutting above the aorta. The aorta was cannulated with a blunted 23-gauge needle and the hearts were fastened to the cannula with a 4-0 suture tied around the aorta. The hearts were then subjected to 5 minutes of retrograde perfusion with Perfusion Buffer (NaCl [120.4 mM], KCl [14.7 mM], KH_2PO_4 [0.6 mM], Na_2HPO_4], $MgSO_4 \cdot 7H_2O$ [1.2 millimolar (mM)], Na-HEPES [10 mM], $NaHCO_3$ [4.6 mM], Taurine [30 mM], 2,3-butanedione monoxime [10 mM], D-glucose [5.5 mM]) via the Langendorff technique (Skrzypiec-Spring, Grotthus, Szelag, & Schulz, 2007). To remove the extracellular matrix, the hearts were then digested for 20 minutes via Langendorff retrograde perfusion with 40 milliliters (ml) of Digestion Buffer (50 ml Perfusion buffer, 6.25 microliters (µl) of 100 mM $CaCl_2$, and 18 milligrams (mg) Liberase TH Research Grade [Cat. No. 05401151001, Roche Diagnostics]). Following the digestion, the hearts were removed from the cannula and placed into a 35 millimeter (mm) petri dish containing 2.5 ml of Digestion Buffer. The hearts were manually torn apart and triturated to disperse cardiomyocytes, which were filtered through a 200 µm Nylon Mesh (Cat. No. 146487, Spectrum Labs) into a 15 ml conical tube to remove any remaining clumps of tissue. The petri dish was then washed with 2.5 ml of Myocyte Stopping Buffer 1 (9 ml Perfusion Buffer, 1 ml Fetal Bovine Serum, 12.5 µl of 10 mM $CaCl_2$), which was filtered into the 15 ml conical tube to collect the remaining cardiomyocytes. The cardiomyocytes were allowed to settle by gravity for 10 minutes. The supernatant was then removed and replaced with 10 ml of Myocyte Stopping Buffer 2 (28.5 ml Perfusion Buffer, 1.5 ml Fetal Bovine Serum, 12.5 µl

of 10 mM CaCl$_2$). Serial reintroduction of CaCl$_2$ was then added to the cardiomyocyte solution as follows: 50 µl of 10 mM CaCl$_2$ for 4 minutes, 50 µl of 10 mM CaCl$_2$ for 4 minutes, 100 µl of 10 mM CaCl$_2$ for 4 minutes, 30 µl of 100 mM CaCl$_2$ for 4 minutes, and 50 µl of 100 mM CaCl$_2$ for 15 minutes. Cardiomyocytes were triturated between CaCl$_2$ reintroduction steps. Cardiomyocyte yield and quality was determined using the light microscopy imaging feature on the ZOE Fluorescent Cell Imager (Cat. No. 1450031, Bio-Rad Laboratories, Inc.) (**Figure 12**).

Immunofluorescence

Following their isolation, cardiomyocytes from either NTG or cMyBP-C^{110kDa} hearts were cultured for 1 hour on Lab-Tek II Chamber Slides (Cat. No. 154461, Thermo Fisher Scientific Inc.) coated with ECM Gel from Engelbreth-Holm-Swarm murine sarcoma (Cat. No. E6909, Sigma-Aldrich Co. LLC.). After adhering to the chamber slides, cardiomyocytes were washed twice with phosphate buffered saline (PBS) (4°C) and fixed with ice-cold (-20°C) methanol for 1 minute as well as cold (4°C) 4% paraformaldehyde for 3 minutes. Cardiomyocytes were then permeabilized in 0.5% Triton X-100 in PBS for 20 minutes and 0.1% Triton X-100 twice for 15 minutes. Antigen retrieval was performed by placing the cardiomyocytes in antigen retrieval solution (0.1M glycine in PBS, pH 7.4) for 30 minutes followed by washing three times with PBS. Non-specific binding of antibodies was prevented by incubating cells for 30 minutes in blocking solution (0.1% BSA, 0.1% gelatin, 0.1% tween-20, 0.0001%
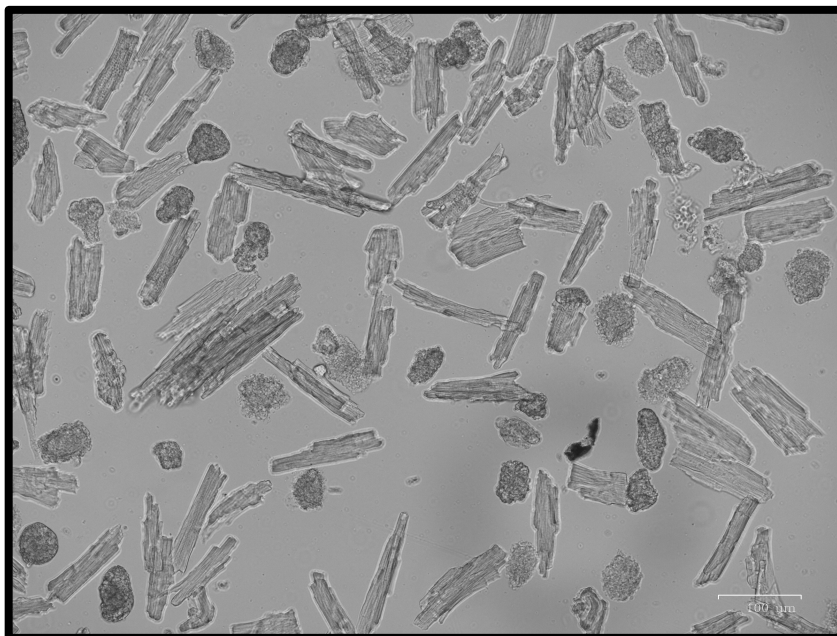
Figure 12. Isolated Mouse Cardiomyocytes. Representative image of mouse cardiomyocytes post-isolation that were used for immunofluorescence studies.

NaN$_3$) diluted 1:1 in PBS. Cardiomyocytes were then incubated overnight at 4°C with combinations of the following primary antibodies diluted 1:200 in blocking solution: MYBPC3 (E-7) antibody (Cat. No. sc-137180, Santa Cruz Biotechnology, Inc.), Anti-C5 fragment of MYBPC3 IgG (custom made antibody gifted from Dr. Saul Winegrad), Anti-c-Myc antibody produced in rabbit (Cat. No. C3956, Sigma-Aldrich Co. LLC.), Anti-α-Actinin antibody produced in rabbit (Cat. No. A2543, Sigma-Aldrich Co. LLC.), and Monoclonal Anti-α-Actinin (Sarcomeric) antibody produced in mouse (Cat. No. A7811, Sigma-Aldrich Co. LLC.). Following washing three times with PBS, the cardiomyocytes were then incubated in the dark for 1 hour at 4°C with a combination of Goat anti-rabbit IgG (H+L) Secondary Antibody, Alexa Fluor 488 conjugate (Cat. No. A-11008, Thermo Fisher Scientific Inc.) and Goat anti-Mouse IgG (H+L) Secondary Antibody, Alexa Fluor 568 conjugate (Cat. No. A-11004, Thermo fisher Scientific Inc.) secondary antibodies diluted 1:100 in blocking solution. Cardiomyocytes were then washed three times with PBS and covered with VECTASHIELD Hard Set Mounting Medium with DAPI (Cat. No. H-1500, Vector Laboratories, Inc.) and a coverslip that was sealed to the slide with nail polish. Cardiomyocytes were then imaged as described below.

Two-Photon Fluorescence and SHG Microscopy of Cardiomyocytes

The immunofluorescence labeled cardiomyocytes from NTG and cMyBP-C^{110kDa} hearts were imaged using a hybrid of two-photon fluorescence and SHG microscopy and an LSM 710 system (Carl Zeiss) with a two-photon laser with 70

femtosecond pulses (MaiTai, DeepSee, eHp, Spectraphysics) and NDD detectors. A C-Apchromat 40x/1.20 NA W Korr objective was used to image α-actinin, cMyBP-C and the c-Myc-labeled cMyBP-C[110kDa] TG protein under a two-photon fluorescence modality using a 780 nm two-photon excitation wavelength, with appropriate emission filters (500-550 nm, green cMyBP-C or c-Myc-cMyBP-C[110kDa] TG protein labeled with Alexa Fluor 488 and 570-615 nm, red α-actinin labeled with Alexa fluor 568). The same excitation was used to create a SHG image as described previously (Sivaguru et al., 2010; Sivaguru, Fried, Miller, & Fouke, 2014). Briefly, the frequency doubled label-free SHG signals from myosin based on the inherent non-centrosymmetric nature of its molecular structure using the same excitation of 780 nm. Note that this is the same wavelength used for two-photon fluorescence of the aforementioned molecules α-actinin, cMyBP-C, and the c-Myc-labeled cMyBP-C[110kDa] Tg protein in backward/reflected direction using NDD detectors. Simultaneously, the myosin signals were collected in the forward direction using the TPMT of the LSM 710 detector after passing the emission beam through a 690 nm short pass filter to block any stray IR signals. This was coupled with a SHG filter in the range of 380-400 nm, centered at 390 nm, which is exactly twice the frequency of the excitation beam of 780 nm (Sivaguru et al., 2014). The image acquisition parameters, which included digital zoom (4X), pixel size (52x52 nm in XY), 1024x1024 total pixel dimension constituting ~53x53 µm size of frame XY, with an 8-bit dynamic range, four line averages and ~4.4% laser power, 1.58 us pixel dwell time and a master

gain of ~655-690 across the channels, were kept constant across the different immunofluorescence labeled cardiomyocyte samples acquired from NTG and cMyBP-C^{110kDa} mouse hearts. Raw data are pseudocolored to their emission wavelength (blue-SHG, green cMyBP-C or the c-Myc-labeled cMyBP-C^{110kDa} TG protein, red α-actinin) and adjusted to reveal the entire dynamic range in min/max intensity profile to best represent the image in the program Zen 2012 (Carl Zeiss).

Cardiac Muscle Organization Analysis

To examine whole heart morphology, hearts from NTG and cMyBP-C^{110kDa} animals were processed and imaged as described previously (Sivaguru et al., 2015). Four-month old NTG and cMyBP-C^{110kDa} animals were heparinized in 0.25 ml 1000 USP/ml heparin sodium (Sagent Pharmaceuticals) to prevent blood clots from forming during heart removal. Mice were then anesthetized with 5% isoflurane and subjected to cervical dislocation. Hearts were rapidly excised from the chest taking care to ensure the aorta remained attached. The hearts were then cannulated through the aorta, as described previously, and perfused with 5 ml of ice-cold cardioplegic solution (50 mM KCL, 5% dextrose, 1x PBS) to allow for complete cardiac muscle relaxation. Afterwards, the hearts were perfused with 5 ml of ice-cold NOTOXhisto fixative (Cat. No. 614-05, Science Device Laboratory). Each heart was then dehydrated in a graded ethanol series (25%, 50%, 75%, and 100% in PBS under vacuum) for a total time of approximately 30 to 45 minutes per step. The dehydrated hearts were then taken through

increasing benzyl alcohol:benzyl benzoate (BABB)-to-ethanol ratios (1:2, 1:1, 2:1) for 2 hours per step, and placed three times in absolute BABB until the heart sank and appeared clear (approximately 45 minutes to 2 hours depending on the heart size). Each heart was then rehydrated using a decreasing ethanol series from 100% to 25% for approximately 2 to 3 hours and was then labeled with a Periodic Acid-Schiff (PAS) kit (Cat. No. 395B, Sigma-Aldrich Co. LLC.) for 30 minutes according to the manufacturer's protocol until the hearts turned translucent purple. The hearts were then washed, and dehydrated through the ethanol series and BABB:ethanol series as before ending with three 100% BABB washes. Cleared and labeled hearts were placed in a custom-made cover glass-bottom dish (#1.5 or 0.17 mm) to which a glass tube was glued. The diameter of the glass tube and height of the BABB solution were adjusted and the cover glass of the glass tube was sealed with glue (Loctite, Prism, 46040, Electron Microscopy Sciences). To prevent evaporation and tissue movement from drafts during imaging, the top chamber was closed with a cover glass. Heart samples were imaged on a Zeiss LSM 710 NLO system with a two-photon laser (Mai Tai eHP with DeepSee, Newport Corporation), 488 and 561 nm single photon lasers with a regular photomultiplier tube or a 32-channel quasar spectral detector to characterize the emission peaks for PAS-stained samples. The 780 nm excitation wavelength was used to exploit the peak power of the two-photon laser and improve the penetration depth and excite the PAS dye. A Zeiss LSM 700 system with 488 and 55 nm lasers were used for single-photon microscopy tiling. The

images were stitched with 0% overlap using the native Zeiss 2 Black Edition software. Two-dimensional image calculations were performed using Zeiss Axiovision software to obtain morphometric measurements of heart length, width, height, ventricular area, and muscle and myocardial wall dimensions. Each measurement was made from four different locations, which were averaged. The whole-heart, atrial and ventricular volumes were traced in 40 to 50 µm steps through the z-axis using the Surpass module (Contour Tracing Algorithm) in the Imaris Suite software (version 8.0, Bitplane, Inc.). The whole-heart volume was created with the Isosurface module in Imaris following background subtraction, smoothing, and thresholding for the muscle based on the muscle volume intensity. The high-resolution snapshots and movies were made in Imaris. The final images and their intensities were adjusted at min/max display settings to optimize the dynamic range of the gray values of a given image.

Cardiac Myofilament Isolation

Protein analysis was performed using homogenized whole-heart tissue from NTG and cMyBP-C[110kDa] animals with myofilament-enriched fractions. Homogenization was performed using a mechanical bead beater, F-60 buffer (60 mM KCl, 30 mM Imidazole, 2 mM $MgCl_2$) with protease (Roche) and phosphatase (cocktail I [Cat. No. p5726] and II [Cat. No. p0044], Sigma-Aldrich Co. LLC.) inhibitors for myofilament isolations and with or without 1% Triton-X 100. Briefly, the hearts were minced with a scalpel and transferred to a homogenization tube with beads in F60 buffer without Triton-X 100. Hearts were

homogenized twice for 40 seconds while being placed on ice for 5 minutes in between homogenization steps. The samples were centrifuged at 13,000 rpm for 10 minutes at 4°C. The supernatant was then saved (total protein fraction) and F-60 buffer with Triton-X 100 was added to the homogenization tubes. Samples were mixed with a pipette tip, vortexed, homogenized for 30 seconds, and centrifuged as before followed by discarding of the supernatant. This was repeated seven more times. After the final wash, F-60 buffer without Triton-X 100 was added to the samples, which were then vortexed, homogenized for 30 seconds, and centrifuged as before. Urea buffer (50 mM Tris-HCL, pH 7.5, 4 M Urea, 1 M thiourea, 0.4% CHAPS, 20 mM spermine, 20 mM DTT) was then added into heart homogenate samples, which were mixed, vortexed, and centrifuged as before. The resulting supernatant was the myofilament fraction, which was quantified by the Bradford assay (Cat. No. 23236, Thermo Fisher Scientific Inc.) and diluted to 1 µg/ml with 2X gel loading dye. Myofilament samples from NTG and cMyBP-C^{110kDa} hearts were then resolved on 4-15% SDS-PAGE gel cassettes (Cat. No. 456-1083, Bio-Rad Laboratories, Inc.) and stained with Coomassie Brilliant Blue to detect protein (**Figure 13**).

Western Blot Analysis

Western blot analysis to detect FL cMyBP-C, the cMyBP-C^{110kDa} TG protein, and phosphorylation sites of cMyBP-C at serine residues 273, 282, and 302, as well as phosphorylation of cTnI at serine residues 23/24 in NTG and cMyBP-C^{110kDa} myofilament fractions was performed using a Bio-Rad transfer
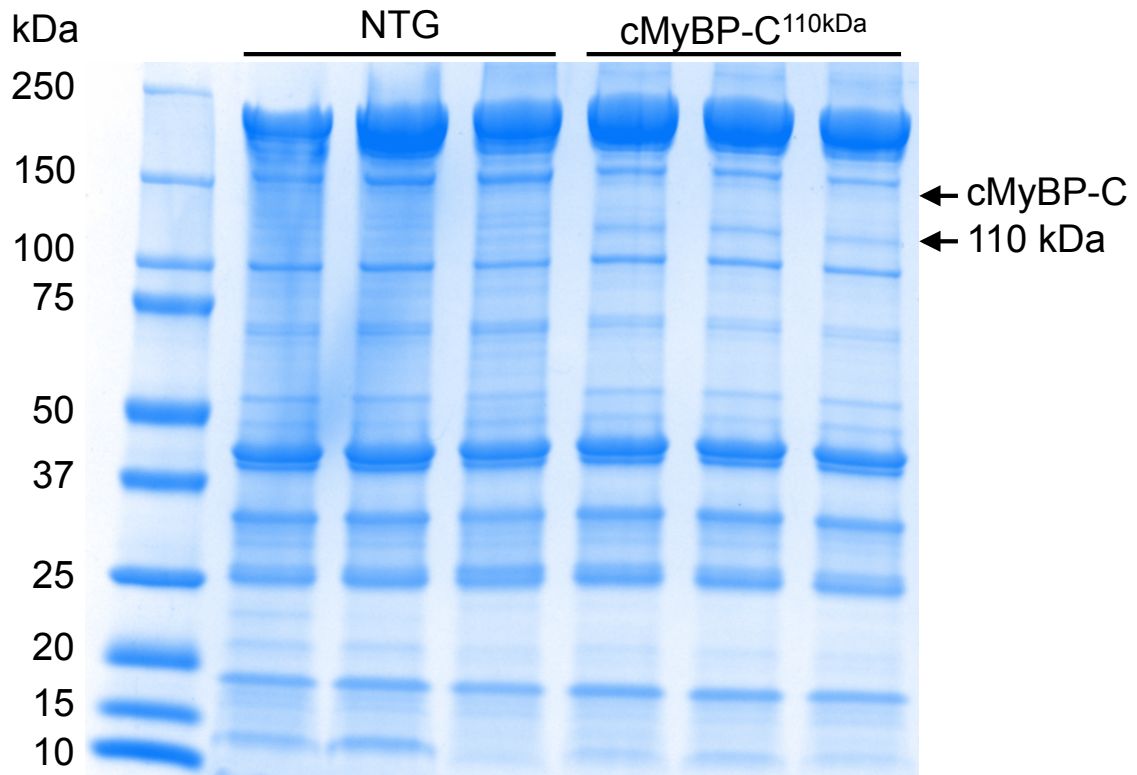
Figure 13. Myofilament Fractions from NTG and cMyBP-C^{110kDa} Hearts. Following myofilament fractionation of NTG and cMyBP-C^{110kDa} hearts, myofilament fractions were run on diagnostic 4-15% SDS-PAGE and stained with Coomassie Brilliant Blue. These samples were then used for Western Blot analysis of the expression levels of total FL cMyBP-C and the cMyBP-C^{110kDa} TG protein as well as for the level of phosphorylation of cMyBP-C at serine residues 273, 282, and 302 and phosphorylation of cTnI at serines 23/24. n = 3 hearts per group.

system. Briefly, myofilament fractions from NTG and cMyBP-C^{110kDa} hearts were resolved on 4-15% SDS-PAGE as described above. Proteins were then transferred to nitrocellulose membranes for 3 hours at 300 milliamps at 4°C. To ensure protein transfer, the membranes were stained with Ponceau S solution (Cat. No. 500-0205, Sigma-Aldrich Co. LLC.) followed by destaining with tris-buffered saline containing 1% Tween-20 (TBS-T) for 5 minutes. To prevent non-specific binding of antibodies, membranes were blocked for 30 minutes with Western Blocking Reagent (Cat. No. 11921673001, Sigma-Aldrich Co. LLC.) diluted 1:10 in TBS-T. Membranes were then incubated overnight at room temperature with the following primary antibodies diluted in blocking solution: anti-cMyBP-C^{C2-14} (Copeland et al., 2010) to detect cMyBP-C's N' region (C0 domain), anti-cMyBP-C^{C10} to detect cMyBP-C's C' region (C10 domain), anti-c-Myc (Cat. No. MA1-980, Thermo Fisher Scientific Inc.) to specifically detect the c-Myc-tagged cMyBP-C^{110kDa} protein, anti-cMyBP-C phosphorylation site-specific antibodies to detect cMyBP-C phosphorylation levels at serine residues 273, 282, and 302 (Govindan, McElligott, et al., 2012), anti-cTnI (Cat No. MAB3150, EMD Millipore Corporation), and an anti-cTnI serine 23/24 phosphorylation site-specific antibody (Cat. No. 4004S, Cell Signaling Technology, Inc.) to detect cTnI phosphorylation levels at serine residues 23/24. The next day, the membranes were washed three times for 5 minutes with TBS-T and were then incubated for 1 hour at room temperature with either donkey anti-mouse IgG-HRP (Cat. No. sc-2314, Santa Cruz Biotechnology, Inc.) or donkey anti-rabbit IgG-HRP (Cat.

No. sc-2305, Santa Cruz Biotechnology, Inc.) secondary antibodies diluted in blocking solution. All membranes were exposed to Amersham ECL Prime Western Blotting Detection reagent (Cat. No. RPN2232, General Electric Company) and were imaged using a Chemidoc XRS+ System with Image Lab Software (Cat. No. 1708265, Bio-Rad Laboratories). Protein and phosphorylation levels were quantified by densitometry using ImageJ (NIH), with the target protein or phosphorylation target normalized to β-actin.

mRNA Isolation and qPCR Analysis

Minced heart tissue from NTG and cMyBP-C^{110kDa} mice was homogenized in 1mL of TriZol (BioRad) using a bead homogenizer, and total RNA was isolated using the Aurum Total RNA Fatty and Fibrous Tissue Kit (Cat. No. 732-6820, Bio-Rad Laboratories) per the manufacturers instructions. Synthesis of cDNA from the mRNA samples was performed using the iScript cDNA synthesis kit (Cat. No. 170-8891, Bio-Rad Laboratories) with 1µg of mRNA template used in each reaction. Templates for qPCR analysis were also generated using no reverse transcriptase, which were used as negative controls. Gene expression levels were analyzed using TaqMan primers recognizing *MYBPC3* with FAM dye (Cat. No. Mm.PT.53a.42655843.g, Integrated DNA Technologies, Inc.), *MYH7*-FAM (Cat. No. Mm.PT.53a.17465550.g, Integrated DNA Technologies, Inc.), *NPPA*-FAM (Cat. No. Mm.PT.56a.10008284.g, Integrated DNA Technologies, Inc.), and *GAPDH*-VIC Dye, (Cat. No. 4352339E, Thermo Fisher Scientific Inc.) with iTaq Universal Probes Supermix (Cat. 172-5131, Bio-Rad Laboratories) and

analyzed using a CFX96 Touch Real-Time PCR Detection System (Cat. No. 1855196, Bio-Rad Laboratories). The cycle protocol was 94°C for 10 minutes, followed by 40 cycles at 94°C for 15 seconds and 60°C for 60 seconds. Analysis of qPCR data was performed using the ΔΔCq method, normalized to the geometric mean of *GAPDH* values and corrected for primer efficiency as described previously (Pfaffl, 2001)

RNA-Seq

Total RNA was isolated from four hearts from NTG and three hearts from cMyBP-C^{110kDa} mice using the same isolation method as described for qPCR analysis above. The four samples from the NTG hearts and the three samples for the cMyBP-C^{110kDa} hearts were pooled by genotype prior to sequencing. These samples were then used for RNA-sequencing at the Loyola Genomics Facility under the direction of Michael Zilliox and Gina Kuffel at Loyola University Chicago. The quality of the total RNA was confirmed with the use of an Agilent 2100 Bioanalzyer. Using the TruSeq® Stranded mRNA Library Prep kit (Cat. No. RS-122-2201, Illumina, Inc.), the mRNA in the total RNA was converted into a library of template molecules of known strand origin. Specifically, the mRNA was isolated using poly-T oligos attached to magnetic beads. The resulting mRNA was fragmented and reverse transcribed. The product cDNA was amplified and sequencing adapters and barcodes were ligated onto the fragments for each respective sample to create cDNA libraries ready for sequencing. The samples were sequenced on the Illumina HiSeq platform rendering 100 bp paired-end

reads. The reads for each sample were aligned to University of California, Santa Cruz's hg19 build of the human genome using STAR aligner. Aligned reads were counted and assigned to genes assuming a negative binomial distribution and DESeq2 was used to perform differential expression.

Mouse Papillary Muscle Extraction

To perform mechanical measurements of muscle function in NTG and cMyBP-C^{110kDa} hearts at 3-months of age, whole hearts were rapidly excised and underwent retrograde perfusion with 1X Krebs-Henseleit Buffer (68.91 g NaCl, 3.727 g KCl, 12 ml of 1 M MgCl$_2$, 2.04 g NaH$_2$PO$_4$ diluted in 1 L for 10X and then diluted to 1X in 500 ml followed by the addition of 1 g D-glucose, 0.84 g NaHCO3, and 0.76 g BDM) via the aorta. The heart was cut to carefully expose the papillary muscles in the LV (**Figure 14**). Papillary muscles were excised under a dissecting scope (Zeiss Discover.V8 Stereo, PlanAPO S 0.63x FWD 81 mm) and permeabilized overnight in 1% Triton X-100 pre-diluted to 10% in mounting relaxing solution (6.3 mM ATP, 6.48 mM MgCl$_2$, 10mM EGTA, 10 mM Na$_2$CrP, 49.76 mM Kprop, 100 mM BES, pH 7.0) at 4°C to remove the cell membrane and membrane-bound proteins. The papillary muscles were then further trimmed into fiber bundles of approximately 1 mm in length under the dissecting microscope. Straight fiber bundles were selected based upon uniformity and attached at each end with aluminum t-clips. NTG and cMyBP-C^{110kDa} papillary muscle and whole heart images were taken under the dissecting scope using an attached digital camera (Canon EOS Rebel T3i). Each fiber
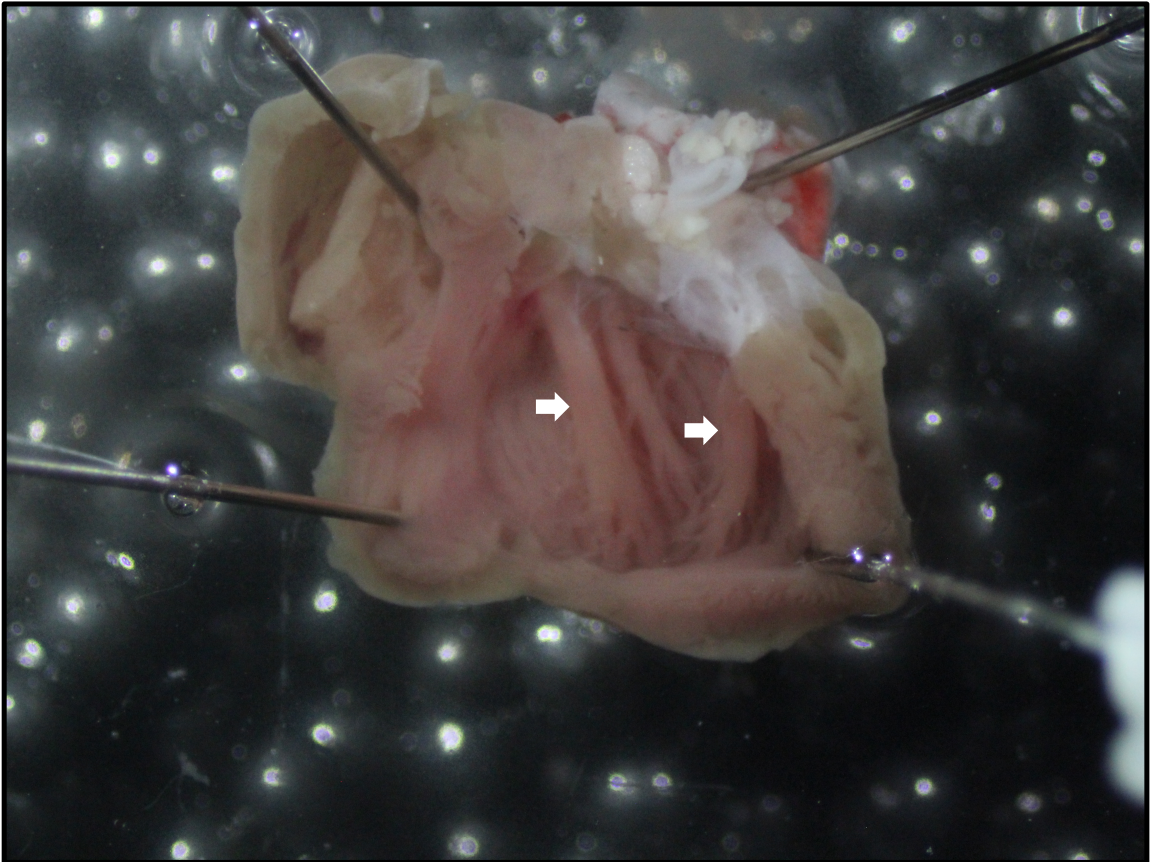
Figure 14. Mouse Papillary Muscle Extraction. Representative image of a mouse heart cut open through the LV to expose the papillary muscles (indicated by white arrows). Papillary muscles were extracted from NTG and cMyBP-C^{110kDa} hearts and were then permeabilized, trimmed, and used to perform mechanical measurements of muscle function using the Force-ATPase assay.

bundle was gently cleansed by washing with fresh relaxing solution on ice and was used within 12 hours. The t-clipped fibers were attached to a force transducer (BAM21-LC; World Precision Instruments) and a high-speed length controller (Aurora Scientific, Inc.). Muscle dimensions (cross-sectional area, length, and volume) were determined using an ocular micrometer mounted in the dissection microscope (resolution, ~10 μm). These muscle dimensions were used to normalize contractile force, sarcomere length, and ATPase activity. Sarcomere length was measured in a passive relaxed condition by laser diffraction as previously described (de Tombe & ter Keurs, 1990), adjusted to and maintained at 2 μm. Briefly, a helium-neon laser beam was directed through the isolated muscle fiber bundle, in which the muscle striation pattern splits the laser beam into a diffraction pattern (**Figure 15**). The striations of the muscle fiber bundle acted as a grating, with known angles of diffraction, and the projected pattern was then used to measure average sarcomere length.

Force-ATPase Assay

Following their preparation, the permeabilized T-clipped papillary muscle fibers from NTG and cMyBP-C^{110kDa} hearts were used on a force-ATPase assay to determine maximal force production, Ca^{2+} sensitivity of force development, tension cost, k$_{tr}$, and cross-bridge stiffness. The permeabilized fibers were incubated for 3 minutes in relaxing solution followed by 3 minutes in preactivating solution before measuring force in activating solution (Witayavanitkul et al., 2014). Activating solution contained 20 mM Ca^{2+}-EGTA, 1.55 mM potassium
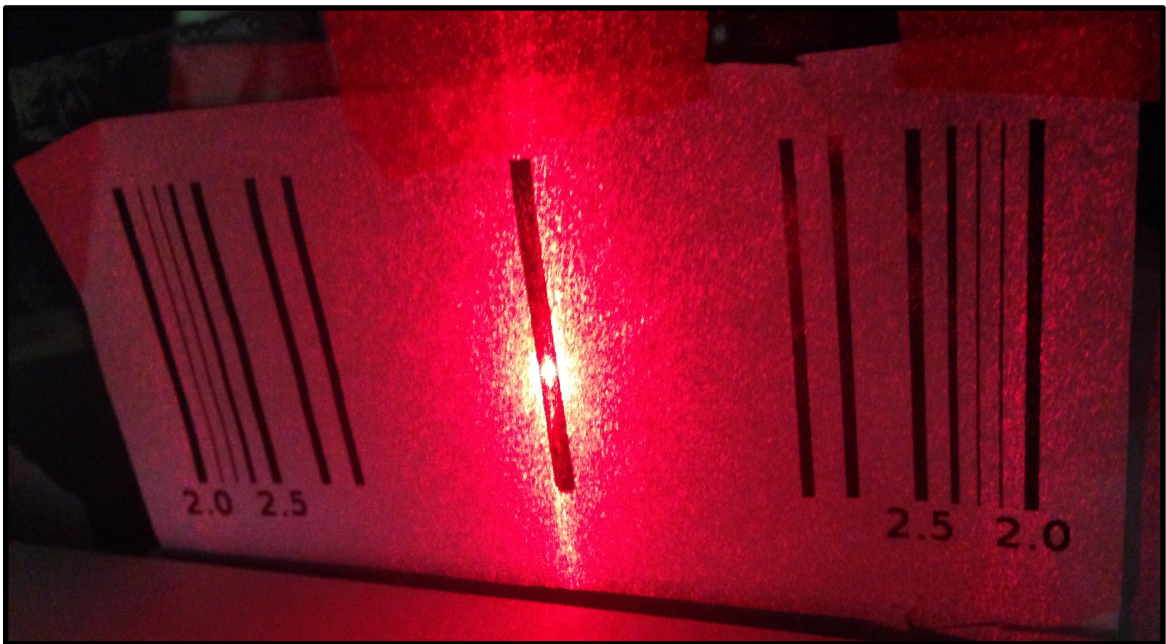
Figure 15. Setting Sarcomere Length by Laser Diffraction. Sarcomere length was measured in a passive relaxed condition by laser diffraction using a helium-neon laser beam directed through the isolated muscle fiber bundle. The muscle striation pattern splits the laser beam into a diffraction pattern and this was used to set and maintain the sarcomere length at 2 µm depicted by laser light intensities at 2.0 in the figure.

propionate, 6.59 mM $MgCl_2$, 100 mM N,N-bis (2-hydroxyethyl) taurine; N,N-Bis-(2-hydroxyethyl)-2-aminoethanesulfonic acid, 5 mM sodium azide, 1 mM DTT, 10 mM phosphoenolpyruvate, 0.01 mM oligomycin, 0.1 mM PMSF, and 0.02 mM A2P5, and a commercial protease inhibitor cocktail (Sigma). Relaxing solution was the same as activating solution, but contained 20 mM EGTA, 21.2 mM potassium propionate, 7.11 mM $MgCl_2$, and no calcium. Preactivating solution was the same as the activating solution, but contained 0.5 mM EGTA, 19.5 mM 1,6-diaminohexane-N,N,N,N'-tetraacetic acid, 21.8 mM potassium propionate, and no calcium. All solutions contained 0.5 mg/ml pyruvate kinase and 0.05 mg/ml lactate dehydrogenase (Sigma) and had an ionic strength of 180 mM, 5 mM free ATP, and 1 mM free magnesium. Isometric tension and ATPase activity were measured at various levels of Ca^{2+} activation as previously described (de Tombe & Stienen, 1995; Rundell, Manaves, Martin, & de Tombe, 2005). Briefly, the isolated muscle was exposed to a range of calcium solutions obtained by proportional mixing of activating and relaxing solutions (described below). The force generated and ATP consumed during muscle contraction were measured simultaneously. Force-pCa relationships were determined by titrating the activation and relaxing solutions (Witayavanitkul et al., 2014). Maximal isometric tension was measured at 100% activation solution, followed by sequential washes in relaxing and preactivating solutions for 3 minutes each. Subsequent measurements of isometric tension occurred in solutions titrated with decreasing ratios of activation-to-relaxation solutions: 100%, 95%, 90%, 85%, 80%, 75%,

70%, 60% and 0% activation solution, which corresponded to pCa values of approximately 4.50, 5.11, 5.38, 5.58, 5.74, 5.96, 6.07, 6.25, and 10.00, respectively, as determined by the Fabiato program (van der Velden, Moorman, & Stienen, 1998). The integrity of the fibers was tested afterwards by measuring maximal tension after the experiment (100% activation). Any fibers that did not maintain 80% or greater maximal tension were excluded from analysis. Force-ATPase relationship was determined using an optical absorbance enzyme assay (Guth & Wojciechowski, 1986). Briefly, ATP consumption was determined by measuring the absorbance of UV light at a wavelength of 340 nm. ATP hydrolyses into ADP and inorganic phosphate inside the fiber, which is stoichiometrically coupled to the oxidation of NADH to NAD+. This oxidization reaction is catalyzed by pyruvate kinase and lactate dehydrogenase in the activating solutions. NADH, but not NAD+, absorbs light specifically at 340 nm. A series of 50 nanoliters (nl) of 10 mM ADP were injected into the activating chamber. Each injection of ADP induced a rapid reduction in fluorescence and allowed the calculation of the rate of ATP consumption, determined by measuring the fluorescent decay rate at 340 nm. After completion of the Force-ATPase assay, papillary muscles underwent a rapid release-restretch maneuver in order to break previously formed cross-bridges and allow cross-bridges to reform. The k_{tr} was then measured at maximal activation, as previously described (Rundell et al., 2005; Swartz & Moss, 1992). Force-pCa and Force-ATPase relationships were fitted with a modified Hill equation (Chandra et al., 2001; Rundell et al.,

2005; Sumandea, Pyle, Kobayashi, de Tombe, & Solaro, 2003). Stiffness and tension costs were fit linearly to the force-stiffness and force-ATPase data, respectively. Stiffness is a measure of attached cross-bridges and is proportional to tension. Stiffness is measured by applying rapid, oscillating length changes and recording the change in force (Δforce/Δlength) (Ford, Huxley, & Simmons, 1977).

Statistical Analysis

All data are represented as the mean ± standard error of the mean (SEM). Statistical analysis was performed using Graph Pad Prism (version 6.0). Data were analyzed using a one-way ANOVA with a Tukey's post-hoc test or a Student's t-test where appropriate. Statistical significance was defined as $P < 0.05$.

CHAPTER FIVE

RESULTS

cMyBP-C^{110kDa} Transgenic Mouse Line Characterization

To determine whether cMyBP-C^{110kDa} mice expressed the cMyBP-C^{110kDa} TG protein missing the N'-C0-C1f region of cMyBP-C compared to NTG animals, which should not express the cMyBP-C^{110kDa} TG protein, I performed Western blot analysis using antibodies against the N' and C' regions of cMyBP-C. Using the previously reported cMyBP-C^{C2-14} antibody that binds the C0 domain of cMyBP-C (Copeland et al., 2010), endogenous FL cMyBP-C protein expression was detected in myofilament fractions from NTG and cMyBP-C^{110kDa} hearts (**Figure 16A**). Endogenous FL cMyBP-C expression was significantly reduced ($p < 0.001$) in myofilament fractions from cMyBP-C^{110kDa} compared to NTG animals (**Figure 16C**). The cMyBP-C^{110kDa} mice were expected to have marginal expression of endogenous FL cMyBP-C as these animals were developed on a NTG background and would likely still express some of the endogenous FL protein. Importantly, the cMyBP-C^{C2-14} N' antibody did not detect the cMyBP-C^{110kDa} TG protein as this protein does not contain the C0 domain to which this antibody binds. The minimal expression levels of endogenous FL cMyBP-C in cMyBP-C^{110kDa} myofilament fractions indicated that the cMyBP-C^{110kDa} TG protein
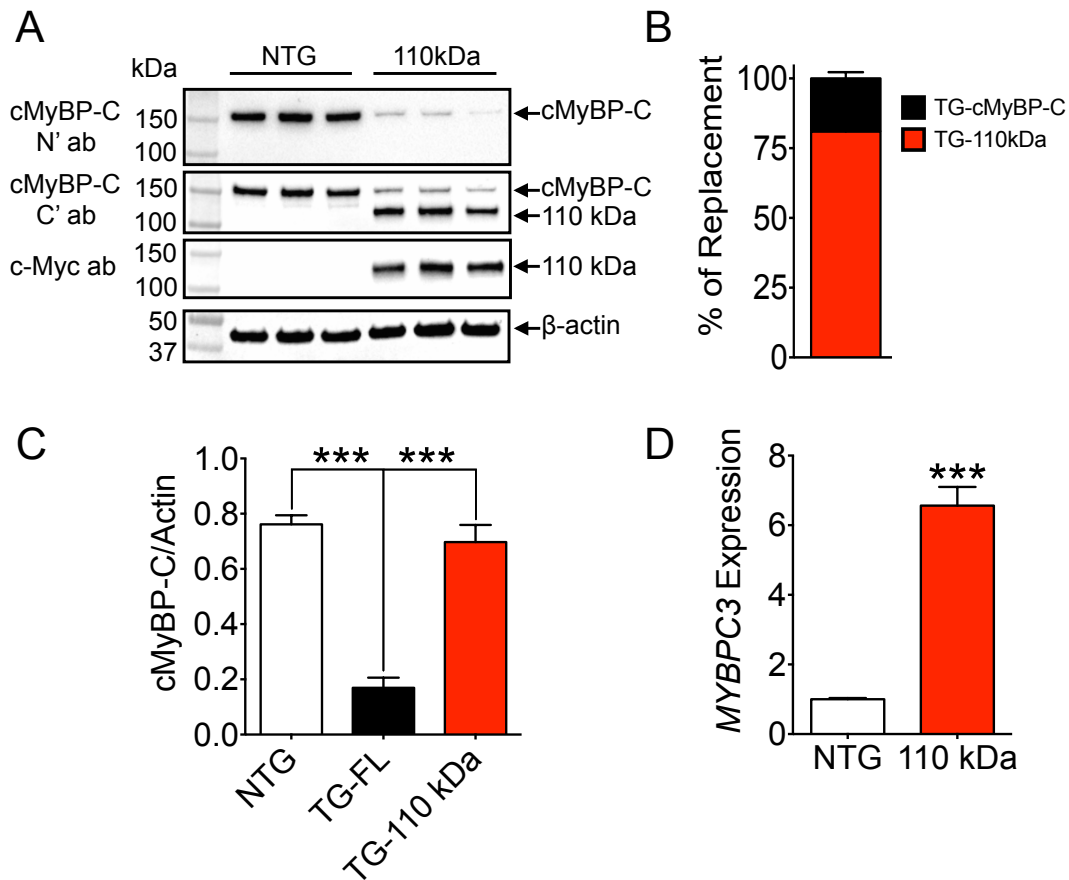
Figure 16. cMyBP-C^{110kDa} Transgenic Mouse Line Characterization. (A) Western blot analysis using cardiac myofilament fractions from NTG and cMyBP-C^{110kDa} mice stained with N', C', and c-Myc antibodies to detect endogenous FL cMyBP-C and the cMyBP-C^{110kDa} TG protein (n = 3 hearts per group). (B) Quantification of sarcomeric percent replacement of endogenous FL cMyBP-C with the cMyBP-C^{110kDa} TG protein in cMyBP-C^{110kDa} hearts quantified from Western blot data presented in A. (C) Densitometry quantifications of endogenous FL cMyBP-C from NTG and cMyBP-C^{110kDa} myofilament fractions measured from Western blot data presented in A. (D) qPCR quantifications of *MYBPC3* gene expression normalized to *GAPDH* in whole hearts from NTG and cMyBP-C^{110kDa} mice (n = 4 hearts per group). ***$p < 0.001$.

was located within, and may replace, the endogenous FL protein in cMyBP-C^{110kDa} sarcomeres. Western blot analysis using a C' antibody against cMyBP-C's C10 domain detected the cMyBP-C^{110kDa} TG protein within myofilament fractions from cMyBP-C^{110kDa} hearts but not NTG hearts (**Figure 16A**). The expression of the cMyBP-C^{110kDa} TG protein was detected at 110 kDa and was significantly elevated ($p < 0.001$) compared to the expression of FL cMyBP-C in cMyBP-C^{110kDa} myofilament fractions (**Figure 16C**). As expected, the cMyBP-C^{110kDa} TG protein was not detected in NTG myofilament fractions (**Figure 16A**). Importantly, cMyBP-C^{110kDa} TG protein expression was significantly increased compared to endogenous FL cMyBP-C expression (81 ± 2.2% cMyBP-C^{110kDa} TG protein vs 19 ± 2.2% FL cMyBP-C; $p < 0.0001$) in cMyBP-C^{110kDa} myofilament fractions (**Figure 16B**). The cMyBP-C^{110kDa} TG protein is c-Myc-tagged at its N' region. Therefore, using an anti-c-Myc antibody, the cMyBP-C^{110kDa} TG protein was exclusively detected within cMyBP-C^{110kDa} myofilament fractions and not in those from NTG hearts (**Figure 16A**). The endogenous FL cMyBP-C protein is not c-Myc-tagged. Accordingly, the endogenous FL cMyBP-C protein was not detected by the anti-c-Myc antibody in myofilament fractions from cMyBP-C110^{kDa} and NTG hearts (**Figure 16A**). As the cMyBP-C^{110kDa} mouse is a TG animal, expectedly, the levels of total cardiac *MYBPC3* gene expression (quantified from FL *MYBPC3* mRNA expression in NTG hearts and FL *MYBPC3* plus cMyBP-C^{110kDa}-*MYBPC3* mRNA expression in cMyBP-C^{110kDa} hearts) were significantly augmented ($p < 0.001$) in cMyBP-C^{110kDa} hearts compared to NTG

hearts (**Figure 16D**). Together, these data demonstrate that the cMyBP-C^{110kDa} TG protein is expressed only within cMyBP-C^{110kDa} hearts and replaces endogenous FL cMyBP-C within the cardiac sarcomere, verifying the mouse model.

cMyBP-C^{110kDa} Mice Display Reduced Cardiac Function

After confirming that the cMyBP-C^{110kDa} TG protein is expressed only within cMyBP-C^{110kDa} hearts, I next performed short-axis M-mode echocardiography on NTG and cMyBP-C^{110kDa} mice to evaluate cardiac function in these animals at 3- and 6-months of age (**Figure 17**). No significant difference in IVSd (**Figure 17A**), IVSs (**Figure 17B**), LVIDd (**Figure 17C**), LVPWd (**Figure 17E**), LVPWs (**Figure 17F**), or LV volume at end diastole (**Figure 17I**) was observed between NTG and cMyBP-C^{110kDa} hearts at either 3- or 6-months of age. However, LVIDs (**Figure 17D**) and LV chamber volume at end systole (**Figure 17J**) were significantly increased ($p < 0.05$) in cMyBP-C^{110kDa} compared to NTG hearts at 6-months of age. Crucially, there was a significant decrease ($p < 0.05$) in LV percent EF (**Figure 17G**) and percent FS (**Figure 17H**) in cMyBP-C^{110kDa} hearts compared to NTG hearts at 3-months of age. Percent EF (**Figure 17G**) and percent FS (**Figure 17H**) were even further reduced ($p < 0.0001$) in cMyBP-C^{110kDa} hearts compared to NTG hearts by 6-months of age. Furthermore, percent EF and percent FS were significantly reduced ($p < 0.05$) in cMyBP-C^{110kDa} hearts at 6-months of age compared to cMyBP-C^{110kDa} hearts at 3-months of age, indicating disease progression. Summarized short-axis M-mode
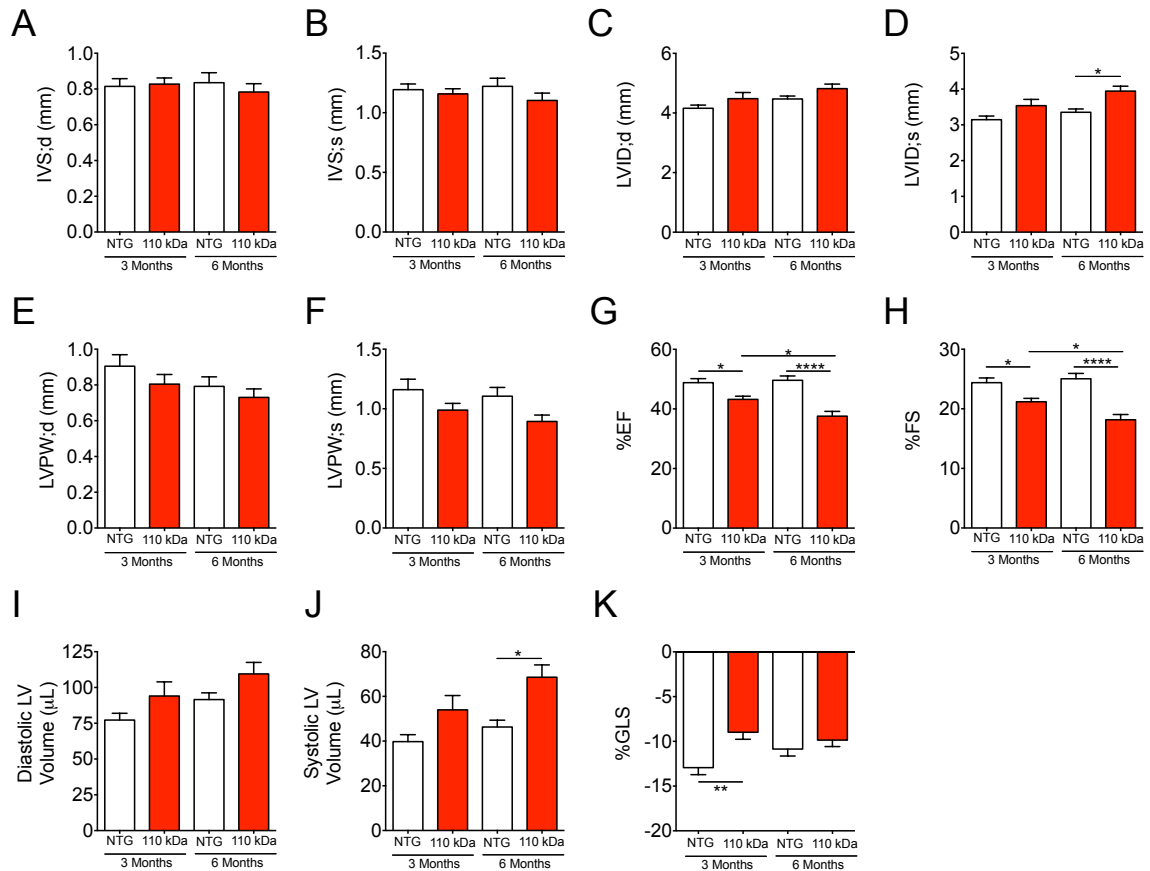
Figure 17. cMyBP-C[110kDa] Mice Display Reduced Cardiac Function. Short-axis M-mode echocardiography data quantified from NTG and cMyBP-C[110kDa] hearts at 3- and 6-months of age depicting (A) IVSd, (B) IVSs, (C) LVIDd, (D) LVIDs, (E) LVPWd, (F) LVPWs, (G) percent EF, (H) percent FS, (I) LV chamber volume during diastole, (J) LV chamber volume during systole, and (K) percent GLS. n = 7-10 hearts per group. *$p < 0.05$, **$p < 0.01$, ****$p < 0.0001$.

echocardiography quantification values by age and genotype are presented in **Table 1**. Summarized short-axis M-mode echocardiography quantification values by age, genotype, and gender are presented in **Table 2**. Finally, percent GLS was significantly reduced in cMyBP-C^{110kDa} hearts compared to NTG hearts at 3-months of age ($p < 0.01$) (**Figure 17K**). Together, these data demonstrate that cMyBP-C^{110kDa} mice develop cardiac dysfunction that begins near 3-months of age and progresses to severity by 6-months of age.

Cardiac Enlargement in cMyBP-C^{110kDa} Mice

Echocardiography analysis revealed overt cardiac dysfunction and increased LV chamber size in cMyBP-C^{110kDa} compared to NTG animals. Therefore, I next performed whole heart cardiac imaging by two-photon confocal microscopy to evaluate cardiac muscle organization, size, and morphology using hearts from cMyBP-C^{110kDa} and NTG animals at 4-months of age. These experiments were performed to better understand if and how the heart compensates and remodels when the N'-C0-C1f region of cMyBP-C is absent to determine whether the N' region of cMyBP-C is necessary for maintaining normal cardiac morphology. Imaging of isolated, perfused whole hearts depicted an increase in the size of cMyBP-C^{110kDa} hearts compared to NTG hearts (**Figure 18A**). This was further confirmed by 2-D confocal microscopy images of whole hearts from NTG and cMyBP-C^{110kDa} animals, which revealed an increase in the size of the LV and RV chambers in cMyBP-C^{110kDa} heart sections compared to those from NTG animals (**Figure 18 B, C**). Quantifications of 3-D confocal

	3-Months		6-Months	
	NTG	**cMyBP-C^{110kDa}**	**NTG**	**cMyBP-C^{110kDa}**
IVS;d (mm)	0.81 ± 0.04	0.83 ± 0.03	0.84 ± 0.06	0.78 ± 0.05
IVS;s (mm)	1.19 ± 0.05	1.16 ± 0.04	1.22 ± 0.07	1.10 ± 0.06
LVID;d (mm)	4.16 ± 0.11	4.48 ± 0.20	4.47 ± 0.10	4.82 ± 0.15
LVID;s (mm)	3.15 ± 0.10	3.54 ± 0.18	3.35 ± 0.09	3.94 ± 0.14
LVPW;d (mm)	0.90 ± 0.06	0.80 ± 0.05	0.79 ± 0.05	0.73 ± 0.05
LVPW;s (mm)	1.16 ± 0.09	0.99 ± 0.06	1.11 ± 0.07	0.89 ± 0.05
%EF	48.81 ± 1.35	43.20 ± 1.06	49.60 ± 1.45	37.58 ± 1.61
%FS	24.38 ± 0.79	21.18 ± 0.57	25.04 ± 0.90	18.17 ± 0.88
LV Volume;d (µl)	77.22 ± 4.76	94.07 ± 9.86	91.55 ± 4.69	109.50 ± 8.04
LV Volume;s (µl)	39.75 ± 3.12	53.99 ± 6.38	46.29 ± 3.06	68.55 ± 5.54
%GLS	-12.94 ± 0.73	-8.98 ± 0.74	-10.86 ± 0.74	-9.86 ± 0.72

d = diastole; EF = Ejection Fraction; GLS = Global Longitudinal Strain; FS = Fractional Shortening; IVS = Interventricular Septum; LVID = Left Ventricular Internal Diameter; LVPW = Left Ventricular Posterior Wall; s = systole

Table 1. Short-Axis M-Mode Echocardiography Data from NTG and cMyBP-C^{110kDa} Mice at 3- and 6-Months of Age.

	3-Months				6-Months			
	NTG Female	NTG Male	cMyBP-C[110kDa] Female	cMyBP-C[110kDa] Male	NTG Female	NTG Male	cMyBP-C[110kDa] Female	cMyBP-C[110kDa] Male
IVS;d (mm)	0.79 ± 0.06	0.86 ± 0.06	0.79 ± 0.06	0.85 ± 0.04	0.81 ± 0.08	0.88 ± 0.04	0.67 ± 0.06	0.85 ± 0.04
IVS;s (mm)	1.16 ± 0.06	1.25 ± 0.07	1.08 ± 0.07	1.21 ± 0.05	1.20 ± 0.10	1.27 ± 0.01	0.97 ± 0.13	1.18 ± 0.04
LVID;d (mm)	3.99 ± 0.09	4.44 ± 0.13	4.24 ± 0.27	4.64 ± 0.29	4.40 ± 0.14	4.62 ± 0.07	4.36 ± 0.08	5.09 ± 0.12
LVID;s (mm)	3.00 ± 0.10	3.39 ± 0.13	3.32 ± 0.21	3.68 ± 0.25	3.29 ± 0.13	3.48 ± 0.05	3.55 ± 0.14	4.18 ± 0.10
LVPW;d (mm)	0.92 ± 0.05	0.89 ± 0.18	0.79 ± 0.05	0.81 ± 0.09	0.76 ± 0.06	0.86 ± 0.12	0.71 ± 0.09	0.74 ± 0.06
LVPW;s (mm)	1.17 ± 0.13	1.14 ± 0.13	1.03 ± 0.08	0.96 ± 0.08	1.05 ± 0.05	1.22 ± 0.20	0.91 ± 0.07	0.88 ± 0.08
%EF	49.58 ± 1.92	47.52 ± 1.82	44.19 ± 1.59	42.55 ± 1.47	50.05 ± 2.22	48.69 ± 0.21	38.78 ± 3.24	36.85 ± 1.94
%FS	24.78 ± 1.15	23.72 ± 1.06	21.66 ± 0.90	20.86 ± 0.77	25.31 ± 1.37	24.50 ± 0.14	18.69 ± 1.77	17.85 ± 1.07
LV Volume;d (μl)	69.75 ± 3.86	89.67 ± 6.16	81.96 ± 11.86	102.14 ± 14.25	88.24 ± 6.62	98.17 ± 3.42	86.08 ± 3.56	123.55 ± 6.74
LV Volume;s (μl)	35.29 ± 2.90	47.19 ± 4.33	45.78 ± 6.63	59.46 ± 9.47	44.25 ± 4.41	50.37 ± 1.70	52.92 ± 4.86	77.93 ± 4.49
%GLS	-11.54 ± 0.64	-14.8 ± 0.46	-10.33 ± 1.4	-7.91 ± 0.55	-9.45 ± 0.63	-12.70 ± 1.17	-9.79 ± 1.19	-9.9 ± 1.02

d = diastole; EF = Ejection Fraction; GLS = Global Longitudinal Strain; FS = Fractional Shortening; IVS = Interventricular Septum; LVID = Left Ventricular Internal Diameter; LVPW = Left Ventricular Posterior Wall; s = systole

Table 2. Short-Axis M-Mode Echocardiography Data from NTG and cMyBP-C[110kDa] Mice at 3- and 6-Months of Age Dichotomized by Gender.
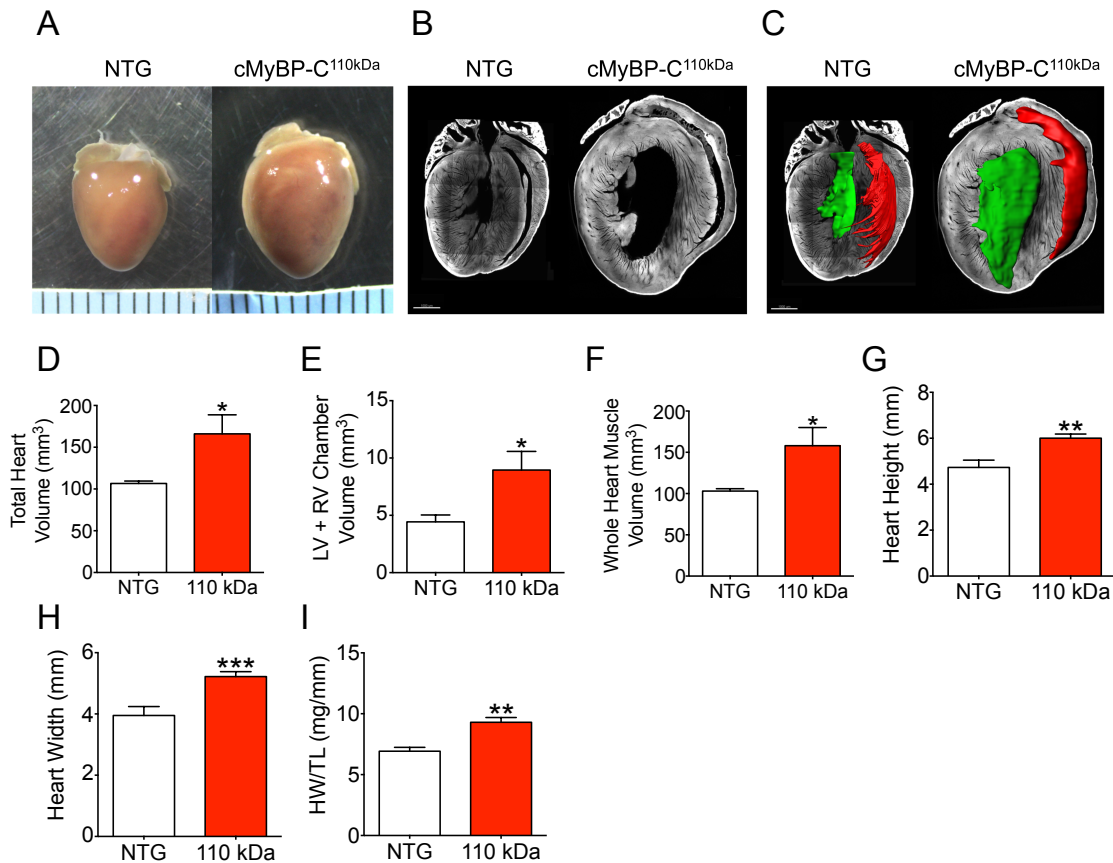
Figure 18. Cardiac Enlargement in cMyBP-C^{110kDa} Mice. (A) A representative whole heart image from NTG and cMyBP-C^{110kDa} mice showing relative heart size. (B) 2-D long-axis imaging by confocal microscopy of hearts from NTG and cMyBP-C^{110kDa} mice showing wall thickness and chamber size. (C) 2-D long-axis imaging by confocal microscopy of hearts from NTG and cMyBP-C^{110kDa} mice with RV and LV volumes filled in to represent blood volume. 3-D confocal microscopy images of NTG and cMyBP-C^{110kDa} hearts were used to quantify (D) total heart volume, (E) LV plus RV chamber volume, and (F) whole heart muscle volume. 2-D confocal microscopy images of NTG and cMyBP-C^{110kDa} hearts were used to quantify (G) heart height and (H) heart width. Quantifications in D-H are from n = 5 hearts per group. (I) Quantification of HW/TL ratio in cMyBP-C^{110kDa} and NTG mice (n = 4 hearts per group). Scale bar = 1 mm in B and C. *p < 0.05, **p < 0.01, ***p < 0.001.

microscopy images demonstrated a significant increase ($p < 0.05$) in total heart volume (**Figure 18D**), LV plus RV chamber volume (**Figure 18E**), and whole heart muscle volume (**Figure 18F**) in hearts from cMyBP-C^{110kDa} compared to NTG animals. Additionally, quantifications of 2-D confocal microscopy images demonstrated a significant elevation in both the height ($p < 0.01$) (**Figure 18G**) and width ($p < 0.001$) (**Figure 18H**) of hearts from cMyBP-C^{110kDa} compared to NTG animals. cMyBP-C^{110kDa} mice also had a significant elevation in the ratio of heart weight (HW) to tibia length (TL) compared to NTG mice (**Figure 18I**). Together, these data indicate that the N'-C0-C1f region of cMyBP-C is necessary for maintaining normal global cardiac morphology as the absence of this region leads to pathological remodeling in cMyBP-C^{110kDa} hearts.

Cardiac Hypertrophy Markers are Elevated in cMyBP-C^{110kDa} Mice

Whole isolated heart and confocal microscopy imaging revealed cardiac hypertrophy in cMyBP-C^{110kDa} mice. Therefore, I next determined whether pathological hypertrophy markers were increased in the hearts of cMyBP-C^{110kDa} mice compared to hearts from NTG mice at 7-8 months of age. Indeed, qPCR analysis showed a significant increase in mRNA expression levels of the hypertrophy markers *MYH7* (**Figure 19A**) and *NPPA* (**Figure 19B**) in cMyBP-C^{110kDa} compared to NTG hearts, verifying myocardial hypertrophy in cMyBP-C^{110kDa} hearts at the molecular level. This was further confirmed by RNA-sequencing of mRNA isolated from cMyBP-C^{110kDa} and NTG hearts (**Figure 19C**). As expected, *MYBPC3* gene expression levels were found to be
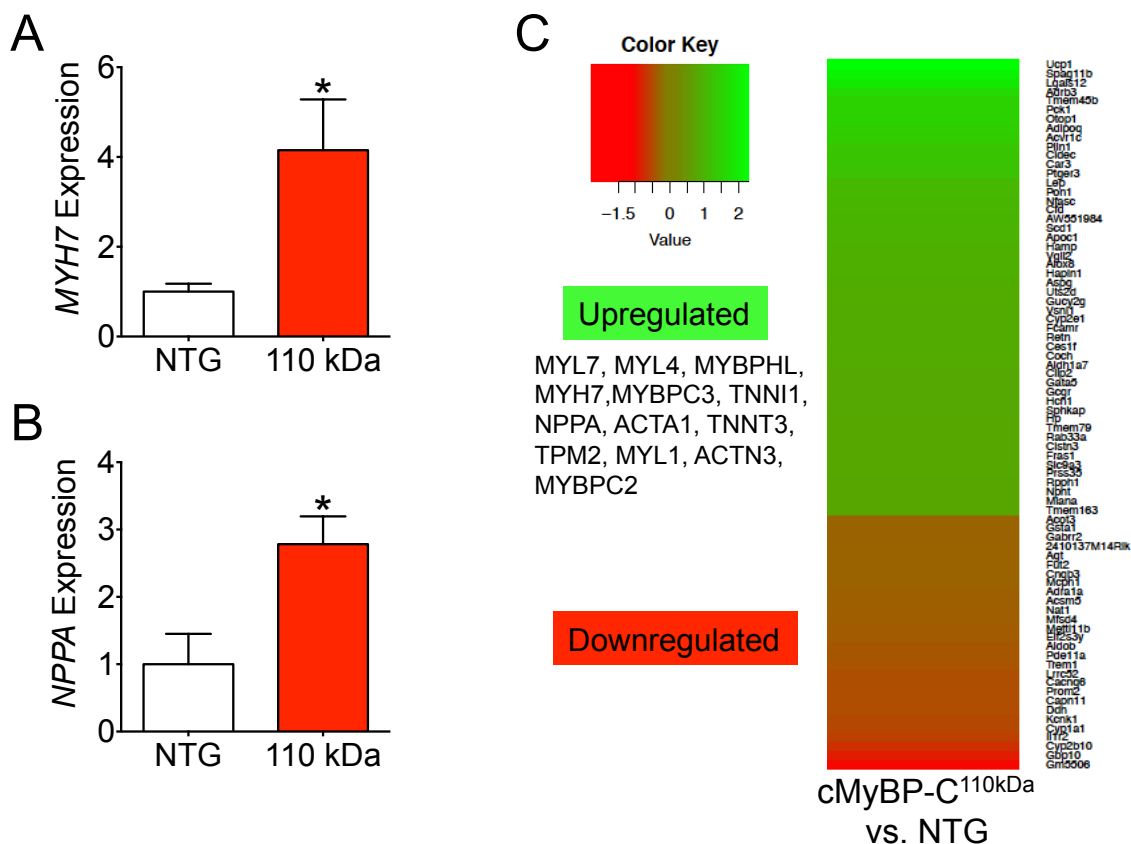
Figure 19. Cardiac Hypertrophy Markers are Elevated in cMyBP-C[110kDa] Hearts. qPCR quantifications of (A) *MYH7* and (B) *NPPA* gene expression levels normalized to *GAPDH* in whole hearts from NTG and cMyBP-C[110kDa] mice (n = 4 hearts per group). Heat map depicting the top 50 upregulated and bottom 29 downregulated genes in cMyBP-C[110kDa] hearts compared to NTG hearts as determined by RNA-sequencing (n = 4 NTG hearts, 3 cMyBP-C[110kDa] hearts, mRNA samples were pooled within each group). Upregulated sarcomeric protein genes are listed to the left of the heat map. *p < 0.05.

upregulated by RNA-sequencing, confirming our qPCR data (**Figure 16D**). Surprisingly, RNA-sequencing further revealed a significant upregulation in several sarcomeric proteins including many skeletal isoforms of these proteins (**Figure 19C**). Importantly, gene expression levels *MYBPC2*, which encodes the fast-skeletal isoform of MyBP-C, were found to be upregulated in cMyBP-C^{110kDa} hearts compared to NTG hearts (**Figure 19C**). The expression of fast-skeletal MyBP-C has been previously detected in cMyBP-C null hearts undergoing dilation (Lin et al., 2013). Total global gene expression changes of the top upregulated and bottom downregulated genes in cMyBP-C^{110kDa} compared to NTG hearts are presented in **Table 3** and **Table 4**, respectively. Together, these data further support that the N'-C0-C1f region of cMyBP-C is necessary for regulating cardiac contraction as its absence leads to overt cardiac hypertrophy at the level of the cardiomyocyte that translates into global cardiac remodeling.

Fibrosis and Sarcomere Area are Increased in cMyBP-C^{110kDa} Hearts

I next sought to investigate whether the cardiac remodeling observed in cMyBP-C^{110kDa} hearts was accompanied by myocardial fibrosis and altered myocyte sarcomere area. H&E and MT staining of myocardial sections from NTG and cMyBP-C^{110kDa} hearts (**Figure 20A**) revealed no significant difference in percent nuclear area (**Figure 20B**) quantified from H&E labeled sections between these groups. However, a highly significant ($p < 0.0001$) elevation in percent fibrosis (**Figure 20C**) quantified from MT labeled sections was observed in cMyBP-C^{110kDa} hearts compared to NTG hearts. This was largely localized

Gene	NTG	cMyBP-C^{110kDa}	FoldChange
Ucp1	6	1194	199.00
Spag11b	1	128	128.00
Lgals12	1	85	85.00
Acsm3	1	70	70.00
Adrb3	3	139	46.33
Tmem45b	6	210	35.00
Pck1	27	942	34.89
Otop1	2	66	33.00
Adipoq	18	497	27.61
Acvr1c	2	53	26.50
Plin1	18	382	21.22
Cidec	26	523	20.12
Car3	179	3282	18.34
Ptger3	4	70	17.50
Lep	10	118	11.80
Pon1	4	46	11.50
Nfasc	10	108	10.80
Cfd	103	1082	10.50
AW551984	6	59	9.83
Scd1	1262	12237	9.70
Apoc1	11	104	9.45
Hamp	35	317	9.06
Vgll2	15	131	8.73
Alox8	10	86	8.60
Hapln1	5	43	8.60
Aspg	10	79	7.90
Uts2d	6	44	7.33
Gucy2g	5	36	7.20
Vsnl1	7	50	7.14
Cyp2e1	64	449	7.02
Fcamr	5	35	7.00
Retn	13	89	6.85
Ces1f	5	34	6.80
Coch	9	61	6.78
Aldh1a7	9	59	6.56
Cilp2	230	1478	6.43
Gata5	17	108	6.35
Gcgr	18	113	6.28
Hcn1	67	417	6.22
Sphkap	31	191	6.16
Hp	115	699	6.08
Tmem79	12	72	6.00
Rab33a	6	36	6.00
Clstn3	20	118	5.90
Fras1	71	416	5.86
Slc9a3	14	82	5.86
Prss35	7	41	5.86
Rpph1	6	35	5.83
Npnt	31	178	5.74

Table 3. Top Upregulated Genes in cMyBP-C^{110kDa} Compared to NTG Hearts by RNA-Sequencing.

Gene	NTG	cMyBP-C^{110kDa}	FoldChange
Mlana	49	277	5.65
Tmem163	212	1182	5.58
Cd207	29	160	5.52
Elovl6	75	413	5.51
Rbp4	18	99	5.50
4833424O15Rik	19	103	5.42
Cdh3	12	65	5.42
Cdo1	156	823	5.28
Mpz	16	84	5.25
Myl7	8057	41920	5.20
Igj	24	123	5.13
Lingo1	52	260	5.00
Gpr81	11	55	5.00
Hydin	11	55	5.00
Prr15l	9	45	5.00
Acaa1b	8	40	5.00
Mybphl	1337	6621	4.95
Stmnd1	7	34	4.86
Rxfp1	36	174	4.83
Prkar2b	107	512	4.79
Dmkn	9	43	4.78
Lrp8	39	186	4.77
Dkk3	1772	8355	4.72
Nsg2	7	33	4.71
Apol9b	7	33	4.71
Fgf12	356	1656	4.65
Myl4	9363	43345	4.63
Vwc2	12	55	4.58
Casq1	446	2040	4.57
Miat	9	41	4.56
Nwd1	9	41	4.56
Capn6	15	68	4.53
Cpne5	95	428	4.51
Lypd1	12	54	4.50
Sln	2373	10632	4.48
Lman1l	23	103	4.48
Myh7	15849	70398	4.44
Ntrk3	49	217	4.43
Dfna5	12	53	4.42
Tbx15	23	101	4.39
Ipcef1	8	35	4.38
Sh2d5	8	35	4.38
Unc5c	15	65	4.33
Frmpd1	19	82	4.32
Ifltd1	152	655	4.31
Adamts19	46	198	4.30
1700055N04Rik	17	73	4.29
Plekha7	313	1341	4.28
E030013I19Rik	13	55	4.23
Arxes2	18	76	4.22
Cacna2d2	278	1157	4.16

Table 3 (Continued). Top Upregulated Genes in cMyBP-C^{110kDa} Compared to NTG Hearts by RNA-Sequencing.

Gene	NTG	cMyBP-C110kDa	FoldChange
Slc7a7	225	931	4.14
Pnpla3	106	438	4.13
Fasn	2008	8291	4.13
Trim10	16	66	4.13
Mybpc3	269005	1108179	4.12
Glb1l2	19	78	4.11
Camk1g	25	102	4.08
Acp5	38	152	4.00
Tnni1	19	76	4.00
Shank2	12	48	4.00
Tmem132e	11	44	4.00
Wnt2b	10	40	4.00
Paqr6	17	67	3.94
Itih2	23	90	3.91
Dkk2	9	35	3.89
Nppa	37866	146881	3.88
Igfbpl1	36	139	3.86
Slc6a7	20	77	3.85
Nnat	30	115	3.83
Sytl1	12	46	3.83
Apol6	34	130	3.82
Gm1078	1876	7087	3.78
Mdfi	52	196	3.77
Sytl2	137	516	3.77
1500015O10Rik	25	94	3.76
Stk32b	52	195	3.75
Ccl3	12	45	3.75
Pitx2	22	82	3.73
Necab3	11	41	3.73
Tub	13	48	3.69
Itih4	101	372	3.68
Gypa	31	113	3.65
Acta1	12784	46462	3.63
Gpr158	16	58	3.63
Sost	45	163	3.62
Lpar3	13	47	3.62
2900041M22Rik	10	36	3.60
Dlgap1	27	97	3.59
Klf8	17	61	3.59
E2f2	47	168	3.57
Flrt1	28	100	3.57
Psd	14	50	3.57
2610307P16Rik	18	64	3.56
Krt8	24	85	3.54
Vdr	61	216	3.54
Cib2	41	145	3.54
Arnt2	19	67	3.53
Cacna2d3	58	203	3.50
Fam180a	12	42	3.50
Ikzf3	15	52	3.47

Table 3 (Continued). Top Upregulated Genes in cMyBP-C110kDa Compared to NTG Hearts by RNA-Sequencing.

Gene	NTG	cMyBP-C110kDa	FoldChange
Cacna1h	1487	5145	3.46
Dock3	31	107	3.45
Apol11b	64	218	3.41
Ppp1r1b	204	694	3.40
Vat1l	10	34	3.40
Cacna1d	123	417	3.39
Car5b	40	135	3.38
Gm11627	22	74	3.36
Cnn1	169	565	3.34
Nrtn	140	465	3.32
Sypl2	68	225	3.31
Diras2	13	43	3.31
Adamts8	63	208	3.30
Epyc	24	79	3.29
Proca1	24	79	3.29
Nox4	60	195	3.25
Camk1d	299	958	3.20
Clic6	18	57	3.17
Ntrk2	55	174	3.16
Bmp3	32	101	3.16
Piezo2	41	129	3.15
Krt7	35	110	3.14
Tro	75	235	3.13
Wnt2	16	50	3.13
Fcho1	33	103	3.12
Slc4a1	111	345	3.11
Trim46	38	118	3.11
Greb1	31	96	3.10
Peg12	13	40	3.08
Fbln7	40	123	3.08
Lck	15	46	3.07
Cyp26b1	417	1273	3.05
Dok5	20	61	3.05
Ifitm10	21	64	3.05
Prdm6	19	57	3.00
Ngef	14	42	3.00
Gpr75	13	39	3.00
Gpr21	13	39	3.00
Syn1	13	39	3.00
Bmp10	756	2262	2.99
Rgs1	51	152	2.98
Neb	281	835	2.97
Edn3	317	940	2.97
Bnc1	24	71	2.96
A2m	37	109	2.95
Clec11a	45	132	2.93
Wisp1	100	293	2.93
Inhba	14	41	2.93
Drp2	27	79	2.93

Table 3 (Continued). Top Upregulated Genes in cMyBP-C110kDa Compared to NTG Hearts by RNA-Sequencing.

Gene	NTG	cMyBP-C[110kDa]	FoldChange
Ptgs2	311	909	2.92
Stra6	12	35	2.92
Xylb	12	35	2.92
Scml2	31	90	2.90
Col4a6	156	450	2.88
Faim2	17	49	2.88
Gja5	704	2029	2.88
Pou2f2	24	69	2.88
Adcy1	341	979	2.87
Aif1l	124	356	2.87
Xlr4a	15	43	2.87
Epha1	14	40	2.86
Srcin1	20	57	2.85
Slc4a11	12	34	2.83
Bex4	12	34	2.83
Gpr162	58	164	2.83
Bend6	40	113	2.83
Xpnpep2	40	113	2.83
Nr5a2	34	96	2.82
Nkain2	16	45	2.81
1600029D21Rik	16	45	2.81
Comp	335	940	2.81
Olfm1	462	1295	2.80
Srgap3	66	185	2.80
Kcnn4	14	39	2.79
Fam167a	18	50	2.78
Cdcp1	18	50	2.78
Adam33	133	369	2.77
Selp	31	86	2.77
Dio2	75	208	2.77
Upk1b	77	213	2.77
Zfp579	466	1286	2.76
Adig	48	132	2.75
Prrt1	28	77	2.75
Sfrp5	245	670	2.73
Col14a1	822	2245	2.73
Hs6st2	26	71	2.73
Scara3	146	398	2.73
Lrrn4	98	267	2.72
Ebi3	21	57	2.71
Pou2af1	21	57	2.71
Kcnq5	14	38	2.71
Irs3	14	38	2.71
Ephb2	31	84	2.71
Duox2	17	46	2.71
Mpzl2	27	73	2.70
Gli1	93	251	2.70
Nlrp5-ps	23	62	2.70
Flywch2	13	35	2.69
Mfap4	535	1440	2.69

Table 3 (Continued). Top Upregulated Genes in cMyBP-C[110kDa] Compared to NTG Hearts by RNA-Sequencing.

Gene	NTG	cMyBP-C110kDa	FoldChange
Fgfr2	42	113	2.69
Rbm47	32	86	2.69
Map3k9	16	43	2.69
St8sia1	16	43	2.69
Panx2	74	198	2.68
Ptprv	24	64	2.67
Prss12	15	40	2.67
Stk32a	44	117	2.66
Stard10	2321	6152	2.65
Gpr39	17	45	2.65
Rnf43	18	47	2.61
Podn	1425	3719	2.61
Tnnt3	28	73	2.61
Rab3b	91	236	2.59
Cybrd1	63	163	2.59
4833418N02Rik	24	62	2.58
Galnt12	24	62	2.58
Enkur	35	90	2.57
1190002F15Rik	14	36	2.57
Vstm5	14	36	2.57
Mmp3	262	673	2.57
Nkain4	67	172	2.57
Pycr1	30	77	2.57
Ap1s3	27	69	2.56
Nov	253	646	2.55
Gpr114	20	51	2.55
Spsb4	285	726	2.55
Cit	44	112	2.55
Slc1a7	35	89	2.54
Clec4a2	50	127	2.54
Shisa2	63	160	2.54
H1fx	26	66	2.54
Acsbg1	26	66	2.54
9330179D12Rik	34	86	2.53
Tpm2	2002	5061	2.53
3-Sep	57	144	2.53
Rpp25	84	212	2.52
Edil3	24	60	2.50
Esr1	14	35	2.50
Atp6v0a4	14	35	2.50
Xist	4181	10414	2.49
Gas2l3	99	246	2.48
Slc38a1	458	1136	2.48
Chad	25	62	2.48
Mum1l1	90	223	2.48
Kif1a	132	327	2.48
Brsk1	105	260	2.48
1700034H15Rik	19	47	2.47
Ms4a1	19	47	2.47
6330403K07Rik	17	42	2.47

Table 3 (Continued). Top Upregulated Genes in cMyBP-C110kDa Compared to NTG Hearts by RNA-Sequencing.

Gene	NTG	cMyBP-C^{110kDa}	FoldChange
Gbp8	30	74	2.47
Slc1a3	102	251	2.46
Timp1	85	209	2.46
Nlrc3	66	162	2.45
Krt18	58	142	2.45
Mthfd2	112	274	2.45
A830082K12Rik	27	66	2.44
Snora81	18	44	2.44
Rspo1	77	188	2.44
Col8a2	39	95	2.44
Gpx3	14720	35760	2.43
Upk3b	368	894	2.43
Rgs11	28	68	2.43
Lat	21	51	2.43
Snord47	14	34	2.43
Fcrla	14	34	2.43
Dlg2	82	199	2.43
Slc24a2	144	349	2.42
Myl1	1861	4504	2.42
Lrrc55	55	133	2.42
Snca	331	800	2.42
Efhd1	224	541	2.42
Gng2	429	1035	2.41
Scand1	267	644	2.41
Itga8	370	892	2.41
C530008M17Rik	191	460	2.41
Ikbke	89	214	2.40
Neto2	92	221	2.40
Olfml2a	100	240	2.40
Atp2a1	70	168	2.40
Slc26a3	35	84	2.40
Crb2	25	60	2.40
Esco2	20	48	2.40
Gpr173	20	48	2.40
Enpp6	93	223	2.40
Met	66	158	2.39
Vsig4	85	203	2.39
Plac8	31	74	2.39
Heatr8	39	93	2.38
Cilp	439	1043	2.38
Rasl11a	48	114	2.38
Cep72	32	76	2.38
Csrp2	611	1450	2.37
Fmod	278	659	2.37
Gjc3	30	71	2.37
Gm12409	22	52	2.36
Spp1	22	52	2.36
Nipal2	58	137	2.36
Sox9	75	177	2.36
Atp10a	129	304	2.36

Table 3 (Continued). Top Upregulated Genes in cMyBP-C^{110kDa} Compared to NTG Hearts by RNA-Sequencing.

Gene	NTG	cMyBP-C^{110kDa}	FoldChange
Ube2c	62	146	2.35
Actn3	17	40	2.35
Stx1b	17	40	2.35
Kcnd1	17	40	2.35
Actg2	54	127	2.35
Kcnj10	20	47	2.35
Slc12a8	29	68	2.34
Tmem158	35	82	2.34
Megf6	291	679	2.33
Rasal3	42	98	2.33
Fkbp1b	30	70	2.33
Mfap2	94	219	2.33
Fam46c	101	235	2.33
AI854703	40	93	2.33
Armcx4	535	1242	2.32
Rn45s	126192	292902	2.32
Col12a1	69	160	2.32
Cdkn2b	19	44	2.32
Loxl4	51	118	2.31
Lamc3	48	111	2.31
Sema3d	159	367	2.31
Ier2	3085	7115	2.31
Cx3cr1	151	348	2.30
2210404O09Rik	23	53	2.30
Gprasp2	143	329	2.30
Alas2	2830	6501	2.30
Ifi27l2a	492	1129	2.29
Omd	34	78	2.29
Fgl2	2255	5173	2.29
Pirt	378	866	2.29
Kmo	21	48	2.29
Fdx1l	46	105	2.28
Rps6ka6	50	114	2.28
Pcdhgc4	25	57	2.28
Mlph	43	98	2.28
Akap5	176	401	2.28
Stard6	18	41	2.28
Lif	40	91	2.28
Pam	44909	101993	2.27
Tspan8	15	34	2.27
Dhh	34	77	2.26
Cd46	23	52	2.26
Ltbp2	211	477	2.26
Aass	35	79	2.26
Lefty1	43	97	2.26
Lgals3	291	656	2.25
Susd5	100	225	2.25
Fhdc1	20	45	2.25
Lrrn3	16	36	2.25
Klra2	16	36	2.25

Table 3 (Continued). Top Upregulated Genes in cMyBP-C^{110kDa} Compared to NTG Hearts by RNA-Sequencing.

Gene	NTG	cMyBP-C[110kDa]	FoldChange
Cdk1	57	128	2.25
Unc5a	140	314	2.24
Gnal	25	56	2.24
A230056P14Rik	25	56	2.24
Sox5	96	215	2.24
Slc27a3	59	132	2.24
Mt3	52	116	2.23
Gnao1	1371	3057	2.23
Junb	4148	9249	2.23
C2	120	267	2.23
Pvt1	40	89	2.23
5033406O09Rik	18	40	2.22
Beta-s	38840	86291	2.22
Slc25a1	361	801	2.22
Caskin1	23	51	2.22
Fam60a	56	124	2.21
Cd79a	42	93	2.21
Megf10	47	104	2.21
Mir208a	38	84	2.21
Cpz	24	53	2.21
Lrrn2	352	777	2.21
Prnd	347	765	2.20
1810041L15Rik	35	77	2.20
Adamts20	20	44	2.20
Tmem30b	15	33	2.20
Prph	15	33	2.20
Cebpa	262	576	2.20
Chst4	56	123	2.20
Fzd2	159	349	2.19
Bex1	52	114	2.19
Msantd1	26	57	2.19
Itgb7	79	173	2.19
Sertad4	301	659	2.19
1700084E18Rik	16	35	2.19
Tcf7	43	94	2.19
Jsrp1	27	59	2.19
Prox2	38	83	2.18
Ccl8	60	131	2.18
Gm20605	82	179	2.18
ORF63	88	192	2.18
Tbc1d1	1384	3019	2.18
Sbk2	481	1049	2.18
Mybpc2	1040	2267	2.18
4933436C20Rik	167	364	2.18
Grhl1	28	61	2.18
1700109H08Rik	28	61	2.18
Zbtb7c	135	294	2.18
Ms4a4b	17	37	2.18
Iglon5	17	37	2.18
2410076I21Rik	17	37	2.18

Table 3 (Continued). Top Upregulated Genes in cMyBP-C[110kDa] Compared to NTG Hearts by RNA-Sequencing.

Gene	NTG	cMyBP-C[110kDa]	FoldChange
Shisa4	182	396	2.18
Hoxb3	23	50	2.17
Fam198a	58	126	2.17
Emb	94	204	2.17
Mbp	272	590	2.17
Scml4	95	206	2.17
Camkk1	90	195	2.17
B230312C02Rik	18	39	2.17
Fam167b	18	39	2.17
Thrsp	990	2144	2.17
Fam227a	49	106	2.16
Snai1	68	147	2.16
Fam84a	31	67	2.16
Adamts17	25	54	2.16
Itgae	19	41	2.16
AU023871	26	56	2.15
Blk	33	71	2.15
Tusc5	170	365	2.15
Kcnn3	41	88	2.15
Aacs	242	519	2.14
Gpm6a	391	838	2.14
Cep55	21	45	2.14
Ccl12	86	184	2.14
Twist1	58	124	2.14
Gdf10	124	265	2.14
Nat8l	207	442	2.14
Fam83g	30	64	2.13
Chst10	23	49	2.13
B3gnt9	205	436	2.13
Zdhhc15	48	102	2.13
Ccr7	24	51	2.13
Slc13a4	24	51	2.13
Pdzd7	16	34	2.13
Cd24a	236	501	2.12
Cfb	150	318	2.12
Aldh3a1	25	53	2.12
Cxcr6	25	53	2.12
Olfr920	17	36	2.12
Itga11	174	368	2.11
Cpt1c	184	389	2.11
5031414D18Rik	79	167	2.11
Lrp2	36	76	2.11
Tsku	136	287	2.11
Lrfn3	73	154	2.11
Bdh2	28	59	2.11
Osr1	86	181	2.10
Cxcl1	575	1209	2.10
Tbxa2r	89	187	2.10
Slc41a2	91	191	2.10

Table 3 (Continued). Top Upregulated Genes in cMyBP-C[110kDa] Compared to NTG Hearts by RNA-Sequencing.

Gene	NTG	cMyBP-C^{110kDa}	FoldChange
Dbp	3262	6845	2.10
Npy1r	187	392	2.10
Olfml1	168	352	2.10
Cdh24	21	44	2.10
Rbp1	537	1125	2.09
Cnbd2	33	69	2.09
Nphp4	68	142	2.09
Casp3	81	169	2.09
Aoah	60	125	2.08
1700056E22Rik	24	50	2.08
Mmp23	371	772	2.08
Cd79b	50	104	2.08
Cyp2s1	89	185	2.08
Myl9	2139	4446	2.08
Lpar2	26	54	2.08
Peg3	288	598	2.08
Lrrc17	171	355	2.08
Baiap3	53	110	2.08
Cd180	40	83	2.08
Morn4	81	168	2.07
Rnf165	27	56	2.07
Arl5c	42	87	2.07
Ccnb1	28	58	2.07
Sec14l5	86	178	2.07
Ube2l6	976	2016	2.07
Foxc1	291	601	2.07
Alx4	31	64	2.06
Map1a	498	1028	2.06
Gabra3	142	293	2.06
G530011O06Rik	64	132	2.06
Gpr35	32	66	2.06
Itih5	595	1227	2.06
Pamr1	178	367	2.06
Efcc1	50	103	2.06
Pygl	310	638	2.06
Sall1	69	142	2.06
Prdm1	180	370	2.06
Fstl3	235	483	2.06
Nap1l5	164	337	2.05
Phgdh	76	156	2.05
Fos	4929	10110	2.05
Kcnj15	60	123	2.05
Plagl1	365	748	2.05
Dct	167	342	2.05
Unc13d	63	129	2.05
Rgs14	42	86	2.05
Xylt1	21	43	2.05
Pcdhb9	22	45	2.05
Tmprss5	22	45	2.05

Table 3 (Continued). Top Upregulated Genes in cMyBP-C^{110kDa} Compared to NTG Hearts by RNA-Sequencing.

Gene	NTG	cMyBP-C^{110kDa}	FoldChange
Igf1	732	1496	2.04
Il22ra1	23	47	2.04
Itga10	162	331	2.04
Lss	96	196	2.04
Ptn	98	200	2.04
Dennd2d	49	100	2.04
Hivep3	75	153	2.04
Rab36	52	106	2.04
Tat	27	55	2.04
Cdon	541	1101	2.04
Shisa3	91	185	2.03
Cd44	614	1247	2.03
Cd22	35	71	2.03
Gm1673	36	73	2.03
Pak1	75	152	2.03
Fst	38	77	2.03
Col18a1	799	1619	2.03
Brdt	43	87	2.02
Galnt6	47	95	2.02
Zfp273	64	129	2.02
Sv2a	193	389	2.02
Zfp951	66	133	2.02
Tubb3	68	137	2.01
Slc22a17	276	556	2.01
Ephx3	75	151	2.01
Hist1h2be	78	157	2.01
Mycn	89	179	2.01
Lair1	102	205	2.01
Smim1	313	629	2.01
2610203C20Rik	502	1005	2.00
Grin2c	131	262	2.00
2210404O07Rik	55	110	2.00
Basp1	53	106	2.00
Tvp23a	45	90	2.00
Slc18a2	43	86	2.00
Klhl29	38	76	2.00
Havcr2	35	70	2.00
Treml2	34	68	2.00
Zfp184	32	64	2.00
Twist2	31	62	2.00
Gng4	29	58	2.00
Efcab4b	29	58	2.00
Cyp7b1	26	52	2.00
Rasgef1c	23	46	2.00
Mirg	17	34	2.00

Table 3 (Continued). Top Upregulated Genes in cMyBP-C^{110kDa} Compared to NTG Hearts by RNA-Sequencing.

Gene	NTG	cMyBP-C^{110kDa}	FoldChange
Gm5506	109	10	10.9
Gbp10	392	52	7.538461538
Cyp2b10	159	31	5.129032258
Il1r2	39	10	3.9
Cyp1a1	80	24	3.333333333
Kcnk1	85	26	3.269230769
Ddn	34	11	3.090909091
Capn11	182	59	3.084745763
Cacng6	78	26	3
Prom2	45	15	3
Lrrc52	106	36	2.944444444
Trem1	40	15	2.666666667
Pde11a	46	18	2.555555556
Aldob	1107	434	2.550691244
Eif2s3y	2224	934	2.381156317
Mettl11b	56	24	2.333333333
Mfsd4	382	167	2.28742515
Nat1	36	16	2.25
Acsm5	550	252	2.182539683
Adra1a	814	381	2.13648294
Mcph1	373	178	2.095505618
Cngb3	176	84	2.095238095
Fut2	54	26	2.076923077
Agt	666	323	2.061919505
2410137M14Rik	45	22	2.045454545
Gabrr2	134	66	2.03030303
Gsta1	71	35	2.028571429
Acot3	34	17	2

Table 4. Bottom Downregulated Genes in cMyBP-C^{110kDa} Compared to NTG Hearts by RNA-Sequencing.
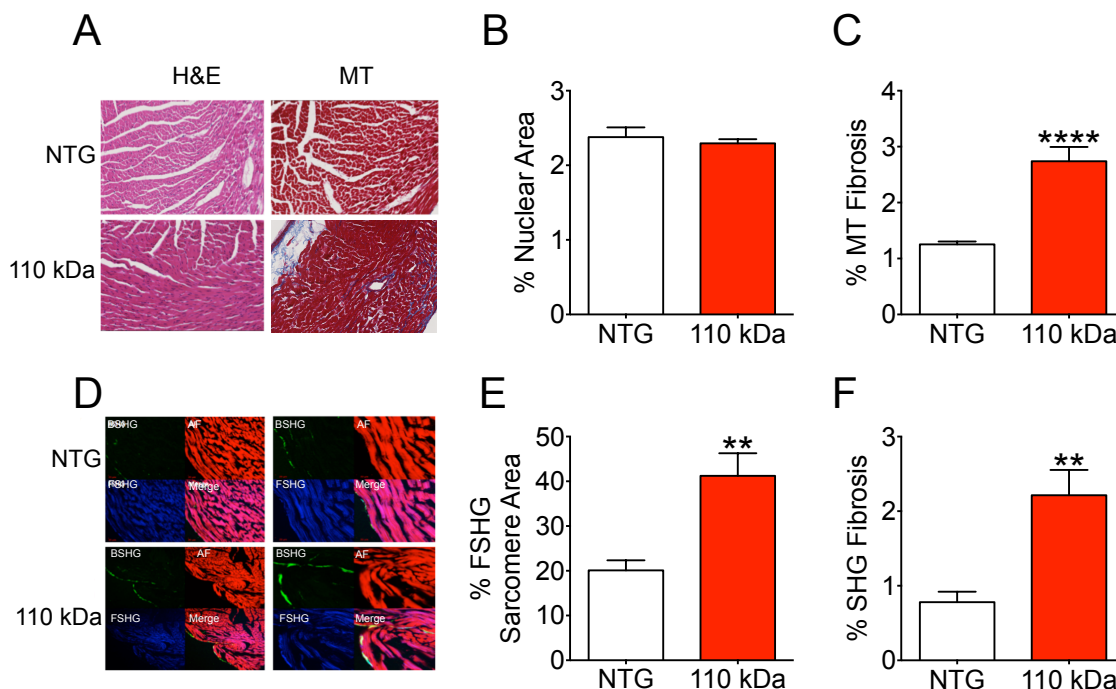
Figure 20. Fibrosis and Sarcomere Area are Increased in cMyBP-C^{110kDa} Hearts. (A) Representative H&E and MT stained myocardial sections from cMyBP-C^{110kDa} and NTG hearts. Quantification of percent (B) nuclear area and (C) MT fibrosis obtained from measurements of H&E and MT labeled myocardial sections from cMyBP-C^{110kDa} and NTG hearts (n = 3 NTG hearts, 53 sections and 5 cMyBP-C^{110kDa} hearts, 74 sections). (D) Representative SHG imaged myocardial sections from cMyBP-C^{110kDa} and NTG hearts (left). Images are magnified in the right panels. Green channel is backward SHG (BSHG) depicting predominantly collagen fibers, red channel is autofluorescence (AF) and blue channel is forward directed SHG (FSHG) showing sarcomere pattern and their merge. Quantifications of (E) percent FSHG sarcomere area and (F) percent SHG fibrosis obtained from SHG imaged myocardial sections from cMyBP-C^{110kDa} and NTG hearts (n = 3 NTG hearts, 12 sections and 5 cMyBP-C^{110kDa} hearts, 19 sections). *$p < 0.01$, ****$p < 0.0001$.

around the cardiac vasculature and may be due to the observed increase in blood vessel size in the hearts of cMyBP-C^{110kDa} animals. However, fibrosis was also detected within the interstitial tissue. Next, SHG imaging of myocardial sections from cMyBP-C^{110kDa} and NTG hearts was implemented to detect sarcomere area with forward directed SHG (FSHG) and collagen deposition with backward directed SHG (BSHG) (**Figure 20D**). Quantification of FSHG images demonstrated a significant increase ($p < 0.01$) in percent sarcomere area in cMyBp-C^{110kDa} myocardial sections (**Figure 20E**), which corresponded to the increase in heart size observed in cMyBP-C^{110kDa} hearts (**Figure 18**). In line with the MT data, quantification of BSHG images demonstrated a significant elevation ($p < 0.01$) in percent fibrosis in cMyBP-C^{110kDa} myocardial sections compared to NTG sections (**Figure 20F**). Together, these data signify that myocardial fibrosis accompanies the cardiac remodeling that results from contractile dysfunction in cMyBP-C^{110kDa} mice due to the absence of the N'-C0-C1f region of cMyBP-C.

cMyBP-C^{110kDa} Incorporates Properly into the Cardiac Sarcomere

cMyBP-C^{110kDa} mice develop contractile dysfunction, myocardial hypertrophy, and fibrosis (**Figures 17-20**). Therefore, I next elucidated whether this pathology was specifically due to the absence of the C0-C1f region of cMyBP-C in the cMyBP-C^{110kDa} TG protein or whether the dysfunction and morphological changes seen in cMyBP-C^{110kDa} hearts was due to aberrant mislocalization of the cMyBP-C^{110kDa} protein acting as a poison polypeptide, which has been previously demonstrated for the C0-C1f fragment of cMyBP-C

(Govindan, Sarkey, et al., 2012; Witayavanitkul et al., 2014). To address this question, I isolated single cardiomyocytes from 3-month old NTG and cMyBP-C^{110kDa} hearts and performed immunofluorescence imaging to detect cMyBP-C, the cMyBP-C^{110kDa} TG protein, and α-actinin (**Figure 21**). I coupled this with SHG imaging to simultaneously detect myosin structure. As expected, myosin localized within the A-band of the sarcomere between α-actinin at the Z-line with no overlap in the I-band (**Figure 21**). Myocytes from NTG and cMyBP-C^{110kDa} hearts were stained with an antibody targeted towards cMyBP-C's N' region (C0 domain), which detected only endogenous FL cMyBP-C (**Figure 21A**). In both NTG and cMyBP-C^{110kDa} myocytes, the classical staining pattern of two cMyBP-C bands between the Z-lines of the sarcomere (stained with α-actinin) was observed, demonstrating proper localization of endogenous cMyBP-C in both groups of animals (**Figure 21A**). However, the staining of endogenous cMyBP-C in cMyBP-C^{110kDa} myocytes was faint and nearly undetectable indicating low levels of endogenous FL cMyBP-C within the sarcomeres of cMyBP-C^{110kDa} myocytes (**Figure 21A**). This corresponds to the Western blot data that suggested only 19% incorporation of endogenous FL cMyBP-C in cMyBP-C^{110kDa} myofilament fractions (**Figure 16B**). Myocytes were then stained with an antibody targeted towards cMyBP-C's more C-terminal region (C5 domain) to identify endogenous FL cMyBP-C in NTG and cMyBP-C^{110kDa} myocytes as well as the cMyBP-C^{110kDa} TG protein in cMyBP-C^{110kDa} myocytes (**Figure 21B**). In both NTG and cMyBP-C^{110kDa} myocytes, the classical staining pattern of two
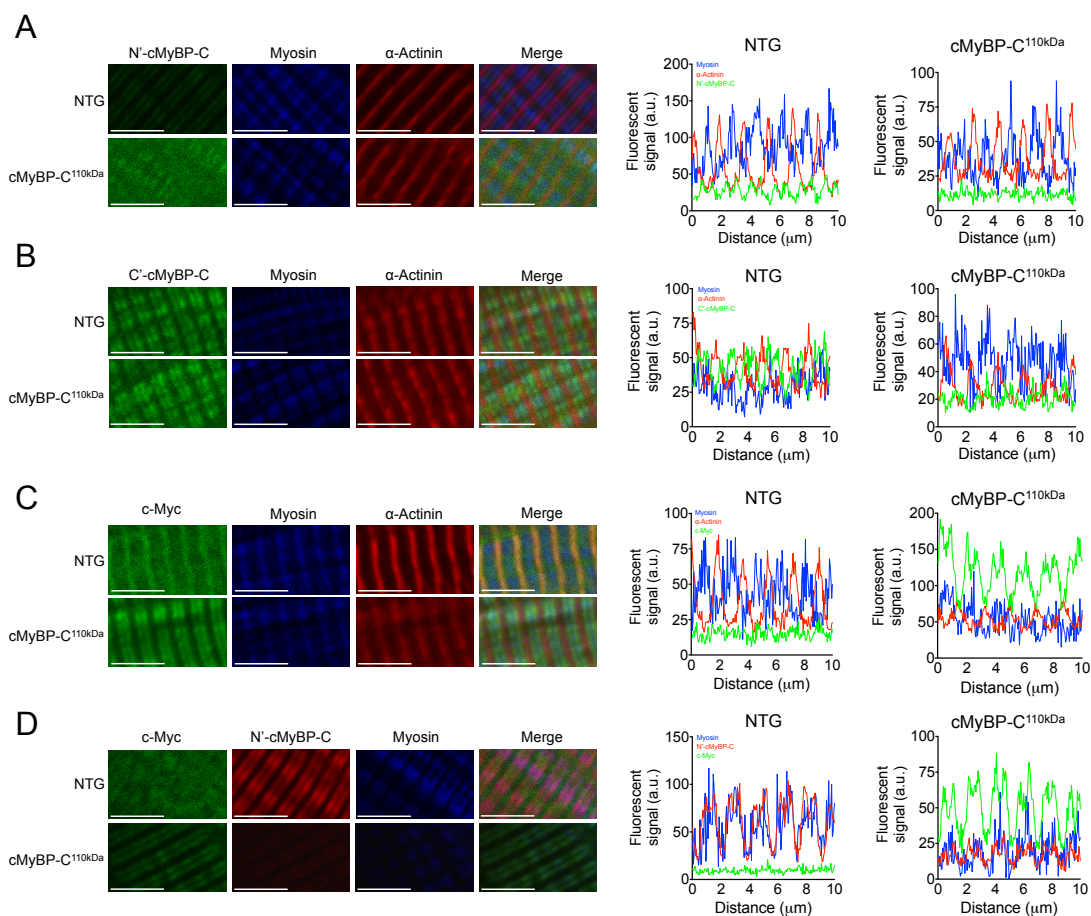
Figure 21. cMyBP-C^{110kDa} Incorporates Properly into the Cardiac Sarcomere.
Single cardiomyocytes were isolated from NTG and cMyBP-C^{110kDa} hearts. (A)
Myocytes were labeled with antibodies against cMyBP-C's N' region (C0 domain)
(green) and α-actinin (red). SHG imaging was implemented to show myosin
structure (blue). Also depicted is the merge of all three signals and fluorescence
line scans. (B) Myocytes were labeled and imaged as in A but using and antibody
against cMyBP-C's more C' region (C5 domain) (green), which depicts
endogenous cMyBP-C in NTG and cMyBP-C^{110kDa} myocytes as well as the
cMyBP-C^{110kDa} TG protein in cMyBP-C^{110kDa} myocytes. (C) Myocytes were
labeled and imaged as in A and B but using an antibody against c-Myc (green),
which shows only the c-Myc-tagged cMyBP-C^{110kDa} TG protein. (D) Myocytes
were labeled and imaged as in A-C but using antibodies against c-Myc (green)
and cMyBP-C's N' region (red) with no staining for α-actinin. As in C, the c-Myc
signal was seen only in myocytes from cMyBP-C^{110kDa} hearts. Endogenous
cMyBP-C was detected in both NTG and cMyBP-C^{110kDa} myocytes. Scale bar =
5μm.

cMyBP-C bands between the Z-lines of the sarcomere (stained with α-actinin) was observed (**Figure 21B**). As staining with an antibody against cMyBP-C's N' region showed low levels of endogenous FL cMyBP-C (**Figure 21A**) and staining with an antibody targeted towards cMyBP-C's C5 domain indicated increased expression of cMyBP-C similar to the levels observed in NTG myocytes (**Figure 21B**), it was likely that the anti-C5 domain antibody was detecting the cMyBP-C^{110kDa} TG protein within the sarcomeres of cMyBP-C^{110kDa} myocytes and that the TG protein was localizing at the C-zone. Therefore, to test this, myocytes from NTG and cMyBP-C^{110kDa} hearts were stained for an antibody directed against c-Myc, which targeted only the c-Myc-tagged cMyBP-C^{110kDa} TG protein. The signal observed by staining for c-Myc depicted a doublet pattern of the c-Myc-tagged-cMyBP-C^{110kDa} TG protein between the Z-lines in cMyBP-C^{110kDa} myocytes with no staining observed in NTG myocytes (**Figure 21C**). This implied proper localization of the cMyBP-C^{110kDa} protein. Importantly, the lack of c-Myc staining at the Z-lines suggested the cMyBP-C^{110kDa} transgenic protein does not aberrantly localize throughout the sarcomere but localizes specifically within the A-band and possibly within the C-zone. To determine definitively that the cMyBP-C^{110kDa} TG protein localizes within the C-zone of the A-band, myocytes from NTG and cMyBP-C^{110kDa} hearts were stained with antibodies against c-Myc and cMyBP-C's N' region. As in **Figure 21C**, the c-Myc signal was observed in myocytes from cMyBP-C^{110kDa} hearts, but not NTG hearts (**Figure 21D**). Additionally, using the antibody targeted against cMyBP-C's N' region,

endogenous FL cMyBP-C was detected in both NTG and cMyBP-C^{110kDa} myocytes (**Figure 21D**). Merging of the c-Myc and endogenous FL cMyBP-C signals in cMyBP-C^{110kDa} myocytes showed co-localization and complete overlap of endogenous cMyBP-C and the cMyBP-C^{110kDa} TG protein in the classical doublet pattern, confirming that the cMyBP-C^{110kDa} TG protein localizes within the C-zone of the cardiac sarcomere in cMyBP-C^{110kDa} hearts along with endogenous cMyBP-C (**Figure 21D**). Together, these data confirm that the dysfunction and morphological changes observed in cMyBP-C^{110kDa} hearts was instigated by the absence of the C0-C1f region of cMyBP-C and not aberrant mislocalization of the cMyBP-C^{110kDa} TG protein within cMyBP-C^{110kDa} sarcomeres. This further supports a critical role for the N'-C0-C1f region of cMyBP-C in regulating cardiac function at the level of the sarcomere.

cMyBP-C Phosphorylation is Elevated in cMyBP-C^{110kDa} Hearts

To determine whether phosphorylation at serine residues 273, 282, and 302 within the M domain of cMyBP-C was altered in cMyBP-C^{110kDa} hearts during HF compared to NTG hearts, I performed Western blot analysis using myofilament fractions from 7-month old NTG and cMyBP-C^{110kDa} hearts (**Figure 22**). Antibodies targeted against phosphorylated serine residues 273, 282, and 302 were used, as have been previously reported (Copeland et al., 2010). Intriguingly, phosphorylation at serine residue 273 of the endogenous FL cMyBP-C from cMyBP-C^{110kDa} myofilament fractions was significantly higher ($p < 0.001$) than that of the cMyBP-C^{110kDa} TG protein in these fractions and was also
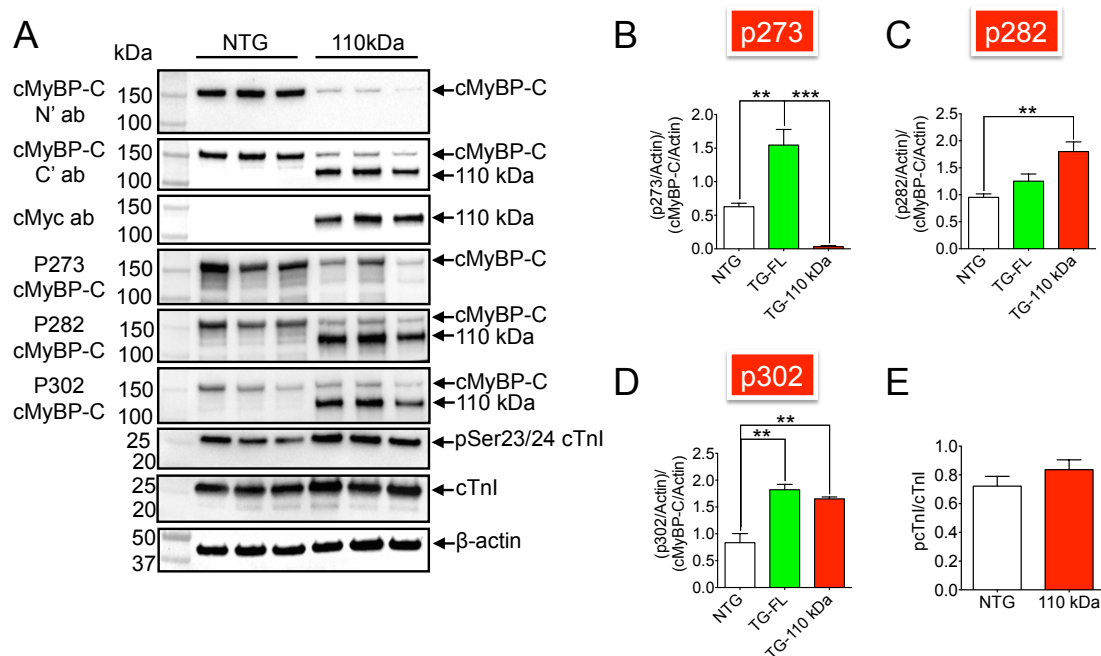
Figure 22. cMyBP-C Phosphorylation is Elevated in cMyBP-C[110kDa] Hearts.
(A) Western blot analysis presented in **Figure 16A** and including phosphorylation of serine residues 273, 282, and 302 of cMyBP-C and phosphorylation of cTnI and serine residues 23/24. Densitometry analysis of the phosphorylation levels of endogenous FL cMyBP-C from NTG and cMyBP-C[110kDa] (TG-FL) myofilament fractions and the cMyBP-C[110kDa] TG protein (TG-110 kDa) from cMyBP-C[110kDa] myofilament fractions at serine residues (B) 273, (C) 282, and (D) 302 as well as at serine residues (E) 23/24 of cTnI. n = 3 hearts per group. $**p < 0.01$, $***p < 0.001$.

significantly higher ($p < 0.01$) than that of the endogenous FL cMyBP-C from NTG myofilament fractions (**Figure 22 A, B**). Importantly, phosphorylation of serine residue 273 in the cMyBP-C^{110kDa} TG protein was absent (**Figure 22 A, B**). This was likely due to the disruption of the PKA recognition motif for phosphorylation of serine residue 273 in the cMyBP-C^{110kDa} TG protein by the removal of the N'-C0-C1f region of cMyBP-C (removal of residues 1-271). Phosphorylation of serine residue 282 of the cMyBP-C^{110kDa} TG protein in cMyBP-C^{110kDa} myofilament fractions was significantly higher ($p < 0.01$) than that of endogenous FL cMyBP-C in NTG myofilament fractions (**Figure 22 A, C**). Strikingly, phosphorylation at serine residue 282 of both the endogenous FL cMyBP-C and cMyBP-C^{110kDa} TG protein from cMyBP-C^{110kDa} was significantly elevated ($p < 0.01$) than that of endogenous FL cMyBP-C in NTG myofilament fractions (**Figure 22 A, D**). No difference in phosphorylation of cTnI at serine residues 23/24 between NTG and cMyBP-C^{110kDa} samples was detected (**Figure 22 A, E**). Together, these data suggest that both endogenous FL cMyBP-C and the cMyBP-C^{110kDa} TG protein are hyperphosphorylated at specific serine residues within the M domain in cMyBP-C^{110kDa} sarcomeres, which may play a functional role in the contractile dysfunction observed in cMyBP-C^{110kDa} hearts.

Maximum Force and k_{tr} are Increased in cMyBP-C^{110kDa} Hearts

The experiments performed as part of my **Specific Aim 2** determined how the absence of the N'-C0-C1f region of cMyBP-C in cMyBP-C^{110kDa} hearts alters myofilament function to elucidate whether this region is necessary for controlling

physiological contraction kinetics in the heart. Therefore, I performed a steady-state fiber force-ATPase experiment using isolated cardiac LV papillary muscle fibers from 3-month old cMyBP-C^{110kDa} and NTG mice. I performed these experiments using animals at 3-months of age as this was prior to severe global cardiac dysfunction and would allow me to determine the mechanism(s) by which the absence of the N'-C0-C1f region of cMyBP-C instigates sarcomeric contractile dysfunction leading to whole-heart dysfunction and remodeling (**Figures 17-20**). The parameters that I measured included force production, Ca^{2+} sensitivity of force development, tension cost, cross-bridge stiffness, and rate of tension redevelopment (k_{tr}). Intriguingly, LV papillary fibers from cMyBP-C^{110kDa} hearts generated significantly more force ($p < 0.01$) at maximum Ca^{2+} compared to those from NTG hearts (**Figure 23 A, B**). However, no difference was observed in Ca^{2+} sensitivity of force development (**Figure 24 A, B**), tension cost (**Figure 25 A, B**), and cross-bridge stiffness (**Figure 26**) between cMyBP-C^{110kDa} and NTG fibers. Remarkably, the rate of tension redevelopment (k_{tr}) was significantly higher ($p < 0.05$) than that of NTG fibers (**Figure 27**). Together, these data demonstrate the underlying contractile abnormalities that occur in cMyBP-C^{110kDa} sarcomeres that likely give rise to global heart dysfunction in these animals.
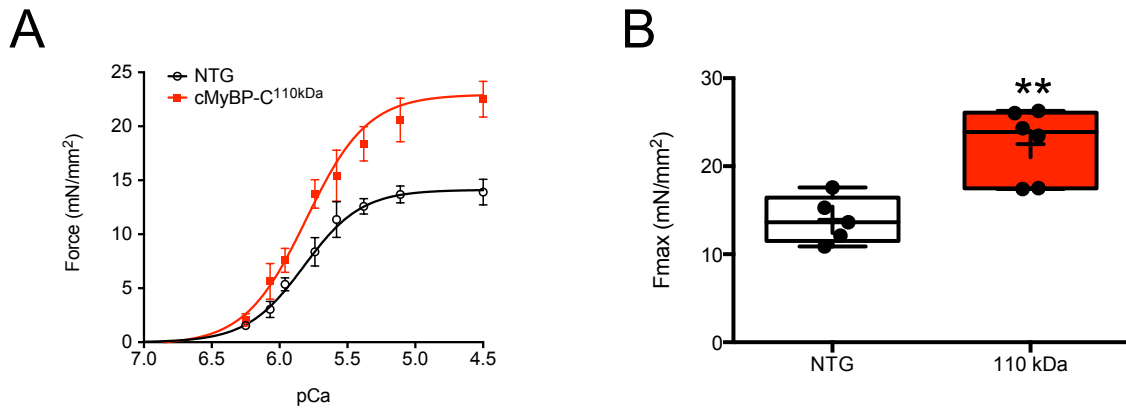
Figure 23. Maximum Force is Increased in cMyBP-C^{110kDa} Hearts. (A) Force-pCa curves depicting force production at various pCa values for NTG and cMyBP-C^{110kDa} LV papillary muscle fibers at 3-months of age. (B) Maximum force produced by NTG and cMyBP-C^{110kDa} fibers derived from force-pCa curves in A. Mean values plotted as "+" symbols. n = 5 fibers from 5 NTG hearts and 6 fibers from 6 cMyBP-C^{110kDa} hearts. **$p < 0.01$.
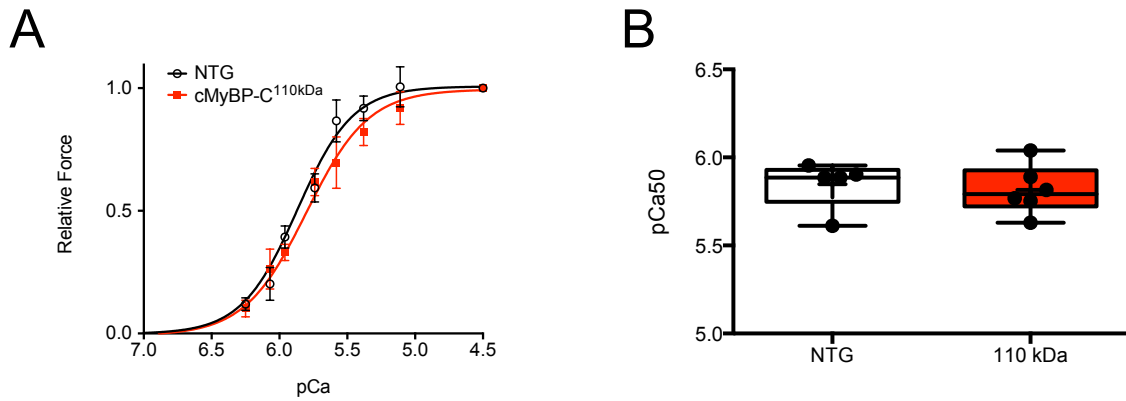
Figure 24. Ca^{2+} Sensitivity of Force Development is Preserved in cMyBP-C^{110kDa} Hearts. (A) Force-pCa curves depicting normalized force production at various pCa values for NTG and cMyBP-C^{110kDa} fibers at 3-months of age. (B) pCa50 (Ca^{2+} sensitivity) values derived from normalized force-pCa curves in A. Mean values plotted as "+" symbols. n = 5 fibers from 5 NTG hearts and 6 fibers from 6 cMyBP-C^{110kDa} hearts.
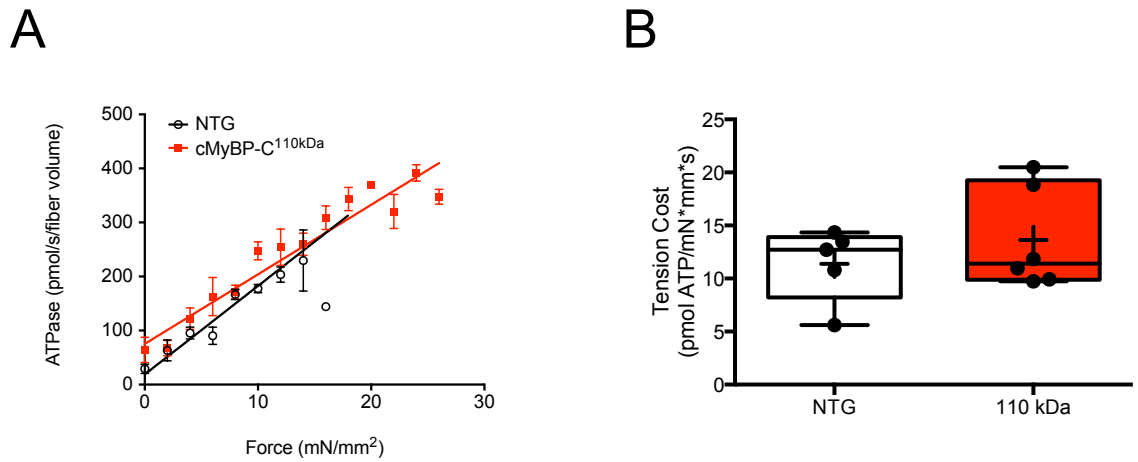
Figure 25. Tension Cost is Unaltered in cMyBP-C[110kDa] Hearts. (A) Force-ATPase curves depicting ATPase activity for NTG and cMyBP-C[110kDa] fibers at 3-months of age. (B) Tension cost values derived from force-ATPase values in A. Mean values plotted as "+" symbols. n = 5 fibers from 5 NTG hearts and 6 fibers from 6 cMyBP-C[110kDa] hearts.

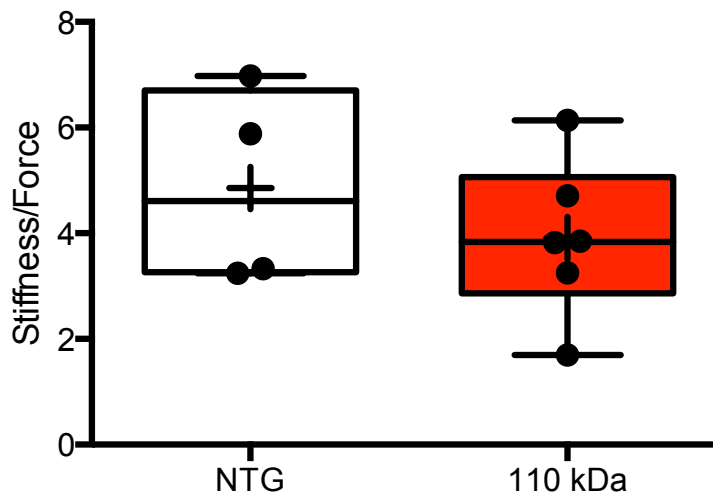**Figure 26. Cross-bridge stiffness is Unchanged in cMyBP-C110kDa Hearts.** Cross-bridge stiffness normalized to force for NTG and cMyBP-C110kDa fibers at 3-months of age. Mean values plotted as "+" symbols. n = 4 fibers from 4 NTG hearts and 6 fibers from 6 cMyBP-C110kDa hearts.
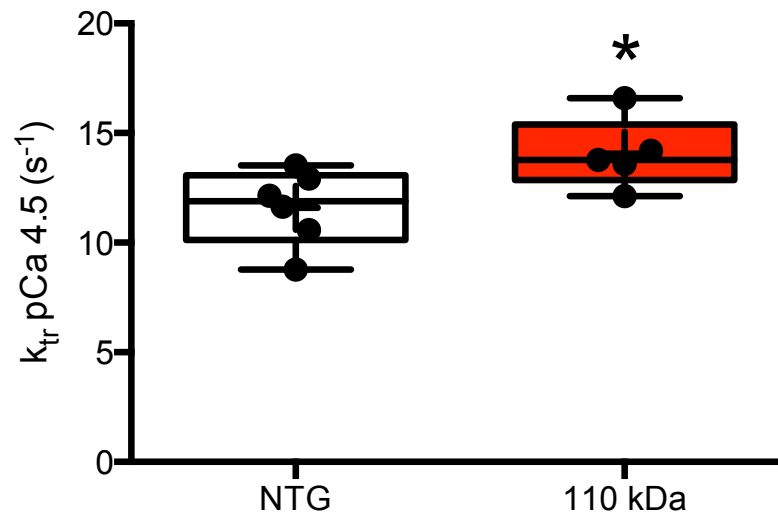
Figure 27. Rate of Tension Redevelopment (k_{tr}) is Increased in cMyBP-C^{110kDa} Hearts. k_{tr} generated by NTG and cMyBP-C^{110kDa} fibers at 3-months of age following a rapid slack-restretch maneuver. Mean values plotted as "+" symbols. n = 6 fibers from 6 NTG hearts and 5 fibers from 5 cMyBP-C^{110kDa} hearts. *$p < 0.05$.

CHAPTER SIX

DISCUSSION

The data reported in this work support my central hypothesis that the N'-C0-C1f region of cMyBP-C is critical for normal cardiac function *in vivo*. Indeed, the results of my experiments demonstrate that the absence of the N'-C0-C1f region of cMyBP-C in the cardiac sarcomeres of cMyBP-C^{110kDa} mice leads to a significant reduction in percent FS by 3-months of age that is even further reduced by 6-months of age (**Figure 17**). Crucially, the cMyBP-C^{110kDa} protein was expressed at high levels in the hearts of cMyBP-C^{110kDa} mice (**Figure 16**) and localized properly within the C-zone of cMyBP-C^{110kDa} sarcomeres (**Figure 21**). The dysfunction that developed in cMyBP-C^{110kDa} hearts led to pathological cardiac remodeling producing LV and RV chamber enlargement (**Figure 18**) and a significant elevation in both sarcomere area (**Figure 20**) and in markers of pathological myocardial hypertrophy (**Figure 19**). Additionally, the remodeling observed in cMyBP-C^{110kDa} hearts led to a significant elevation in myocardial fibrosis (**Figure 20**), which likely contributed to the dysfunction seen in the hearts of these animals. Importantly, the dysfunction and remodeling that developed at the whole organ level in cMyBP-C^{110kDa} hearts was likely instigated by the contractile deficiencies produced within cMyBP-C^{110kDa} sarcomeres due to the absence of the N'-C0-C1f region of cMyBP-C. Specifically, using a steady-state force-ATPase assay with isolated, permeabilized papillary muscle fibers from

cMyBP-C^{110kDa} hearts and NTG hearts for comparison, I observed a significant increase in maximum force and k$_{tr}$ produced by cMyBP-C^{110kDa} fibers (**Figures 23, 27**). This indicates contractile abnormalities at the level of the cardiac sarcomere (Specific Aim 2) that generates overt cardiac dysfunction (Specific Aim 1) within cMyBP-C^{110kDa} animals. Finally, at the molecular level, I detected hyperphosphorylation of cMyBP-C in both FL cMyBP-C and the cMyBP-C^{110kDa} TG protein from cMyBP-C^{110kDa} cardiac myofilament fractions, which may play a role in the dysfunction observed in cMyBP-C^{110kDa} hearts (**Figure 22**).

The critical finding of this study was that cMyBP-C^{110kDa} animals developed severe cardiac contractile dysfunction and myocardial remodeling. The remodeling within cMyBP-C^{110kDa} hearts led to LV and RV chamber enlargement with no significant differences in LV and septal wall thicknesses between cMyBP-C^{110kDa} and NTG hearts. However, it is important to note that the LV and septal wall thicknesses were reduced in cMyBP-C^{110kDa} hearts compared to NTG hearts, however, again, this difference was not significant. Although, expectedly, if cardiac function continues to worsen beyond 6-months of age in cMyBP-C^{110kDa} hearts it is likely that thinning of the LV and septal walls would be evident producing a cardiac phenotype consistent with DCM. Intriguingly, the DCM phenotype has been previously observed in the homozygous mutant cMyBP-C t/t mouse model developed in the Seidman lab, which expresses less than 10 percent of a truncated form of cMyBP-C that does not incorporate into the cardiac sarcomere and that develops depressed systolic contractility and

diastolic dysfunction (McConnell et al., 1999). The t/t mouse is essentially a functional knockout of cMyBP-C produced by a knock-in mutation in the *MYBPC3* gene that was developed on the FVB/N background. In contrast, the cMyBP-C^{110kDa} mouse is a TG mouse model produced by the TG expression of a N' truncated cMyBP-C protein that lacks the N'-C0-C1f region of cMyBP-C developed on the C57BL/6 background. Interestingly, these two animals develop a similar phenotype, but which is more severe in the t/t mouse model (McConnell et al., 1999) likely due to the complete absence of cMyBP-C in the cardiac sarcomere rather than only the absence of the N' region. However, the t/t mouse is not a true genetic model of *MYBPC3* ablation as it still expresses a small amount of cMyBP-C. Interestingly, the cMyBP-C genetic knockout mouse model developed on the SV/129 background by the Moss lab in the early 2000's develops a phenotype consistent with hypertrophic cardiomyopathy and harbors both systolic and diastolic dysfunction (Harris et al., 2002).

Understanding how and why the heart remodels to produce HFpEF, as in HCM, or HFrEF, as in DCM, is truly fascinating. Importantly, there are three possible reasons that I speculate may produce the differences observed in cardiac remodeling and function (HCM vs. DCM) between cMyBP-C knockout, t/t, and cMyBP-C^{110kDa} animals. The first possibility is that all three mouse models were developed on different mouse strains. As such, these different mouse strains may respond differently to mutations of cMyBP-C. Another possibility is the fact that the cMyBP-C knockout mouse is a homozygous *MYBPC3* knockout

mouse model while the t/t mouse is a homozygous *MYBPC3* knock-in mouse model and the cMyBP-C^{110kDa} mouse is a TG model due to truncation of the *MYBPC3* gene. As such, these methods to produce truncation or knockout of cMyBP-C could lead to different expression levels of cMyBP-C or responses of the heart to these manipulations between the mouse models. Finally, one obvious possibility, as stated above, is that the absence of the N' region of cMyBP-C in cMyBP-C^{110kDa} animals produces a different form of contractile deficiency at the level of the sarcomere than occurs in cMyBP-C knockout and t/t mice, which lack FL cMyBP-C. This would suggest an important role for the C' region of cMyBP-C in regulating cardiac function in addition to the N' region of cMyBP-C.

Previously, work performed using the t/t mouse model has shown that the absence of cMyBP-C in this model leads to a shorter myosin cross-bridge lifetime when the myosin isoform is controlled and a compression of the cardiac myofilament lattice induced by rigor (Palmer et al., 2011). Additionally, it was demonstrated that a constitutively unphosphorylated form of cMyBP-C developed on the t/t background (AllP-$_{t/t}$) had the same effect suggesting that the presence and phosphorylation of cMyBP-C at it's N' region provides structural support and radial rigidity to the myofilament lattice (Palmer et al., 2011). Stated differently, this suggests that the cMyBP-C provides radial rigidity to the myofilament lattice through its N' region and that disruption of phosphorylation of cMyBP-C is sufficient to abolish this structural role of the N' region of cMyBP-C and shorten

cross-bridge lifetime (Palmer et al., 2011). Intriguingly, this may explain why an elevation in phosphorylation of cMyBP-C from cMyBP-C^{110kDa} hearts was observed in this study. During HF, cMyBP-C has been shown to be dephosphorylated (Sadayappan et al., 2006a; Tong, Gaffin, Zawieja, & Muthuchamy, 2004). However, more recently, cMyBP-C has been shown to be hyperphosphorylated following MI as the hearts became decompensated (Toepfer et al., 2016). Extrapolating the findings by Palmer *et al.* that both the absence or dephosphorylation of cMyBP-C leads to structural alterations and shortened cross-bridge lifetime, it is possible that when cMyBP-C is absent or dephosphorylated, the restraint it places on myosin heads from interacting with actin is abolished leading to increased cross-bridge cycling rate and decreased cross-bridge lifetime. Here, I found that the absence of the N'-C0-C1f region of cMyBP-C led to increased rate of tension redevelopment after a rapid slack-restretch maneuver and an increase in maximal force production at maximum levels of Ca^{2+} suggesting decreased cross-bridge lifetime and increased cross-bridge cycling rate as was observed on studies with t/t mice. The increase in k_{tr} in cMyBP-C^{110kDa} fibers may also indicate that more fibers are binding faster, which could lead to the increase in maximal force observed in these fibers. Furthermore, it is possible that the hyperphosphorylation of cMyBP-C in cMyBP-C^{110kDa} sarcomeres may act as a compensatory mechanism that attempts to increase cross-bridge lifetime and slow cross-bridge cycling rate. However, while this may be effective in FL cMyBP-C, this effort is futile in the N' truncated

cMyBP-C^{110kDa} protein. Yet, the exact mechanism by which this would occur is difficult to determine as it is currently thought that the phosphorylation of cMyBP-C at low Ca^{2+} relieves cMyBP-C's constraint on myosin heads and may activate the thin filament and accelerate cross-bridge kinetics (Tong, Stelzer, Greaser, Powers, & Moss, 2008) while at high Ca^{2+}, cMyBP-C binding to the thin filament may slow thin filament sliding within the C-zone. Therefore, in the cMyBP-C^{110kDa} mouse model, the hyperphosphorylation of the cMyBP-C^{110kDa} TG protein may increase cross-bridge cycling kinetics at low Ca^{2+} further accounting for the increased k$_{tr}$ but may act to slow cross-bridge cycling rate and increase cross-bridge lifetime at high Ca^{2+} levels due to more molecules of cMyBP-C binding to actin. However, again, this effort at high Ca^{2+} would be fruitless in an N' truncated form of cMyBP-C such as the cMyBP-C^{110kDa} protein. Additionally, the ablation of the PKA phosphorylation motif for phosphorylation of serine 273 in the cMyBP-C^{110kDa} TG protein may play a role in the ability (or inability) of this protein to regulate contraction.

Additional work by Palmer *et al*. using the intact heart, trabeculae, and skinned fibers from t/t mice indicated that t/t ventricles display reduced peak elastance and an abbreviation of systolic elastance time course (Palmer, Georgakopoulos, et al., 2004). This was also observed in the cMyBP-C knockout mouse model (Palmer, Georgakopoulos, et al., 2004). Furthermore, t/t mice displayed earlier time-to-peak trabecular tension, increased unloaded shortening velocity in skinned muscle strips, and reduced myofilament stiffness at diastolic

calcium concentrations (Palmer, Georgakopoulos, et al., 2004). Conclusively, t/t mice exhibited abnormal sarcomere shortening velocity and abbreviated muscle stiffening (Palmer, Georgakopoulos, et al., 2004). Additionally, Palmer *et al*. demonstrated reduced cross-bridge dependent stiffness of skinned myocardium from t/t mice (Palmer, McConnell, et al., 2004). In the present study, no difference in stiffness normalized to force production was observed between cMyBP-C[110kDa] and NTG skinned fibers, indicating a potential role for the more C' region of cMyBP-C in regulating cross-bridge dependent stiffness within the sarcomere. Importantly, much of the current understanding of the role cMyBP-C plays in regulating cardiac contractile function comes from studies on the cMyBP-C knockout mouse. As mentioned previously, isolated cardiac myocytes from cMyBP-C knockout hearts develop a reduction in myofilament Ca^{2+} sensitivity of tension (Harris et al., 2002), deficit in diastolic relaxation and increased LA myofilament Ca^{2+} sensitivity (Pohlmann et al., 2007), acceleration of stretch activation (Stelzer, Dunning, et al., 2006) and force development (Stelzer, Fitzsimons, et al., 2006), and loss of PKA mediated stretch activation (Stelzer, Patel, et al., 2006). Furthermore, cMyBP-C knockout mice failed to compensate for increased load and demonstrated a significant reduction in systolic and diastolic function when challenged with pressure overload (Brickson et al., 2007). Finally, ablation of cMyBP-C led to radial displacement of myosin cross-bridges in cMyBP-C knockout myofibrils compared to wild-type controls (Colson et al., 2007). Interestingly, cMyBP-C knockout LV myocytes had a reduction in Ca^{2+}

sensitivity of tension (Harris et al., 2002), while isolated knockout LA had an increase in sensitivity to external Ca^{2+}. In contrast, papillary muscle fibers from the cMyBP-C^{110kDa} mice used in this study showed no difference in Ca^{2+} sensitivity of force development compared to fibers from NTG controls, indicating that regions beyond the N'-C0-C1f region of cMyBP-C may be implicated in cMyBP-C's regulation of myocardial Ca^{2+} sensitivity of tension.

As mentioned previously, in this study, isolated, permeabilized papillary muscle fibers from cMyBP-C^{110kDa} hearts generated a significant elevation in maximal force production and k_{tr} compared to fibers from NTG controls at 3-months of age. This may be the underlying contractile abnormality within the cardiac sarcomeres of these animals that leads to global cardiac remodeling and dysfunction. Interestingly, no clear difference in sarcomere organization (data not shown; collaboration with Dr. Roger Craig) was observed between cMyBP-C^{110kDa} and NTG animals, likely due to previous observations that the C' region is the portion of cMyBP-C important for its incorporation into the C-zone of the cardiac sarcomere (Freiburg & Gautel, 1996; Gilbert et al., 1999; Miyamoto et al., 1999; Okagaki et al., 1993; Pfuhl & Gautel, 2012). Recently, our group has generated a mouse model that harbors a frameshift mutation within the C' C10 domain of cMyBP-C that leads to aberrant mislocalization of cMyBP-C at the Z-lines of the cardiac sarcomere and contractile dysfunction (unpublished data), which we also observed by adenoviral expression of this mutant form of cMyBP-C in adult rat cardiomyocytes (Kuster et al., 2015). This further suggests the

importance of the C' region of cMyBP-C in the localization of cMyBP-C within the sarcomere. However, the findings that I present here clearly demonstrate that the cMyBP-C^{110kDa} TG protein properly localizes to the C-zone of the cardiac sarcomere and, therefore, the cardiac dysfunction observed is likely instigated by the absence of the N'-C0-C1f region of cMyBP-C and not aberrant mislocalization of this protein, which has its C' region intact allowing for proper incorporation. Intriguingly, the ability of cMyBP-C to slow actin-filament sliding within the C-zone of native thick filaments isolated from NTG hearts was lost on thick filaments from cMyBP-C^{110kDa} hearts (data not shown; collaboration with Dr. David Warshaw and Dr. Michael Previs). Particularly important, the cMyBP-C^{110kDa} mouse model was developed based upon several of the following observations. Initially, our group identified this region as a predominant N' cleavage fragment of cMyBP-C following myocardial ischemic injury (Govindan, McElligott, et al., 2012). Furthermore, we discovered that the C0-C1f fragment was sufficient to cause contractile dysfunction in isolated rat ventricular myocytes (Govindan, Sarkey, et al., 2012) and that it could impair myofilament function in human cardiac myofilaments (Witayavanitkul et al., 2014). Later work by Razzaque *et al.* demonstrated that endogenous expression of C0-C1f was sufficient to cause HCM and HF in mice (Razzaque et al., 2013). Most importantly and referring back to our observation that the cMyBP-C^{110kDa} TG protein could not slow actin-filament sliding within the C-zone of native thick filaments from cMyBP-C^{110kDa} hearts, it has been reported that the first 17

residues of the M-domain (the "f" region of C0-C1f) are crucial to the ability of C0-C1f to inhibit actin filament sliding over myosin (Previs et al., 2012; A. Weith et al., 2012). This may implicate a role for the N'-C0-C1f region of cMyBP-C in regulating cMyBP-C's interactions and function at both low and high Ca^{2+} levels. Together, these previous studies and my findings in this study suggest that the N'-C0-C1f region of cMyBP-C is necessary for regulating myofilament function. Therefore, I conclude that the N'-C0-C1f region of cMyBP-C is essential for cMyBP-C's regulation of both actomyosin interactions and cardiac contractile function.

CHAPTER SEVEN

CONCLUSIONS AND FUTURE DIRECTIONS

In conclusion, the data that I have presented here demonstrate that cMyBP-C^{110kDa} mice, which lack the N'-C0-C1f region of cMyBP-C, develop cardiac dysfunction that progresses to severity by 6-months of age. Indeed, cMyBP-C^{110kDa} mice developed a significant deficit in cardiac function at the level of the whole heart and at the tissue fiber level. Furthermore, cMyBP-C^{110kDa} mice developed cardiac enlargement and an elevation in markers of pathological hypertrophy as well as an increase in myocardial fibrosis. Importantly, the cMyBP-C^{110kDa} TG protein localized properly within the C-zone of the cardiac sarcomere along with endogenous FL-cMyBP-C. Together, these data indicate that the N'-C0-C1f region of cMyBP-C is a critical regulator of cardiac function and is necessary for maintaining normal cardiac function. Therefore, this study has been important for expanding the current body of knowledge on cMyBP-C's mechanistic function in both health and disease and may provide a better understanding of which N' domains of cMyBP-C are important for regulating actomyosin function and cardiac contractile function *in vivo*. Translating this clinically, the results of this study could prove important for understanding the cellular mechanisms by which individuals with N' mutations in cMyBP-C develop cardiomyopathies.

Future efforts by our group will focus on further understanding how cMyBP-C regulates cardiac contraction from its N' to C' domains and will specifically focus on how mutations in cMyBP-C lead to both HCM and DCM. As such, we are currently performing genome-wide studies of how cMyBP-C mutations lead to HCM, for example. Specific to the cMyBP-C^{110kDa} TG mouse model, an important future experiment that we are pursuing is to perform X-ray diffraction studies in collaboration with Dr. Thomas Irving at the Illinois Institute of Technology and Argon National Laboratories to elucidate myofilament lattice spacing between actin and myosin filaments in cMyBP-C^{110kDa} sarcomeres compared NTG sarcomeres. We hypothesize that the absence of the N'-C0-C1f region of cMyBP-C disables cMyBP-C from complete binding to myosin's S2 region and may thereby lead to increased proximity of myosin to actin and a decrease in lattice spacing. Furthermore, our group has considered replacing the N' region of cMyBP-C by expressing the N'-C0C2 region of cMyBP-C in cMyBP-C^{110kDa} hearts with the use of adeno-associated virus to determine if we could prevent cardiac dysfunction in these animals.

While cMyBP-C has been well studied since its initially discovery in the early 1970's, it's exact mechanistic function, particularly in relation to its function at low and high Ca^{2+} levels, is still being investigated. It is my hope that the work that I have performed during my dissertation studies has provided a better understanding of cMyBP-C's function and that the cMyBP-C^{110kDa} TG mouse model will be a useful tool to other scientists seeking to answer novel questions

in relation to cMyBP-C's role in regulating cardiac function. Perhaps, together, my work and future work by others using this mouse model will prove to be one step forward in the journey to find cures for human cardiomyopathy caused by cMyBP-C mutations.

REFERENCES

Ababou, A., Gautel, M., & Pfuhl, M. (2007). Dissecting the N-terminal myosin binding site of human cardiac myosin-binding protein C. Structure and myosin binding of domain C2. *J Biol Chem, 282*(12), 9204-9215.

Ababou, A., Rostkova, E., Mistry, S., Le Masurier, C., Gautel, M., & Pfuhl, M. (2008). Myosin binding protein C positioned to play a key role in regulation of muscle contraction: structure and interactions of domain C1. *J Mol Biol, 384*(3), 615-630.

Ackermann, M. A., & Kontrogianni-Konstantopoulos, A. (2010). Myosin binding protein-C slow: an intricate subfamily of proteins. *J Biomed Biotechnol, 2010*, 652065.

Ackermann, M. A., & Kontrogianni-Konstantopoulos, A. (2011). Myosin binding protein-C: a regulator of actomyosin interaction in striated muscle. *J Biomed Biotechnol, 2011*, 636403.

Ahmad, MI. (2012). Biomarkers in Acute Myocardial Infarction. *J Clin Exp, 3*(22).

Aird, W. C. (2011). Discovery of the cardiovascular system: from Galen to William Harvey. *J Thromb Haemost, 9 Suppl 1*, 118-129.

Ambardekar, A. V., & Buttrick, P. M. (2011). Reverse remodeling with left ventricular assist devices: a review of clinical, cellular, and molecular effects. *Circ Heart Fail, 4*(2), 224-233.

Andersen, M. J., Ersboll, M., Axelsson, A., Gustafsson, F., Hassager, C., Kober, L., Borlaug, B. A., Boesgaard, S., Skovgaard, L. T., & Moller, J. E. (2013). Sildenafil and diastolic dysfunction after acute myocardial infarction in patients with preserved ejection fraction: the Sildenafil and Diastolic Dysfunction After Acute Myocardial Infarction (SIDAMI) trial. *Circulation, 127*(11), 1200-1208.

Balke, C. W., & Shorofsky, S. R. (1998). Alterations in calcium handling in cardiac hypertrophy and heart failure. *Cardiovasc Res, 37*(2), 290-299.

Bardswell, S. C., Cuello, F., Kentish, J. C., & Avkiran, M. (2012). cMyBP-C as a promiscuous substrate: phosphorylation by non-PKA kinases and its potential significance. *J Muscle Res Cell Motil, 33*(1), 53-60.

159

Barefield, D., Kumar, M., de Tombe, P. P., & Sadayappan, S. (2014). Contractile dysfunction in a mouse model expressing a heterozygous MYBPC3 mutation associated with hypertrophic cardiomyopathy. *Am J Physiol Heart Circ Physiol*.

Barefield, D., Kumar, M., Gorham, J., Seidman, J. G., Seidman, C. E., de Tombe, P. P., & Sadayappan, S. (2015). Haploinsufficiency of MYBPC3 exacerbates the development of hypertrophic cardiomyopathy in heterozygous mice. *J mol Cell Cardiol, 79*, 234-243.

Barefield, D., & Sadayappan, S. (2010). Phosphorylation and function of cardiac myosin binding protein-C in health and disease. *J mol Cell Cardiol, 48*(5), 866-875.

Barry, W. H., & Bridge, J. H. (1993). Intracellular calcium homeostasis in cardiac myocytes. *Circulation, 87*(6), 1806-1815.

Bennett, P., Craig, R., Starr, R., & Offer, G. (1986). The ultrastructural location of C-protein, X-protein and H-protein in rabbit muscle. *J Muscle Res Cell Motil, 7*(6), 550-567.

Bers, D. M. (2002). Cardiac excitation-contraction coupling. *Nature, 415*(6868), 198-205.

Bezold, K. L., Shaffer, J. F., Khosa, J. K., Hoye, E. R., & Harris, S. P. (2013). A gain-of-function mutation in the M-domain of cardiac myosin-binding protein-C increases binding to actin. *J Biol Chem, 288*(30), 21496-21505.

Bhuiyan, M. S., Gulick, J., Osinska, H., Gupta, M., & Robbins, J. (2012). Determination of the critical residues responsible for cardiac myosin binding protein C's interactions. *J Mol Cell Cardiol, 53*(6), 838-847.

Borlaug, B. A., & Paulus, W. J. (2011). Heart failure with preserved ejection fraction: pathophysiology, diagnosis, and treatment. *Eur Heart J, 32*(6), 670-679.

Brickson, S., Fitzsimons, D. P., Pereira, L., Hacker, T., Valdivia, H., & Moss, R. L. (2007). In vivo left ventricular functional capacity is compromised in cMyBP-C null mice. *Am J Physiol Heart Circ Physiol, 292*(4), H1747-1754.

Burchfield, J. S., Xie, M., & Hill, J. A. (2013). Pathological ventricular remodeling: mechanisms: part 1 of 2. *Circulation, 128*(4), 388-400.

Bursi, F., Weston, S. A., Redfield, M. M., Jacobsen, S. J., Pakhomov, S., Nkomo, V. T., Meverden, R. A., & Roger, V. L. (2006). Systolic and diastolic heart failure in the community. *JAMA, 296*(18), 2209-2216.

Calaghan, S. C., Trinick, J., Knight, P. J., & White, E. (2000). A role for C-protein in the regulation of contraction and intracellular Ca2+ in intact rat ventricular myocytes. *J Physiol, 528 Pt 1*, 151-156.

Cazorla, O., Vassort, G., Garnier, D., & Le Guennec, J. Y. (1999). Length modulation of active force in rat cardiac myocytes: is titin the sensor? *J mol Cell Cardiol, 31*(6), 1215-1227.

Cazorla, O., Wu, Y., Irving, T. C., & Granzier, H. (2001). Titin-based modulation of calcium sensitivity of active tension in mouse skinned cardiac myocytes. *Circ Res, 88*(10), 1028-1035.

Chandra, M., Rundell, V. L., Tardiff, J. C., Leinwand, L. A., De Tombe, P. P., & Solaro, R. J. (2001). Ca(2+) activation of myofilaments from transgenic mouse hearts expressing R92Q mutant cardiac troponin T. *Am J Physiol Heart Circ Physiol, 280*(2), H705-713.

Chatterjee, K., & Rame, J. E. (2008). Systolic heart failure: chronic and acute syndromes. *Crit Care Med, 36*(1 Suppl), S44-51.

Cohn, J. N., Ferrari, R., & Sharpe, N. (2000). Cardiac remodeling--concepts and clinical implications: a consensus paper from an international forum on cardiac remodeling. Behalf of an International Forum on Cardiac Remodeling. *J Am Coll Cardiol, 35*(3), 569-582.

Colson, B. A., Bekyarova, T., Fitzsimons, D. P., Irving, T. C., & Moss, R. L. (2007). Radial displacement of myosin cross-bridges in mouse myocardium due to ablation of myosin binding protein-C. *J Mol Biol, 367*(1), 36-41.

Colson, B. A., Locher, M. R., Bekyarova, T., Patel, J. R., Fitzsimons, D. P., Irving, T. C., & Moss, R. L. (2010). Differential roles of regulatory light chain and myosin binding protein-C phosphorylations in the modulation of cardiac force development. *J Physiol, 588*(Pt 6), 981-993.

Copeland, O., Sadayappan, S., Messer, A. E., Steinen, G. J., van der Velden, J., & Marston, S. B. (2010). Analysis of cardiac myosin binding protein-C phosphorylation in human heart muscle. *J mol Cell Cardiol, 49*(6), 1003-1011.

Cowie, M. R., Mosterd, A., Wood, D. A., Deckers, J. W., Poole-Wilson, P. A., Sutton, G. C., & Grobbee, D. E. (1997). The epidemiology of heart failure. *Eur Heart J, 18*(2), 208-225.

Craig, R., Lee, K. H., Mun, J. Y., Torre, I., & Luther, P. K. (2014). Structure, sarcomeric organization, and thin filament binding of cardiac myosin-binding protein-C. *Pflugers Arch, 466*(3), 425-431.

Craig, R., & Offer, G. (1976). The location of C-protein in rabbit skeletal muscle. *Proc R Soc Lond B Biol Sci, 192*(1109), 451-461.

Dargie, H. (2005). Heart failure post-myocardial infarction: a review of the issues. *Heart, 91 Suppl 2*, ii3-6; discussion ii31, ii43-38.

de Tombe, P. P. (1998). Altered contractile function in heart failure. *Cardiovasc Res, 37*(2), 367-380.

de Tombe, P. P., & Stienen, G. J. (1995). Protein kinase A does not alter economy of force maintenance in skinned rat cardiac trabeculae. *Circ Res, 76*(5), 734-741.

de Tombe, P. P., & ter Keurs, H. E. (1990). Force and velocity of sarcomere shortening in trabeculae from rat heart. Effects of temperature. *Circ Res, 66*(5), 1239-1254.

de Winter, R. J., & Tijssen, J. G. (2012). Non-ST-segment elevation myocardial infarction: revascularization for everyone? *JACC Cardiovasc Interv, 5*(9), 903-905.

Decker, R. S., Decker, M. L., Kulikovskaya, I., Nakamura, S., Lee, D. C., Harris, K., Klocke, F. J., & Winegrad, S. (2005). Myosin binding protein C phosphorylation, myofibril structure, and contractile function during low-flow ischemia. *Circulation, 111*(7), 906-912.

Dhalla, N. S., Kaura, D., Liu, X., & Beamish, R. E. (1996). Mechanisms of subcellular remodelling in post-infarct heart failure. *EXS, 76*, 463-477.

Dhoot, G. K., & Perry, S. V. (2005). Expression of slow skeletal myosin binding C-protein in normal adult mammalian heart. *J Muscle Res Cell Motil, 26*(2-3), 143-148.

Dorn, G. W., 2nd. (2009). Novel pharmacotherapies to abrogate postinfarction ventricular remodeling. *Nat Rev Cardiol, 6*(4), 283-291.

Ehler, E., Rothen, B. M., Hammerle, S. P., Komiyama, M., & Perriard, J. C. (1999). Myofibrillogenesis in the developing chicken heart: assembly of Z-disk, M-line and the thick filaments. *J Cell Sci, 112 (Pt 10)*, 1529-1539.

Ferguson, J. L., Beckett, G. J., Stoddart, M., Walker, S. W., & Fox, K. A. (2002). Myocardial infarction redefined: the new ACC/ESC definition, based on cardiac troponin, increases the apparent incidence of infarction. *Heart, 88*(4), 343-347.

Flashman, E., Korkie, L., Watkins, H., Redwood, C., & Moolman-Smook, J. C. (2008). Support for a trimeric collar of myosin binding protein C in cardiac and fast skeletal muscle, but not in slow skeletal muscle. *FEBS Lett, 582*(3), 434-438.

Flashman, E., Redwood, C., Moolman-Smook, J., & Watkins, H. (2004). Cardiac myosin binding protein C: its role in physiology and disease. *Circ Res, 94*(10), 1279-1289.

Flashman, E., Watkins, H., & Redwood, C. (2007). Localization of the binding site of the C-terminal domain of cardiac myosin-binding protein-C on the myosin rod. *Biochem J, 401*(1), 97-102.

Ford, L. E., Huxley, A. F., & Simmons, R. M. (1977). Tension responses to sudden length change in stimulated frog muscle fibres near slack length. *J Physiol, 269*(2), 441-515.

Francis, G. S., & McDonald, K. M. (1992). Left ventricular hypertrophy: an initial response to myocardial injury. *Am J Cardiol, 69*(18), 3G-7G; discussion 7G-9G.

Freiburg, A., & Gautel, M. (1996). A molecular map of the interactions between titin and myosin-binding protein C. Implications for sarcomeric assembly in familial hypertrophic cardiomyopathy. *Eur J Biochem, 235*(1-2), 317-323.

Fuchs, F., & Smith, S. H. (2001). Calcium, cross-bridges, and the Frank-Starling relationship. *News Physiol Sci, 16*, 5-10.

Fuchs, F., & Wang, Y. P. (1996). Sarcomere length versus interfilament spacing as determinants of cardiac myofilament Ca2+ sensitivity and Ca2+ binding. *J mol Cell Cardiol, 28*(7), 1375-1383.

Fukuda, N., Sasaki, D., Ishiwata, S., & Kurihara, S. (2001). Length dependence of tension generation in rat skinned cardiac muscle: role of titin in the Frank-Starling mechanism of the heart. *Circulation, 104*(14), 1639-1645.

Furst, D. O., Vinkemeier, U., & Weber, K. (1992). Mammalian skeletal muscle C-protein: purification from bovine muscle, binding to titin and the characterization of a full-length human cDNA. *J Cell Sci, 102 (Pt 4)*, 769-778.

Gao, W. D., Atar, D., Liu, Y., Perez, N. G., Murphy, A. M., & Marban, E. (1997). Role of troponin I proteolysis in the pathogenesis of stunned myocardium. *Circ Res, 80*(3), 393-399.

Gautel, M., Zuffardi, O., Freiburg, A., & Labeit, S. (1995). Phosphorylation switches specific for the cardiac isoform of myosin binding protein-C: a modulator of cardiac contraction? *EMBO J, 14*(9), 1952-1960.

Gheorghiade, M., Sopko, G., De Luca, L., Velazquez, E. J., Parker, J. D., Binkley, P. F., Sadowski, Z., Golba, K. S., Prior, D. L., Rouleau, J. L., & Bonow, R. O. (2006). Navigating the crossroads of coronary artery disease and heart failure. *Circulation, 114*(11), 1202-1213.

Gilbert, R., Cohen, J. A., Pardo, S., Basu, A., & Fischman, D. A. (1999). Identification of the A-band localization domain of myosin binding proteins C and H (MyBP-C, MyBP-H) in skeletal muscle. *J Cell Sci, 112 (Pt 1)*, 69-79.

Go, A. S., Mozaffarian, D., Roger, V. L., Benjamin, E. J., Berry, J. D., Blaha, M. J., Dai, S., Ford, E. S., Fox, C. S., Franco, S., Fullerton, H. J., Gillespie, C., Hailpern, S. M., Heit, J. A., Howard, V. J., Huffman, M. D., Judd, S. E., Kissela, B. M., Kittner, S. J., Lackland, D. T., Lichtman, J. H., Lisabeth, L. D., Mackey, R. H., Magid, D. J., Marcus, G. M., Marelli, A., Matchar, D. B., McGuire, D. K., Mohler, E. R., 3rd, Moy, C. S., Mussolino, M. E., Neumar, R. W., Nichol, G., Pandey, D. K., Paynter, N. P., Reeves, M. J., Sorlie, P. D., Stein, J., Towfighi, A., Turan, T. N., Virani, S. S., Wong, N. D., Woo, D., Turner, M. B., on behalf of the American Heart Association Statistics, Committee, & Stroke Statistics, Subcommittee. (2013). Heart Disease and Stroke Statistics--2014 Update: A Report From the American Heart Association. *Circulation*. 129(3), e28-e292.

Gordin, J. S., & Fonarow, G. C. (2016). New medications for heart failure. *Trends Cardiovasc Med*.

Govindan, S., Kuster, D. W., Lin, B., Kahn, D. J., Jeske, W. P., Walenga, J. M., Leya, F., Hoppensteadt, D., Fareed, J., & Sadayappan, S. (2013). Increase in cardiac myosin binding protein-C plasma levels is a sensitive and cardiac-specific biomarker of myocardial infarction. *Am J Cardiovasc Dis, 3*(2), 60-70.

Govindan, S., McElligott, A., Muthusamy, S., Nair, N., Barefield, D., Martin, J. L., Gongora, E., Greis, K. D., Luther, P. K., Winegrad, S., Henderson, K. K., & Sadayappan, S. (2012). Cardiac myosin binding protein-C is a potential diagnostic biomarker for myocardial infarction. *J mol Cell Cardiol, 52*(1), 154-164.

Govindan, S., Sarkey, J., Ji, X., Sundaresan, N. R., Gupta, M. P., de Tombe, P. P., & Sadayappan, S. (2012). Pathogenic properties of the N-terminal region of cardiac myosin binding protein-C in vitro. *J Muscle Res Cell Motil, 33*(1), 17-30.

Gruen, M., & Gautel, M. (1999). Mutations in beta-myosin S2 that cause familial hypertrophic cardiomyopathy (FHC) abolish the interaction with the regulatory domain of myosin-binding protein-C. *J Mol Biol, 286*(3), 933-949.

Gruen, M., Prinz, H., & Gautel, M. (1999). cAPK-phosphorylation controls the interaction of the regulatory domain of cardiac myosin binding protein C with myosin-S2 in an on-off fashion. *FEBS Lett, 453*(3), 254-259.

Gulick, J., Hewett, T. E., Klevitsky, R., Buck, S. H., Moss, R. L., & Robbins, J. (1997). Transgenic remodeling of the regulatory myosin light chains in the mammalian heart. *Circ Res, 80*(5), 655-664.

Gupta, S., Prahash, A. J., & Anand, I. S. (2000). Myocyte contractile function is intact in the post-infarct remodeled rat heart despite molecular alterations. *Cardiovasc Res, 48*(1), 77-88.

Guth, K., & Wojciechowski, R. (1986). Perfusion cuvette for the simultaneous measurement of mechanical, optical and energetic parameters of skinned muscle fibres. *Pflugers Arch, 407*(5), 552-557.

Gutierrez, C., & Blanchard, D. G. (2004). Diastolic heart failure: challenges of diagnosis and treatment. *Am Fam Physician, 69*(11), 2609-2616.

Haissaguerre, M., Vigmond, E., Stuyvers, B., Hocini, M., & Bernus, O. (2016). Ventricular arrhythmias and the His-Purkinje system. *Nat Rev Cardiol, 13*(3), 155-166.

Hall, T. S., Hallen, J., Agewall, S., Atar, D., & Jensen, T. (2012). Changes in diagnosing non-ST-segment elevation myocardial infarction after the introduction of a new high-sensitivity cardiac troponin T assay: a single-centre experience. *Clin Lab, 58*(9-10), 1029-1036.

Harris, S. P., Bartley, C. R., Hacker, T. A., McDonald, K. S., Douglas, P. S., Greaser, M. L., Powers, P. A., & Moss, R. L. (2002). Hypertrophic cardiomyopathy in cardiac myosin binding protein-C knockout mice. *Circ Res, 90*(5), 594-601.

Harris, S. P., Rostkova, E., Gautel, M., & Moss, R. L. (2004). Binding of myosin binding protein-C to myosin subfragment S2 affects contractility independent of a tether mechanism. *Circ Res, 95*(9), 930-936.

Hartzell, H. C., & Sale, W. S. (1985). Structure of C protein purified from cardiac muscle. *J Cell Biol, 100*(1), 208-215.

Heidenreich, P. A., Albert, N. M., Allen, L. A., Bluemke, D. A., Butler, J., Fonarow, G. C., Ikonomidis, J. S., Khavjou, O., Konstam, M. A., Maddox, T. M., Nichol, G., Pham, M., Pina, I. L., Trogdon, J. G., American Heart Association Advocacy Coordinating, Committee, Council on Arteriosclerosis, Thrombosis, Vascular, Biology, Council on Cardiovascular, Radiology, Intervention, Council on Clinical, Cardiology, Council on, Epidemiology, Prevention, & Stroke, Council. (2013). Forecasting the impact of heart failure in the United States: a policy statement from the American Heart Association. *Circ Heart Fail, 6*(3), 606-619.

Heidenreich, P. A., Trogdon, J. G., Khavjou, O. A., Butler, J., Dracup, K., Ezekowitz, M. D., Finkelstein, E. A., Hong, Y., Johnston, S. C., Khera, A., Lloyd-Jones, D. M., Nelson, S. A., Nichol, G., Orenstein, D., Wilson, P. W., Woo, Y. J., American Heart Association Advocacy Coordinating, Committee, Stroke, Council, Council on Cardiovascular, Radiology, Intervention, Council on Clinical, Cardiology, Council on, Epidemiology, Prevention, Council on, Arteriosclerosis, Thrombosis, Vascular, Biology, Council on, Cardiopulmonary, Critical, Care, Perioperative, Resuscitation, Council on Cardiovascular, Nursing, Council on the Kidney in Cardiovascular, Disease, Council on Cardiovascular, Surgery, Anesthesia, Interdisciplinary Council on Quality of, Care, & Outcomes, Research. (2011). Forecasting the future of cardiovascular disease in the United States: a policy statement from the American Heart Association. *Circulation, 123*(8), 933-944.

Herron, T. J., Rostkova, E., Kunst, G., Chaturvedi, R., Gautel, M., & Kentish, J. C. (2006). Activation of myocardial contraction by the N-terminal domains of myosin binding protein-C. *Circ Res, 98*(10), 1290-1298.

Hofmann, P. A., & Fuchs, F. (1988). Bound calcium and force development in skinned cardiac muscle bundles: effect of sarcomere length. *J mol Cell Cardiol, 20*(8), 667-677.

Horowits, R., Kempner, E. S., Bisher, M. E., & Podolsky, R. J. (1986). A physiological role for titin and nebulin in skeletal muscle. *Nature, 323*(6084), 160-164.

Howarth, J. W., Ramisetti, S., Nolan, K., Sadayappan, S., & Rosevear, P. R. (2012). Structural insight into unique cardiac myosin-binding protein-C motif: a partially folded domain. *J Biol Chem, 287*(11), 8254-8262.

Hsueh, W. A., Law, R. E., & Do, Y. S. (1998). Integrins, adhesion, and cardiac remodeling. *Hypertension, 31*(1 Pt 2), 176-180.

Jia, W., Shaffer, J. F., Harris, S. P., & Leary, J. A. (2010). Identification of novel protein kinase A phosphorylation sites in the M-domain of human and murine cardiac myosin binding protein-C using mass spectrometry analysis. *J Proteome Res, 9*(4), 1843-1853.

Johnson, M. (1998). The beta-adrenoceptor. *Am J Respir Crit Care Med, 158*(5 Pt 3), S146-153.

Julian, F. J., Moss, R. L., & Waller, G. S. (1981). Mechanical properties and myosin light chain composition of skinned muscle fibres from adult and new-born rabbits. *J Physiol, 311*, 201-218.

Kampourakis, T., Yan, Z., Gautel, M., Sun, Y. B., & Irving, M. (2014). Myosin binding protein-C activates thin filaments and inhibits thick filaments in heart muscle cells. *Proc Natl Acad Sci U S A, 111*(52), 18763-18768.

Karsai, A., Kellermayer, M. S., & Harris, S. P. (2013). Cross-species mechanical fingerprinting of cardiac myosin binding protein-C. *Biophys J, 104*(11), 2465-2475.

Kass, D. A., Yamazaki, T., Burkhoff, D., Maughan, W. L., & Sagawa, K. (1986). Determination of left ventricular end-systolic pressure-volume relationships by the conductance (volume) catheter technique. *Circulation, 73*(3), 586-595.

Kensler, R. W., Shaffer, J. F., & Harris, S. P. (2011). Binding of the N-terminal fragment C0-C2 of cardiac MyBP-C to cardiac F-actin. *J Struct Biol, 174*(1), 44-51.

Kim, S. E., Lee, J. H., Park, D. G., Han, K. R., & Oh, D. J. (2010). Acute Myocardial Infarction by Right Coronary Artery Occlusion Presenting as Precordial ST Elevation on Electrocardiography. *Korean Circ J, 40*(10), 536-538.

Knoll, R. (2012). Myosin binding protein C: implications for signal-transduction. *J Muscle Res Cell Motil, 33*(1), 31-42.

Konhilas, J. P., Irving, T. C., & de Tombe, P. P. (2002). Myofilament calcium sensitivity in skinned rat cardiac trabeculae: role of interfilament spacing. *Circ Res, 90*(1), 59-65.

Kontrogianni-Konstantopoulos, A., Ackermann, M. A., Bowman, A. L., Yap, S. V., & Bloch, R. J. (2009). Muscle giants: molecular scaffolds in sarcomerogenesis. *Physiol Rev, 89*(4), 1217-1267.

Kranias, E. G., & Hajjar, R. J. (2012). Modulation of cardiac contractility by the phospholamban/SERCA2a regulatome. *Circ Res, 110*(12), 1646-1660.

Kreuzberg, M. M., Willecke, K., & Bukauskas, F. F. (2006). Connexin-mediated cardiac impulse propagation: connexin 30.2 slows atrioventricular conduction in mouse heart. *Trends Cardiovasc Med, 16*(8),

Kunst, G., Kress, K. R., Gruen, M., Uttenweiler, D., Gautel, M., & Fink, R. H. (2000). Myosin binding protein C, a phosphorylation-dependent force regulator in muscle that controls the attachment of myosin heads by its interaction with myosin S2. *Circ Res, 86*(1), 51-58.

Kuster, D. W., Barefield, D., Govindan, S., & Sadayappan, S. (2013). A sensitive and specific quantitation method for determination of serum cardiac Myosin binding protein-C by electrochemiluminescence immunoassay. *J Vis Exp*(78).

Kuster, D. W., Bawazeer, A. C., Zaremba, R., Goebel, M., Boontje, N. M., & van der Velden, J. (2012). Cardiac myosin binding protein C phosphorylation in cardiac disease. *J Muscle Res Cell Motil, 33*(1), 43-52.

Kuster, D. W., Cardenas-Ospina, A., Miller, L., Liebetrau, C., Troidl, C., Nef, H. M., Mollmann, H., Hamm, C. W., Pieper, K. S., Mahaffey, K. W., Kleiman, N. S., Stuyvers, B. D., Marian, A. J., & Sadayappan, S. (2014). Release kinetics of circulating cardiac myosin binding protein-C following cardiac injury. *Am J Physiol Heart Circ Physiol, 306*(4), H547-556.

Kuster, D. W., Govindan, S., Springer, T. I., Martin, J. L., Finley, N. L., & Sadayappan, S. (2015). A hypertrophic cardiomyopathy-associated MYBPC3 mutation common in populations of South Asian descent causes contractile dysfunction. *J Biol Chem, 290*(9), 5855-5867.

Kuster, D. W., Sequeira, V., Najafi, A., Boontje, N. M., Wijnker, P. J., Witjas-Paalberends, E. R., Marston, S. B., Dos Remedios, C. G., Carrier, L., Demmers, J. A., Redwood, C., Sadayappan, S., & van der Velden, J. (2013). GSK3beta phosphorylates newly identified site in the proline-alanine-rich region of cardiac myosin-binding protein C and alters cross-bridge cycling kinetics in human: short communication. *Circ Res, 112*(4), 633-639.

Kusuoka, H., & Marban, E. (1992). Cellular mechanisms of myocardial stunning. *Annu Rev Physiol, 54*, 243-256.

Lanner, J. T., Georgiou, D. K., Joshi, A. D., & Hamilton, S. L. (2010). Ryanodine receptors: structure, expression, molecular details, and function in calcium release. *Cold Spring Harb Perspect Biol, 2*(11), a003996.

Lin, B., Govindan, S., Lee, K., Zhao, P., Han, R., Runte, K. E., Craig, R., Palmer, B. M., & Sadayappan, S. (2013). Cardiac Myosin binding protein-C plays no regulatory role in skeletal muscle structure and function. *PLoS One, 8*(7), e69671.

Lu, Y., Kwan, A. H., Trewhella, J., & Jeffries, C. M. (2011). The C0C1 fragment of human cardiac myosin binding protein C has common binding determinants for both actin and myosin. *J Mol Biol, 413*(5), 908-913.

Luther, P. K., & Craig, R. (2011). Modulation of striated muscle contraction by binding of myosin binding protein C to actin. *Bioarchitecture, 1*(6), 277-283.

Luther, P. K., Winkler, H., Taylor, K., Zoghbi, M. E., Craig, R., Padron, R., Squire, J. M., & Liu, J. (2011). Direct visualization of myosin-binding protein C bridging myosin and actin filaments in intact muscle. *Proc Natl Acad Sci U S A, 108*(28), 11423-11428.

Luther, PK, Bennett, PM, Knupp, C, Craig, R, Padron, R, Harris, SP, Patel, J, & Moss, RL. (2008). Understanding the organisation and role of myosin binding protein C in normal striated muscle by comparison with MyBP-C knockout cardiac muscle. *J Mol Biol, 384*(1), 60-72.

Lynch, T. L., & Sadayappan, S. (2014). Surviving the infarct: A profile of cardiac myosin binding protein-C pathogenicity, diagnostic utility, and proteomics in the ischemic myocardium. *Proteomics Clin Appl*. 8(7-8), 569-77.

Lynch IV, T. L., Sivaguru, M., Velayutham, M., Cardounel, A. J., Michels, M., Barefield, D., Govindan, S., Dos Remedios, C., van der Velden, J., & Sadayappan, S. (2015). Oxidative Stress in Dilated Cardiomyopathy Caused by MYBPC3 Mutation. *Oxid Med Cell Longev, 2015*, 424751.

Maron, B. J., & Maron, M. S. (2013). Hypertrophic cardiomyopathy. *Lancet, 381*(9862), 242-255.

Matsumura, Y., Kusuoka, H., Inoue, M., Hori, M., & Kamada, T. (1993). Protective effect of the protease inhibitor leupeptin against myocardial stunning. *J Cardiovasc Pharmacol, 22*(1), 135-142.

McConnell, B. K., Jones, K. A., Fatkin, D., Arroyo, L. H., Lee, R. T., Aristizabal, O., Turnbull, D. H., Georgakopoulos, D., Kass, D., Bond, M., Niimura, H., Schoen, F. J., Conner, D., Fischman, D. A., Seidman, C. E., & Seidman, J. G. (1999). Dilated cardiomyopathy in homozygous myosin-binding protein-C mutant mice. *J Clin Invest, 104*(12), 1771.

McDonald, K. S., & Moss, R. L. (1995). Osmotic compression of single cardiac myocytes eliminates the reduction in Ca2+ sensitivity of tension at short sarcomere length. *Circ Res, 77*(1), 199-205.

McNally, E. M., Golbus, J. R., & Puckelwartz, M. J. (2013). Genetic mutations and mechanisms in dilated cardiomyopathy. *J Clin Invest, 123*(1), 19-26.

Merlo, M., Pivetta, A., Pinamonti, B., Stolfo, D., Zecchin, M., Barbati, G., Di Lenarda, A., & Sinagra, G. (2014). Long-term prognostic impact of therapeutic strategies in patients with idiopathic dilated cardiomyopathy: changing mortality over the last 30 years. *Eur J Heart Fail, 16*(3), 317-324.

Miyamoto, C. A., Fischman, D. A., & Reinach, F. C. (1999). The interface between MyBP-C and myosin: site-directed mutagenesis of the CX myosin-binding domain of MyBP-C. *J Muscle Res Cell Motil, 20*(7), 703-715.

Moller, J. E., Pellikka, P. A., Hillis, G. S., & Oh, J. K. (2006). Prognostic importance of diastolic function and filling pressure in patients with acute myocardial infarction. *Circulation, 114*(5), 438-444.

Moolman-Smook, J., Flashman, E., de Lange, W., Li, Z., Corfield, V., Redwood, C., & Watkins, H. (2002). Identification of novel interactions between domains of Myosin binding protein-C that are modulated by hypertrophic cardiomyopathy missense mutations. *Circ Res, 91*(8), 704-711.

Moos, C. (1981). Fluorescence microscope study of the binding of added C protein to skeletal muscle myofibrils. *J Cell Biol, 90*(1), 25-31.

Moos, C., Mason, C. M., Besterman, J. M., Feng, I. N., & Dubin, J. H. (1978). The binding of skeletal muscle C-protein to F-actin, and its relation to the interaction of actin with myosin subfragment-1. *J Mol Biol, 124*(4), 571-586.

Morano, I. (1999). Tuning the human heart molecular motors by myosin light chains. *J Mol Med (Berl), 77*(7), 544-555.

Morano, I., Hadicke, K., Grom, S., Koch, A., Schwinger, R. H., Bohm, M., Bartel, S., Erdmann, E., & Krause, E. G. (1994). Titin, myosin light chains and C-protein in the developing and failing human heart. *J mol Cell Cardiol, 26*(3), 361-368.

Moss, R. L., & Fitzsimons, D. P. (2002). Frank-Starling relationship: long on importance, short on mechanism. *Circ Res, 90*(1), 11-13.

Moss, R. L., Fitzsimons, D. P., & Ralphe, J. C. (2015). Cardiac MyBP-C regulates the rate and force of contraction in mammalian myocardium. *Circ Res, 116*(1), 183-192.

Mozaffarian, D., Benjamin, E. J., Go, A. S., Arnett, D. K., Blaha, M. J., Cushman, M., Das, S. R., de Ferranti, S., Despres, J. P., Fullerton, H. J., Howard, V. J., Huffman, M. D., Isasi, C. R., Jimenez, M. C., Judd, S. E., Kissela, B. M., Lichtman, J. H., Lisabeth, L. D., Liu, S., Mackey, R. H., Magid, D. J., McGuire, D. K., Mohler, E. R., 3rd, Moy, C. S., Muntner, P., Mussolino, M. E., Nasir, K., Neumar, R. W., Nichol, G., Palaniappan, L., Pandey, D. K., Reeves, M. J., Rodriguez, C. J., Rosamond, W., Sorlie, P. D., Stein, J., Towfighi, A., Turan, T. N., Virani, S. S., Woo, D., Yeh, R. W., Turner, M. B., American Heart Association Statistics, Committee, & Stroke Statistics, Subcommittee. (2016). Heart Disease and Stroke Statistics-2016 Update: A Report From the American Heart Association. *Circulation, 133*(4), e38-e360.

Mukherjee, R., & Spinale, F. G. (1998). L-type calcium channel abundance and function with cardiac hypertrophy and failure: a review. *J mol Cell Cardiol, 30*(10), 1899-1916.

Mun, J. Y., Gulick, J., Robbins, J., Woodhead, J., Lehman, W., & Craig, R. (2011). Electron microscopy and 3D reconstruction of F-actin decorated with cardiac myosin-binding protein C (cMyBP-C). *J Mol Biol, 410*(2), 214-225.

Mun, J. Y., Previs, M. J., Yu, H. Y., Gulick, J., Tobacman, L. S., Beck Previs, S., Robbins, J., Warshaw, D. M., & Craig, R. (2014). Myosin-binding protein C displaces tropomyosin to activate cardiac thin filaments and governs their speed by an independent mechanism. *Proc Natl Acad Sci U S A, 111*(6), 2170-2175.

Nyland, L. R., Palmer, B. M., Chen, Z., Maughan, D. W., Seidman, C. E., Seidman, J. G., Kreplak, L., & Vigoreaux, J. O. (2009). Cardiac myosin binding protein-C is essential for thick-filament stability and flexural rigidity. *Biophys J, 96*(8), 3273-3280.

Oakley, C. E., Chamoun, J., Brown, L. J., & Hambly, B. D. (2007). Myosin binding protein-C: enigmatic regulator of cardiac contraction. *Int J Biochem Cell Biol, 39*(12), 2161-2166.

Oakley, C. E., Hambly, B. D., Curmi, P. M., & Brown, L. J. (2004). Myosin binding protein C: structural abnormalities in familial hypertrophic cardiomyopathy. *Cell Res, 14*(2), 95-110.

Offer, G., Moos, C., & Starr, R. (1973). A new protein of the thick filaments of vertebrate skeletal myofibrils. Extractions, purification and characterization. *J Mol Biol, 74*(4), 653-676.

Okagaki, T., Weber, F. E., Fischman, D. A., Vaughan, K. T., Mikawa, T., & Reinach, F. C. (1993). The major myosin-binding domain of skeletal muscle MyBP-C (C protein) resides in the COOH-terminal, immunoglobulin C2 motif. *J Cell Biol, 123*(3), 619-626.

Olshansky, B., & Sullivan, R. M. (2013). Inappropriate sinus tachycardia. *J Am Coll Cardiol, 61*(8), 793-801.

Palmer, B. M., Georgakopoulos, D., Janssen, P. M., Wang, Y., Alpert, N. R., Belardi, D. F., Harris, S. P., Moss, R. L., Burgon, P. G., Seidman, C. E., Seidman, J. G., Maughan, D. W., & Kass, D. A. (2004). Role of cardiac myosin binding protein C in sustaining left ventricular systolic stiffening. *Circ Res, 94*(9), 1249-1255.

Palmer, B. M., McConnell, B. K., Li, G. H., Seidman, C. E., Seidman, J. G., Irving, T. C., Alpert, N. R., & Maughan, D. W. (2004). Reduced cross-bridge dependent stiffness of skinned myocardium from mice lacking cardiac myosin binding protein-C. *Mol Cell Biochem, 263*(1-2), 73-80.

Palmer, B. M., Sadayappan, S., Wang, Y., Weith, A. E., Previs, M. J., Bekyarova, T., Irving, T. C., Robbins, J., & Maughan, D. W. (2011). Roles for cardiac MyBP-C in maintaining myofilament lattice rigidity and prolonging myosin cross-bridge lifetime. *Biophys J, 101*(7), 1661-1669.

Pepe, F. A. (1975). Structure of muscle filaments from immunohistochemical and ultrastructural studies. *J Histochem Cytochem, 23*(7), 543-562.

Pepe, F. A., Ashton, F. T., Street, C., & Weisel, J. (1986). The myosin filament. X. Observation of nine subfilaments in transverse sections. *Tissue Cell, 18*(4), 499-508.

Pfaffl, M. W. (2001). A new mathematical model for relative quantification in real-time RT-PCR. *Nucleic Acids Res, 29*(9), e45.

Pfuhl, M., & Gautel, M. (2012). Structure, interactions and function of the N-terminus of cardiac myosin binding protein C (MyBP-C): who does what, with what, and to whom? *J Muscle Res Cell Motil, 33*(1), 83-94.

Pinnell, J. Turner, S. Howell, S. (2007). Cardiac muscle physiology. *Continuing Education in Anaesthesia, Critical Care and Pain, 7*(3), 85-88.

Pohlmann, L., Kroger, I., Vignier, N., Schlossarek, S., Kramer, E., Coirault, C., Sultan, K. R., El-Armouche, A., Winegrad, S., Eschenhagen, T., & Carrier, L. (2007). Cardiac myosin-binding protein C is required for complete relaxation in intact myocytes. *Circ Res, 101*(9), 928-938.

Previs, M. J., Beck Previs, S., Gulick, J., Robbins, J., & Warshaw, D. M. (2012). Molecular mechanics of cardiac myosin-binding protein C in native thick filaments. *Science, 337*(6099), 1215-1218.

Ratti, J., Rostkova, E., Gautel, M., & Pfuhl, M. (2011). Structure and interactions of myosin-binding protein C domain C0: cardiac-specific regulation of myosin at its neck? *J Biol Chem, 286*(14), 12650-12658.

Rayment, I., Holden, H. M., Whittaker, M., Yohn, C. B., Lorenz, M., Holmes, K. C., & Milligan, R. A. (1993). Structure of the actin-myosin complex and its implications for muscle contraction. *Science, 261*(5117), 58-65.

Rayment, I., Rypniewski, W. R., Schmidt-Base, K., Smith, R., Tomchick, D. R., Benning, M. M., Winkelmann, D. A., Wesenberg, G., & Holden, H. M. (1993). Three-dimensional structure of myosin subfragment-1: a molecular motor. *Science, 261*(5117), 50-58.

Razumova, M. V., Bezold, K. L., Tu, A. Y., Regnier, M., & Harris, S. P. (2008). Contribution of the myosin binding protein C motif to functional effects in permeabilized rat trabeculae. *J Gen Physiol, 132*(5), 575-585.

Razumova, M. V., Shaffer, J. F., Tu, A. Y., Flint, G. V., Regnier, M., & Harris, S. P. (2006). Effects of the N-terminal domains of myosin binding protein-C in an in vitro motility assay: Evidence for long-lived cross-bridges. *J Biol Chem, 281*(47), 35846-35854.

Razzaque, M. A., Gupta, M., Osinska, H., Gulick, J., Blaxall, B. C., & Robbins, J. (2013). An endogenously produced fragment of cardiac Myosin-binding protein C is pathogenic and can lead to heart failure. *Circ Res, 113*(5), 553-561.

Reichlin, T., Hochholzer, W., Bassetti, S., Steuer, S., Stelzig, C., Hartwiger, S., Biedert, S., Schaub, N., Buerge, C., Potocki, M., Noveanu, M., Breidthardt, T., Twerenbold, R., Winkler, K., Bingisser, R., & Mueller, C. (2009). Early diagnosis of myocardial infarction with sensitive cardiac troponin assays. *N Engl J Med, 361*(9), 858-867.

Reinach, F. C., Masaki, T., & Fischman, D. A. (1983). Characterization of the C-protein from posterior latissimus dorsi muscle of the adult chicken: heterogeneity within a single sarcomere. *J Cell Biol, 96*(1), 297-300.

Robinson, B. F., Epstein, S. E., Beiser, G. D., & Braunwald, E. (1966). Control of heart rate by the autonomic nervous system. Studies in man on the interrelation between baroreceptor mechanisms and exercise. *Circ Res, 19*(2), 400-411.

Rome, E., Offer, G., & Pepe, F. A. (1973). X-ray diffraction of muscle labelled with antibody to C-protein. *Nat New Biol, 244*(135), 152-154.

Rundell, V. L., Manaves, V., Martin, A. F., & de Tombe, P. P. (2005). Impact of beta-myosin heavy chain isoform expression on cross-bridge cycling kinetics. *Am J Physiol Heart Circ Physiol, 288*(2), H896-903.

Rybakova, I. N., Greaser, M. L., & Moss, R. L. (2011). Myosin binding protein C interaction with actin: characterization and mapping of the binding site. *J Biol Chem, 286*(3), 2008-2016.

Saber, W., Begin, K. J., Warshaw, D. M., & VanBuren, P. (2008). Cardiac myosin binding protein-C modulates actomyosin binding and kinetics in the in vitro motility assay. *J mol Cell Cardiol, 44*(6), 1053-1061.

Sadayappan, S., & de Tombe, P. P. (2012). Cardiac myosin binding protein-C: redefining its structure and function. *Biophys Rev, 4*(2), 93-106.

Sadayappan, S., Greis, K. D., & Robbins, J. (2008). Phosphorylation-dependent proteolysis and pathogenesis of cardiac myosin binding protein-C. *J Mol Cell Cardiol, 44*(S44).

Sadayappan, S., Gulick, J., Klevitsky, R., Lorenz, J. N., Sargent, M., Molkentin, J. D., & Robbins, J. (2009). Cardiac myosin binding protein-C phosphorylation in a {beta}-myosin heavy chain background. *Circulation, 119*(9), 1253-1262.

Sadayappan, S., Gulick, J., Osinska, H., Martin, L. A., Hahn, H. S., Dorn, G. W., 2nd, Klevitsky, R., Seidman, C. E., Seidman, J. G., & Robbins, J. (2005). Cardiac myosin binding protein-C phosphorylation and cardiac function. *Circ Res, 97*(11), 1156-1163.

Sadayappan, S., Osinska, H., Klevitsky, R., Lorenz, J. N., Sargent, M., Molkentin, J. D., Seidman, C. E., Seidman, J. G., & Robbins, J. (2006a). Cardiac myosin binding protein C phosphorylation is cardioprotective. *Proc Natl Acad Sci U S A, 103*(45), 16918-16923.

Sadayappan, S., Osinska, H., Klevitsky, R., Lorenz, J. N., Sargent, M., Molkentin, J. D., Seidman, C. E., Seidman, J. G., & Robbins, J. (2006b). Cardiac myosin binding protein-C phosphorylation is cardioprotective. *Proc Natl Acad Sci U S A, 103*(45), 16918-16923.

Sagawa, K. (1981). The end-systolic pressure-volume relation of the ventricle: definition, modifications and clinical use. *Circulation, 63*(6), 1223-1227.

Schultheiss, T., Lin, Z. X., Lu, M. H., Murray, J., Fischman, D. A., Weber, K., Masaki, T., Imamura, M., & Holtzer, H. (1990). Differential distribution of subsets of myofibrillar proteins in cardiac nonstriated and striated myofibrils. *J Cell Biol, 110*(4), 1159-1172.

Severs, N. J. (2000). The cardiac muscle cell. *Bioessays, 22*(2), 188-199.

Shaffer, J. F., Kensler, R. W., & Harris, S. P. (2009). The myosin-binding protein C motif binds to F-actin in a phosphorylation-sensitive manner. *J Biol Chem, 284*(18), 12318-12327.

Silverman, M. E. (1985). William Harvey and the discovery of the circulation of blood. *Clin Cardiol, 8*(4), 244-246.

Sivaguru, M., Durgam, S., Ambekar, R., Luedtke, D., Fried, G., Stewart, A., & Toussaint, K. C., Jr. (2010). Quantitative analysis of collagen fiber organization in injured tendons using Fourier transform-second harmonic generation imaging. *Opt Express, 18*(24), 24983-24993.

Sivaguru, M., Fried, G. A., Miller, C. A., & Fouke, B. W. (2014). Multimodal optical microscopy methods reveal polyp tissue morphology and structure in Caribbean reef building corals. *J Vis Exp*(91), e51824.

Sivaguru, M., Fried, G., Sivaguru, B. S., Sivaguru, V. A., Lu, X., Choi, K. H., Saif, M. T., Lin, B., & Sadayappan, S. (2015). Cardiac muscle organization revealed in 3-D by imaging whole-mount mouse hearts using two-photon fluorescence and confocal microscopy. *Biotechniques, 59*(5), 295-308.

Skrzypiec-Spring, M., Grotthus, B., Szelag, A., & Schulz, R. (2007). Isolated heart perfusion according to Langendorff---still viable in the new millennium. *J Pharmacol Toxicol Methods, 55*(2), 113-126.

Sotolongo, R. P., Smith, M. L., & Margolis, W. S. (1990). Coronary angioplasty in emergency treatment of myocardial infarction in a community-hospital setting. *Tex Heart Inst J, 17*(1), 31-36.

Squire, J. M., Luther, P. K., & Knupp, C. (2003). Structural evidence for the interaction of C-protein (MyBP-C) with actin and sequence identification of a possible actin-binding domain. *J Mol Biol, 331*(3), 713-724.

Squire, J. M., Roessle, M., & Knupp, C. (2004). New X-ray diffraction observations on vertebrate muscle: organisation of C-protein (MyBP-C) and troponin and evidence for unknown structures in the vertebrate A-band. *J Mol Biol, 343*(5), 1345-1363.

Starr, R., & Offer, G. (1971). Polypeptide chains of intermediate molecular weight in myosin preparations. *FEBS Lett, 15*(1), 40-44.

Starr, R., & Offer, G. (1978). The interaction of C-protein with heavy meromyosin and subfragment-2. *Biochem J, 171*(3), 813-816.

Stelzer, J. E., Dunning, S. B., & Moss, R. L. (2006). Ablation of cardiac myosin-binding protein-C accelerates stretch activation in murine skinned myocardium. *Circ Res, 98*(9), 1212-1218.

Stelzer, J. E., Fitzsimons, D. P., & Moss, R. L. (2006). Ablation of myosin-binding protein-C accelerates force development in mouse myocardium. *Biophys J, 90*(11), 4119-4127.

Stelzer, J. E., Patel, J. R., & Moss, R. L. (2006). Protein kinase A-mediated acceleration of the stretch activation response in murine skinned myocardium is eliminated by ablation of cMyBP-C. *Circ Res, 99*(8), 884-890.

Stelzer, J. E., Patel, J. R., Walker, J. W., & Moss, R. L. (2007). Differential roles of cardiac myosin-binding protein C and cardiac troponin I in the myofibrillar force responses to protein kinase A phosphorylation. *Circ Res, 101*(5), 503-511.

Struijker-Boudier, H. A., Smits, J. F., & De Mey, J. G. (1995). Pharmacology of cardiac and vascular remodeling. *Annu Rev Pharmacol Toxicol, 35*, 509-539.

Suga, H., & Sagawa, K. (1974). Instantaneous pressure-volume relationships and their ratio in the excised, supported canine left ventricle. *Circ Res, 35*(1), 117-126.

Sumandea, M. P., Pyle, W. G., Kobayashi, T., de Tombe, P. P., & Solaro, R. J. (2003). Identification of a functionally critical protein kinase C phosphorylation residue of cardiac troponin T. *J Biol Chem, 278*(37), 35135-35144.

Swartz, D. R., & Moss, R. L. (1992). Influence of a strong-binding myosin analogue on calcium-sensitive mechanical properties of skinned skeletal muscle fibers. *J Biol Chem, 267*(28), 20497-20506.

Thygesen, K., Alpert, J. S., Jaffe, A. S., Simoons, M. L., Chaitman, B. R., White, H. D., Joint, E. S. C. Accf A. H. A. W. H. F. Task Force for Universal Definition of Myocardial Infarction, Authors/Task Force Members, Chairpersons, Thygesen, K., Alpert, J. S., White, H. D., Biomarker, Subcommittee, Jaffe, A. S., Katus, H. A., Apple, F. S., Lindahl, B., Morrow, D. A., Subcommittee, E. C. G., Chaitman, B. R., Clemmensen, P. M., Johanson, P., Hod, H., Imaging, Subcommittee, Underwood, R., Bax, J. J., Bonow, J. J., Pinto, F., Gibbons, R. J., Classification, Subcommittee, Fox, K. A., Atar, D., Newby, L. K., Galvani, M., Hamm, C. W., Intervention, Subcommittee, Uretsky, B. F., Steg, P. G., Wijns, W., Bassand, J. P., Menasche, P., Ravkilde, J., Trials, Registries, Subcommittee, Ohman, E. M., Antman, E. M., Wallentin, L. C., Armstrong, P. W., Simoons, M. L., Trials, Registries, Subcommittee, Januzzi, J. L., Nieminen, M. S.,

Gheorghiade, M., Filippatos, G., Trials, Registries, Subcommittee, Luepker, R. V., Fortmann, S. P., Rosamond, W. D., Levy, D., Wood, D., Trials, Registries, Subcommittee, Smith, S. C., Hu, D., Lopez-Sendon, J. L., Robertson, R. M., Weaver, D., Tendera, M., Bove, A. A., Parkhomenko, A. N., Vasilieva, E. J., Mendis, S., Guidelines, E. S. C. Committee for Practice, Bax, J. J., Baumgartner, H., Ceconi, C., Dean, V., Deaton, C., Fagard, R., Funck-Brentano, C., Hasdai, D., Hoes, A., Kirchhof, P., Knuuti, J., Kolh, P., McDonagh, T., Moulin, C., Popescu, B. A., Reiner, Z., Sechtem, U., Sirnes, P. A., Tendera, M., Torbicki, A., Vahanian, A., Windecker, S., Document, Reviewers, Morais, J., Aguiar, C., Almahmeed, W., Arnar, D. O., Barili, F., Bloch, K. D., Bolger, A. F., Botker, H. E., Bozkurt, B., Bugiardini, R., Cannon, C., de Lemos, J., Eberli, F. R., Escobar, E., Hlatky, M., James, S., Kern, K. B., Moliterno, D. J., Mueller, C., Neskovic, A. N., Pieske, B. M., Schulman, S. P., Storey, R. F., Taubert, K. A., Vranckx, P., & Wagner, D. R. (2012). Third universal definition of myocardial infarction. *J Am Coll Cardiol, 60*(16), 1581-1598.

Toepfer, C. N., Sikkel, M. B., Caorsi, V., Vydyanath, A., Torre, I., Copeland, O., Lyon, A. R., Marston, S. B., Luther, P. K., MacLeod, K. T., West, T. G., & Ferenczi, M. A. (2016). A post-MI power struggle: adaptations in cardiac power occur at the sarcomere level alongside MyBP-C and RLC phosphorylation. *Am J Physiol Heart Circ Physiol*, ajpheart 00899 02015.

Tong, C. W., Gaffin, R. D., Zawieja, D. C., & Muthuchamy, M. (2004). Roles of phosphorylation of myosin binding protein-C and troponin I in mouse cardiac muscle twitch dynamics. *J Physiol, 558*(Pt 3), 927-941.

Tong, C. W., Stelzer, J. E., Greaser, M. L., Powers, P. A., & Moss, R. L. (2008). Acceleration of crossbridge kinetics by protein kinase A phosphorylation of cardiac myosin binding protein C modulates cardiac function. *Circ Res, 103*(9), 974-982.

van der Velden, J., Moorman, A. F., & Stienen, G. J. (1998). Age-dependent changes in myosin composition correlate with enhanced economy of contraction in guinea-pig hearts. *J Physiol, 507 (Pt 2)*, 497-510.

Van Eyk, J. E., Powers, F., Law, W., Larue, C., Hodges, R. S., & Solaro, R. J. (1998). Breakdown and release of myofilament proteins during ischemia and ischemia/reperfusion in rat hearts: identification of degradation products and effects on the pCa-force relation. *Circ Res, 82*(2), 261-271.

Vincent, J. L. (2008). Understanding cardiac output. *Crit Care, 12*(4), 174.

Walcott, S., Docken, S., & Harris, S. P. (2015). Effects of cardiac Myosin binding protein-C on actin motility are explained with a drag-activation-competition model. *Biophys J, 108*(1), 10-13.

Walker, C. A., & Spinale, F. G. (1999). The structure and function of the cardiac myocyte: a review of fundamental concepts. *J Thorac Cardiovasc Surg, 118*(2), 375-382.

Weber, F. E., Vaughan, K. T., Reinach, F. C., & Fischman, D. A. (1993). Complete sequence of human fast-type and slow-type muscle myosin-binding-protein C (MyBP-C). Differential expression, conserved domain structure and chromosome assignment. *Eur J Biochem, 216*(2), 661-669.

Weber, K. T., & Brilla, C. G. (1991). Pathological hypertrophy and cardiac interstitium. Fibrosis and renin-angiotensin-aldosterone system. *Circulation, 83*(6), 1849-1865.

Weith, A. E., Previs, M. J., Hoeprich, G. J., Previs, S. B., Gulick, J., Robbins, J., & Warshaw, D. M. (2012). The extent of cardiac myosin binding protein-C phosphorylation modulates actomyosin function in a graded manner. *J Muscle Res Cell Motil, 33*(6), 449-459.

Weith, A., Sadayappan, S., Gulick, J., Previs, M. J., Vanburen, P., Robbins, J., & Warshaw, D. M. (2012). Unique single molecule binding of cardiac myosin binding protein-C to actin and phosphorylation-dependent inhibition of actomyosin motility requires 17 amino acids of the motif domain. *J mol Cell Cardiol, 52*(1), 219-227.

Whitten, A. E., Jeffries, C. M., Harris, S. P., & Trewhella, J. (2008). Cardiac myosin-binding protein C decorates F-actin: implications for cardiac function. *Proc Natl Acad Sci U S A, 105*(47), 18360-18365.

Witayavanitkul, N., Ait Mou, Y., Kuster, D. W., Khairallah, R. J., Sarkey, J., Govindan, S., Chen, X., Ge, Y., Rajan, S., Wieczorek, D. F., Irving, T., Westfall, M. V., de Tombe, P. P., & Sadayappan, S. (2014a). Myocardial infarction-induced N-terminal fragment of cardiac myosin-binding protein C (cMyBP-C) impairs myofilament function in human myocardium. *J Biol Chem, 289*(13), 8818-8827.

Woodhead, J. L., Zhao, F. Q., Craig, R., Egelman, E. H., Alamo, L., & Padron, R. (2005). Atomic model of a myosin filament in the relaxed state. *Nature, 436*(7054), 1195-1199.

Xie, M., Burchfield, J. S., & Hill, J. A. (2013). Pathological ventricular remodeling: therapies: part 2 of 2. *Circulation, 128*(9), 1021-1030.

Xu, Q., Dewey, S., Nguyen, S., & Gomes, A. V. (2010). Malignant and benign mutations in familial cardiomyopathies: insights into mutations linked to complex cardiovascular phenotypes. *J mol Cell Cardiol, 48*(5), 899-909.

Yamamoto, K. (1986). The binding of skeletal muscle C-protein to regulated actin. *FEBS Lett, 208*(1), 123-127.

Yang, Q., Hewett, T. E., Klevitsky, R., Sanbe, A., Wang, X., & Robbins, J. (2001). PKA-dependent phosphorylation of cardiac myosin binding protein C in transgenic mice. *Cardiovasc Res, 51*(1), 80-88.

Yang, Q., Osinska, H., Klevitsky, R., & Robbins, J. (2001). Phenotypic deficits in mice expressing a myosin binding protein C lacking the titin and myosin binding domains. *J Mol Cell Cardiol, 33*(9), 1649-1658.

Yang, Q., Sanbe, A., Osinska, H., Hewett, T. E., Klevitsky, R., & Robbins, J. (1998). A mouse model of myosin binding protein C human familial hypertrophic cardiomyopathy. *J Clin Invest, 102*(7), 1292-1300.

Yang, Q., Sanbe, A., Osinska, H., Hewett, T. E., Klevitsky, R., & Robbins, J. (1999). In vivo modeling of myosin binding protein C familial hypertrophic cardiomyopathy. *Circ Res, 85*(9), 841-847.

Yasuda, M., Koshida, S., Sato, N., & Obinata, T. (1995). Complete primary structure of chicken cardiac C-protein (MyBP-C) and its expression in developing striated muscles. *J mol Cell Cardiol, 27*(10), 2275-2286.

Young, D. B. (2010) *Control of Cardiac Output*. San Rafael (CA).

Zhang, H., Chen, X., Gao, E., MacDonnell, S. M., Wang, W., Kolpakov, M., Nakayama, H., Zhang, X., Jaleel, N., Harris, D. M., Li, Y., Tang, M., Berretta, R., Leri, A., Kajstura, J., Sabri, A., Koch, W. J., Molkentin, J. D., & Houser, S. R. (2010). Increasing cardiac contractility after myocardial infarction exacerbates cardiac injury and pump dysfunction. *Circ Res, 107*(6), 800-809.

Zile, M. R., & Brutsaert, D. L. (2002). New concepts in diastolic dysfunction and diastolic heart failure: Part I: diagnosis, prognosis, and measurements of diastolic function. *Circulation, 105*(11), 1387-1393.

Zoghbi, M. E., Woodhead, J. L., Moss, R. L., & Craig, R. (2008). Three-dimensional structure of vertebrate cardiac muscle myosin filaments. *Proc Natl Acad Sci U S A, 105*(7), 2386-2390.

VITA

Thomas L. Lynch IV was born in Palos Park, Illinois. Before attending Loyola University Chicago, he attended Lewis University in Romeoville, Illinois where he earned the degree Bachelor of Science in Biology with a minor in Chemistry. Thomas graduated from Lewis University as valedictorian, Summa Cum Laude, in 2011. Thomas then joined the Department of Molecular Pharmacology and Therapeutics at Loyola in 2011.

While at Loyola, Thomas was elected Treasurer of the Graduate Student Council from 2013-2014 and Co-President of the Graduate Student Council from 2014-2015. Thomas also served on the Graduate Student Advisory Council from 2012-2015. Thomas was awarded an American Heart Association Predoctoral Fellowship [15PRE22430028] during his time at Loyola, with a funding period from January 1, 2015 through December 31, 2016. He has been a member of the American Heart Association since 2014.

Following graduation, Thomas will begin a postdoctoral research position at the University of Wisconsin–Madison in Madison, Wisconsin in the laboratory of Dr. Richard L. Moss, where he will continue to study cardiac physiology and cardiac myosin binding protein-C in health and disease. Thomas currently lives in Orland Park, Illinois.